

**DEVELOPMENT OF ELECTROCHEMICAL SENSORS CONTAINING  
BIMETALLIC SILVER AND GOLD NANOPARTICLES**

**By**

**Stephen Nzioki Mailu**

*BEd (Sc) First class Honours*

A thesis submitted in fulfillment of the requirements for the degree of Magister  
Scientiae in the Department of Chemistry, University of Western Cape.

The logo of the University of the Western Cape, featuring a stylized classical building with columns and a pediment, with the text "UNIVERSITY of the WESTERN CAPE" below it.

UNIVERSITY of the  
WESTERN CAPE

SUPERVISORS: Prof. Emmanuel I. Iwuoha

Prof. Priscilla G.L Baker

MAY, 2010.

## KEYWORDS

Polyaromatic hydrocarbons (PAHs)

Electrochemical sensor

Overoxidized-polypyrrole composite (PPyox)

Silver-gold bimetallic alloy nanoparticles (Ag-AuNPs)

Polypyrrole polymer (PPy)

Anthracene (AN)

Pyrene (Py)

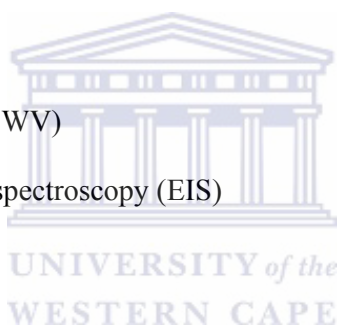
Phenanthrene (PHE)

Cyclic voltammetry (CV)

Square wave voltammetry (SWV)

Electrochemical impedance spectroscopy (EIS)

Bimetallic nanoparticles



## ABSTRACT

Polyaromatic hydrocarbons (PAHs) are ubiquitous environmental pollutants that have been shown to be teratogenic, mutagenic and carcinogenic and pose serious threats to the health of aquatic and human life. Several methods have been developed for their determination such as immunoassay, gas chromatography and high performance liquid chromatography (HPLC) in combination with fluorescence or absorbance detection. However, these methods are known to manifest underlying disadvantages such as complicated pretreatment, high costs and time consuming processes. In this work, a simple, less time consuming electrochemical method in the form of an electrochemical sensor has been developed for the detection of PAHs. The sensor was fabricated by the deposition of silver-gold (1:3) alloy nanoparticles (Ag-AuNPs) on ultrathin overoxidized polypyrrole (PPyox) film which formed a PPyox/Ag-AuNPs composite on glassy carbon electrode (PPyox/Ag-AuNPs/GCE). The silver-gold alloy nanoparticles deposited to form the composite were chemically prepared by simultaneous reduction of silver nitrate ( $\text{AgNO}_3$ ) and chloroauric acid ( $\text{HAuCl}_4$ ) using sodium citrate and characterized by UV-visible spectroscopy technique which confirmed the homogeneous formation of the alloy nanoparticles. Transmission electron microscopy showed that the synthesized nanoparticles were in the range of 20-50 nm. The properties of the composite formed upon deposition of the nanoparticles on the PPyox film were investigated by electrochemical methods. The PPyox/Ag-AuNPs/GCE sensor showed strong catalytic activity towards the oxidation of anthracene, phenanthrene and pyrene, and was able to simultaneously detect anthracene and phenanthrene in a binary mixture of the two. The catalytic peak currents obtained from square wave voltammetry increased linearly with anthracene, phenanthrene and pyrene concentrations in the range of  $3.0 \times 10^{-6}$  to  $3.56 \times 10^{-4}$  M,

$3.3 \times 10^{-5}$  to  $2.83 \times 10^{-4}$  M,  $3.3 \times 10^{-5}$  to  $1.66 \times 10^{-4}$  M and with detection limits of 0.169  $\mu$ M, 1.59  $\mu$ M and 2.70  $\mu$ M, respectively. The PPyox/Ag-AuNPs/GCE sensor is simple, has antifouling properties and is less time consuming with a response time of 4 s.



## DECLARATION

**I declare that** *Development of electrochemical sensors containing bimetallic silver and gold nanoparticles* is my own work, that it has not been submitted for any degree or examination in any other university, and that all sources I have used or quoted have been indicated and acknowledged by means of complete references.

Stephen Nzioki Mailu



UNIVERSITY *of the* May 2010  
WESTERN CAPE

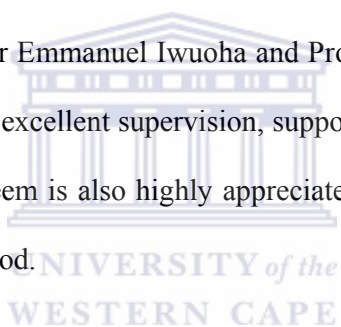
Signed.....

## ACKNOWLEDGEMENTS

The success of this work can be attributed to the assistance, guidance, and prayers of so many people who are hereby gratefully acknowledged. Firstly, I would like to give the Almighty God, all the glory, honour and adoration for giving me the strength and wisdom through the Holy Spirit to complete this work.

Many thanks go to all the members of the church of God where I derived spiritual nourishment.

To my supervisors, Professor Emmanuel Iwuoha and Professor Priscilla G.L Baker, I say a big thank you for your excellent supervision, support and encouragement during this period. Dr. Jaheed Nazeem is also highly appreciated for his continuous support through out my research period.



To the members of the department of Chemistry, University of the Western Cape, South Africa, I say thank you for the good and the cordial working relationship I enjoyed during my studies.

I gratefully acknowledge the National Research Foundation (NRF) of South Africa for funding my research programme. The support of my colleagues in SensorLab, University of the Western Cape, including Peter, Muchindu, Fanelwa, Chinwe, Abdul, Nicolette, Jesmina, Zelo, Natasha, Njomo, Masikini, Lundi, Matinise, Wale and Siphon is gratefully acknowledged. The leadership, role and cooperation from our post-

doctoral fellows: Dr. Amir-Al-Ahmed, Dr. Everlyne Songa, Dr. Omotayo Arotiba, Dr. Tesfaye Waryo and Dr. Faiza Jan Iftikhar, is also acknowledged.

The contributions of my beloved friends: Peter Ndangili, Nicholas Musyoka, Anyona, Everlyne, Njomo, Chinwe, Masikini, Wale and Susan Maingi are highly appreciated.

Much appreciation to all my family members for their love and care during the period of study. My sisters and brothers: Rebecca Mbula, Mary Kamene, Damaris Ngina, Irene Katunge, Nicholas Loki, Richard Kituku and Peter Kinyae, each time you assured me of your moral support while studying, I felt highly encouraged and loved. Thank you so much.

Lastly, to my parents Mrs. Rhodah Mumbi Mailu and Mr. Bredan Mailu Kituku, this is for you. Thank you very much for your love, care, education and upbringing. You are just the best gift from God! Painfully, Daddy passed away at the climax of this work, may his soul rest in peace.

## DEDICATION

This project is dedicated to

The

Almighty God

And

My Parents

Mrs. Rhodah Mumbi Mailu and Mr. Bredan Mailu Kituku.





## LIST OF PUBLICATIONS

- 1. Stephen N. Mailu**, Tesfaye T. Waryo, Peter M. Ndangili, Fanelwa R. Ngece, Abd A. Baleg, Priscilla G. Baker, Emmanuel I. Iwuoha. Determination of anthracene on Ag-Au bimetallic nanoparticles/overoxidized-polypyrrole composite modified glassy carbon electrodes. *Sensors* **2010** (in press).
- 2. Stephen N. Mailu**, Rasaq A. Olowu, Tesfaye T. Waryo, Priscilla G. Baker, Emmanuel I. Iwuoha. Simultaneous determination of anthracene and phenanthrene on Ag-Au bimetallic alloy nanoparticles/overoxidized-polypyrrole composite modified glassy carbon electrode. *Advanced material letters* **2010** (in preparation).
- 3. Stephen N. Mailu**, Tesfaye T. Waryo, Faiza J. Iftikhar, Priscilla G. Baker, Emmanuel I. Iwuoha. Recent advances in synthesis, characterization and application of bimetallic alloy nanoparticles as novel materials in electrochemical sensors and enzyme biosensors. *Electrochemical Acta Chimica*, Review article **2010** (in preparation).

## TABLE OF CONTENTS

<i>Title page</i> .....	i
<i>Keywords</i> .....	ii
<i>Abstract</i> .....	iii
<i>Declaration</i> .....	v
<i>Acknowledgement</i> .....	vi
<i>Dedication</i> .....	viii
<i>List of publications</i> .....	ix
<i>Table of contents</i> .....	<b>Error! Bookmark not defined.</b>
<i>List of figures</i> .....	xvi
<i>List of tables</i> .....	xxiii
<i>List of schemes</i> .....	xxiv
<i>List of abbreviations</i> .....	xxv
CHAPTER 1 .....	1
1.0 INTRODUCTION .....	1
1.1 Background.....	1
1.2 Problem statement.....	4
1.3 Rationale and motivation.....	5
1.4 The aims and objectives of the research.....	7
1.5 Research framework.....	9



1.6	Outline of the thesis. ....	10
CHAPTER 2 .....		12
2.0	LITERATURE REVIEW. ....	12
2.1	Polyaromatic hydrocarbons (PAHs). ....	12
2.1.1	Definition and sources of PAHs. ....	12
2.1.2	Formation of PAHs. ....	13
2.1.3	Properties of PAHs. ....	15
2.1.4	Characteristics of some of the monitored PAHs. ....	17
2.1.4.1	Phenanthrene (PHE). ....	17
2.1.4.2	Anthracene (AN). ....	18
2.1.4.3	Pyrene (Py). ....	19
2.1.5	Toxicological effects of PAHs. ....	20
2.1.5.1	Toxicity of PAHs. ....	20
2.1.5.2	Genotoxicity of PAHs. ....	21
2.1.5.3	Carcinogenicity of PAHs. ....	22
2.1.6	Human exposure to PAHs. ....	23
2.1.7	Methods used in the detection of PAHs. ....	24
2.2	Polymers. ....	27
2.2.1	Conducting polymers (CPs). ....	27
2.2.2	Synthesis of conducting polymers. ....	28
2.2.2.1	Polypyrrole (PPy). ....	29
2.2.2.2	Overoxidation of polypyrrole. ....	33
2.3	Monometallic and bimetallic nanoparticles. ....	35
2.3.1.	Application of nanoparticles in electrochemical sensors and biosensors. ....	35

2.3.1.1	Immobilization of biomolecules. ....	36
2.3.1.2	Catalysis of electrochemical reactions. ....	37
2.3.1.3	Enhancement of electron transfer. ....	38
2.3.1.4	Labeling biomolecules. ....	38
2.3.1.5	Nanoparticles acting as reactant. ....	38
2.3.2	Bimetallic nanoparticles. ....	39
2.3.3	Silver-gold bimetallic alloy nanoparticles (Ag-AuNPs). ....	40
2.3.3.1	Preparation methods for Ag-AuNPs. ....	40
2.4	Chemical sensors. ....	41
2.4.1	Electrochemical sensors. ....	42
2.4.1.1	Potentiometric sensors. ....	42
2.4.1.2	Conductometric sensors. ....	44
2.4.1.3	Amperometric sensors. ....	44
2.5	Characterization techniques. ....	46
2.5.1	Electroanalytical techniques. ....	46
2.5.1.1	Basic components of an electroanalytical system. ....	46
2.5.1.2	Cyclic voltammetry (CV) ....	49
2.5.1.3	Square wave voltammetry (SWV). ....	54
2.5.2	Spectroscopic techniques ....	57
2.5.2.1	Electrochemical impedance spectroscopy (EIS). ....	57
2.5.2.2	UV-visible spectroscopy ....	65
2.5.2.3	Fluorescence spectroscopy. ....	66
2.5.3	Other techniques ....	67
2.5.3.1	Transmission electron microscopy (TEM) ....	67
CHAPTER 3	.....	69

3.0 EXPERIMENTAL SECTION.....	69
3.1 Introduction.....	69
3.2 Reagents and materials .....	69
3.3 Instrumentation.....	70
3.4 Preparation of silver, gold and silver-gold alloy nanoparticles .....	71
3.5 Preparation of glassy carbon electrode (GCE) with nanoparticles .....	72
3.6 Preparation of overoxidized-polypyrrole polymer on GCE (PPyox/GCE).....	72
3.7. Fabrication of overoxidized-polypyrrole/Ag-AuNPs composite on GCE (PPyox/Ag-AuNPs/GCE).....	73
3.8 Electrochemical characterization.....	74
3.8.1 Characterization of the nanoparticles.....	74
3.8.2 Characterization of polypyrrole (PPy).....	75
3.8.3 Characterization of PPyox/GCE and PPyox/Ag-AuNPs/GCE.....	75
3.9 Electrochemical sensor measurements.....	76
3.9.1 Choice of suitable solvent and supporting electrolyte.....	76
3.9.2 Preparation and analysis of the PAHs.....	77
3.9.3 Interferences studies.....	78
CHAPTER 4 .....	79
4.0 RESULTS AND DISCUSSION 1 .....	79
4.1 Characterization of Ag-AuNPs.....	79
4.1.1 UV-visible spectroscopy.....	79
4.1.2 Fluorescence properties of Ag-AuNPs.....	84
4.1.3 Transmission electron microscopy (TEM) .....	85

4.1.4 Electrochemical characterization of Ag-AuNPs.....	86
4.1.4.1 Characterization in neutral medium.....	86
4.1.4.2. Characterization in the presence of $K_3Fe(CN)_6$ redox probe.....	93
4.1.4.3. Impedimetric characterization of Ag-AuNPs/GCE.....	95
4.2 Synthesis and characterization of PPy/GCE.....	99
4.2.1 Characterization of PPy/GCE in 0.1 M $LiClO_4$ .....	99
4.3 Overoxidation of polypyrrole.....	104
4.4 Electrochemical characterization of PPyox/Ag-AuNPs/GCE.....	105
CHAPTER 5.....	108
5.0 RESULTS AND DISCUSSION 2.....	108
5.1 Response of the electrochemical sensor on some monitored PAHs.....	108
5.1.1 Electrocatalytic oxidation of anthracene (AN).....	108
5.1.1.1 Analytical application for anthracene detection.....	113
5.1.1.2. Interferences to AN detection.....	117
5.1.1.3 Stability studies.....	118
5.1.1.4. Reproducibility studies.....	119
5.1.2 Electrocatalytic oxidation of phenanthrene (PHE).....	120
5.1.2.1 Reproducibility studies.....	125
5.1.2.2 Interference studies.....	125
5.1.3. Electrocatalytic oxidation of AN and PHE.....	126
5.1.3.1 Effect of scan rate on the peak current in the binary mixture of AN and PHE.....	129
5.1.3.2. Simultaneous determination of AN and PHE.....	131
5.1.4 Determination of pyrene (Py).....	135

5.1.4.1 Reproducibility. ....	138
CHAPTER 6. ....	139
6.0 CONCLUSION AND RECOMMENDATIONS .....	139
6.1 Conclusion .....	139
6.2 Future work and recommendation: .....	140
References.....	141



## LIST OF FIGURES

<b>FIGURE</b>	<b>TITLE</b>	<b>Page</b>
Figure 1:	The chemical structure of some common 16 US EPA priority PAHs	14
Figure 2:	Structure of phenanthrene	17
Figure 3:	Structure of anthracene	19
Figure 4:	Structure of pyrene	19
Figure 5:	Schematic representation of an electrochemical cell consisting of three electrodes	47
Figure 6:	A typical cyclic voltammogram	51
Figure 7:	A typical SWV containing the forward, reverse and difference currents.	56
Figure 8:	A typical impedance diagram	60
Figure 9:	A typical Nyquist plot	61
Figure 10:	A typical Nyquist plot showing some kinetic parameters	62
Figure 11:	A typical bode plot showing variation of impedance and phase angle with change in frequency	63
Figure 12:	A bode plot showing some kinetic parameters	64
Figure 13:	Randles equivalent circuit for a simple electrochemical cell	64
Figure 14:	UV-visible absorption spectra of Ag, Au, Ag-Au (1:3) alloy nanoparticles and a mixture of pure Ag and Au nanoparticles	80
Figure 15:	UV-visible absorption spectra of Ag, Au and Ag-Au (1:3) alloy nanoparticles after 4 months storage at 25 °C.	81
Figure 16:	UV-visible absorption spectra of Ag-Au alloy nanoparticles	



	with various molar ratios of Ag and Au.	82
Figure 17:	A plot of the wavelength corresponding to the maximum absorbance for varying mole fractions of Ag-Au alloy nanoparticles.	83
Figure 18:	Digital photographs of Au, Ag and Ag-Au alloy (Au mole fraction: (a) 0, (b) 0.1, (c) 0.5, (d) 0.75, (e) 0.9 and (f) 1) nanoparticles	84
Figure 19:	Emission spectra of Au and Ag-Au alloy (Au mole fraction: (a) 0.5, (b) 0.75, (c) 0.9 and (d) 1) nanoparticles with varying Au mole fraction	85
Figure 20:	TEM images of (a) Ag-Au (1:3) bimetallic alloy nanoparticles , (b) pure Ag nanoparticles and (c) pure Au nanoparticles.	86
Figure 21a:	Cyclic voltammograms of bare GCE and AgNPs/GCE in 0.1 M PBS pH 7 at a scan rate of $50 \text{ mV s}^{-1}$ .	87
Figure 21b:	Cyclic voltammograms of bare GCE and AuNPs/GCE in 0.1 M PBS pH 7 at a scan rate of $50 \text{ mV s}^{-1}$ .	88
Figure 21c:	Cyclic voltammograms of bare GCE and Ag-AuNPs/GCE in 0.1 M PBS pH 7 at a scan rate of $50 \text{ mV s}^{-1}$ .	88
Figure 22:	Cyclic voltammograms of Ag-AuNPs/GCE in 0.1M PBS pH 7 at different scan rates.	89
Figure 23a:	Cyclic voltammograms of bare GCE and AgNPs/GCE in 0.1M $\text{LiClO}_4$ at a scan rate of $50 \text{ mV s}^{-1}$	90
Figure 23b:	Cyclic voltammograms of bare GCE and AuNPs/GCE in 0.1 M $\text{LiClO}_4$ at a scan rate of $50 \text{ mV s}^{-1}$ .	91
Figure 23c:	Cyclic voltammograms of bare GCE and Ag-AuNPs/GCE in	

	0.1M LiClO <sub>4</sub> at a scan rate of 50 mV s <sup>-1</sup>	91
Figure 24:	Cyclic voltammograms of Ag-AuNPs/GCE in 0.1M LiClO <sub>4</sub> at different scan rates	92
Figure 25:	A plot of scan rate versus anodic peak current	93
Figure 26:	CVs of bare GCE and Ag-AuNPs/GCE in 5 mM K <sub>3</sub> Fe(CN) <sub>6</sub> solution containing 0.1 M KCl at a scan rate of 50 mV s <sup>-1</sup> .	94
Figure 27:	Nyquist plots of the EIS recorded in the presence of K <sub>4</sub> [Fe(CN) <sub>6</sub> ]/K <sub>3</sub> [Fe(CN) <sub>6</sub> ] (1:1) containing aq. KCl (0.1 M) for the bare GCE and Ag-AuNPs/GCE	96
Figure 28:	Polymerization of pyrrole in 0.1 M LiClO <sub>4</sub>	99
Figure 29:	Multiscan voltammograms of PPy characterization in 0.1 M LiClO <sub>4</sub> at different scan rates: (a) 10 mV s <sup>-1</sup> ; (b) 50 mV s <sup>-1</sup> ; (c) 75 mV s <sup>-1</sup> ; (d) 100 mV s <sup>-1</sup> ; (e) 150 mV s <sup>-1</sup> ; (f) 200 mV s <sup>-1</sup> ; (g) 250 mV s <sup>-1</sup> ; (h) 300 mV s <sup>-1</sup> ; (i) 350 mV s <sup>-1</sup> . (Initial potential: 500 mV).	100
Figure 30:	A plot of current versus scan rate	101
Figure 31:	Cyclic voltammograms of bare GCE and PPy/GCE in 5 mM K <sub>3</sub> Fe(CN) <sub>6</sub> at a scan rate of 50 mV s <sup>-1</sup>	103
Figure 32:	Overoxidation of PPy in 0.1 M NaOH for 420 s	105
Figure 33:	CVs recorded with PPyox/GCE (curve a), bare GCE (curve b) and PPyox/Ag-AuNPs/GCE (curve c) in the presence of K <sub>3</sub> Fe(CN) <sub>6</sub> (5 mM) in aq. KCl (0.1 M): Scan rate: 50 mV s <sup>-1</sup>	107
Figure 34:	CV of 3.56 x 10 <sup>-4</sup> M anthracene at bare GCE, AgNps/GCE, AuNPs/GCE, Ag-AuNPs/GCE, PPyox/GCE and PPyox/Ag-AuNPs/GCE	110

Figure 35:	CVs of PPyox/Ag-AuNPs/GCE upon addition of $3.56 \times 10^{-4}$ M anthracene at different scan rates	112
Figure 36:	A plot of root scan rate versus peak current	113
Figure 37:	CV of PPyox/Ag-AuNPs/GCE in acetonitrile + 0.1 M LiClO <sub>4</sub> with different anthracene concentration: (a) 0, (b) 33, (c) 66, (d) 100, (e) 133, (f) 166, (g) 200, (h) 233, (i) 250, (j) 283, (k) 312, (l) 340, (m) 356 $\mu$ M) at a scan rate of 100 mV s <sup>-1</sup>	114
Figure 38:	A calibration plot showing the relationship between oxidation current and concentration of anthracene	114
Figure 39:	SWV of PPyox/Ag-AuNPs/GCE in acetonitrile + 0.1 M LiClO <sub>4</sub> with different anthracene concentration: (a) 0, (b) 3, (c) 6, (d) 10, (e) 13, (f) 16, (g) 20, (h) 23, (i) 26, (j) 28, (k) 33, (l) 66, (m) 100, (n) 133, (o) 166, (p) 200, (q) 233, (r) 250, (s) 283, (t) 312, (u) 340, (v) 356 $\mu$ M).	115
Figure 40:	A calibration plot showing the relationship between current and concentration of anthracene.	115
Figure 41:	Current-time plot for the electrochemical sensor response to successive addition of 3.0 $\mu$ M anthracene at a constant potential of 1181 mV.	117
Figure 42:	SWV of PPyox/Ag-AuNPs/GCE in acetonitrile and 0.1 M LiClO <sub>4</sub> in anthracene alone and a mixture of anthracene and interferences	118
Figure 43:	SWV of PPyox/Ag-AuNPs/GCE in acetonitrile and 0.1 M LiClO <sub>4</sub> in presence of anthracene ( $3.56 \times 10^{-4}$ M) at the 1 <sup>st</sup> day, 4 <sup>th</sup> day, 8 <sup>th</sup> and 12 <sup>th</sup> day.	119

Figure 44:	CV of $2.5 \times 10^{-4}$ M PHE at bare GCE, Ag-AuNPs/GCE, PPyox/GCE and PPyox/Ag-AuNPs/GCE in acetonitrile and 0.1 M LiClO <sub>4</sub> .	121
Figure 45:	SWV of $2.5 \times 10^{-4}$ M PHE at bare GCE, Ag-AuNPs/GCE, PPyox/GCE and PPyox/Ag-AuNPs/GCE in acetonitrile and 0.1 M LiClO <sub>4</sub> .	121
Figure 46:	Anodic difference SWV of PPyox/Ag-Au NPs/GCE in acetonitrile and 0.1 M LiClO <sub>4</sub> with different PHE concentrations.	122
Figure 47:	A calibration plot showing the relationship between oxidation current and concentration of PHE	123
Figure 48:	CV of PPyox/Ag-AuNPs/GCE in acetonitrile and 0.1 M LiClO <sub>4</sub> at different scan rates upon addition of $2.33 \times 10^{-4}$ M PHE	124
Figure 49:	A plot of root scan rate versus peak current of PHE	124
Figure 50:	SWV of PPyox/Ag-AuNPs/GCE in acetonitrile and 0.1 M LiClO <sub>4</sub> in PHE alone and a mixture of PHE and interferences	126
Figure 51:	Voltammetric curves of $3.56 \times 10^{-4}$ M solution of AN (curve a), $2.30 \times 10^{-4}$ M solution of PHE (curve b) and 0.1 M LiClO <sub>4</sub> supporting electrolyte in acetonitrile (curve c) using PPyox/Ag-AuNPs/GCE.	127
Figure 52:	CVs of PPyox/Ag-AuNPs/GCE in acetonitrile and 0.1 M LiClO <sub>4</sub> (blank) (1) and a mixture of AN and PHE (2) .	128
Figure 53:	SWVs of PPyox/Ag-AuNPs/GCE in acetonitrile and 0.1 M LiClO <sub>4</sub> (blank) (1) and a mixture of AN and PHE (2)	128
Figure 54:	CVs for the binary mixtures of $2.30 \times 10^{-4}$ M AN and $2.30 \times 10^{-4}$ M PHE	128

	<sup>4</sup> M PHE in 0.1 M LiClO <sub>4</sub> and acetonitrile at PPyox/Ag-AuNPs/GCE at different scan rates: (a) 20 (b) 40 (c) 80 (d) 100 (e) 150 (f) 200 (g) 250 (h) 300 (i) 350 (j) 400 (k) 450 mV s <sup>-1</sup>	130
Figure 55:	A plot of root scan rate versus peak current of AN	130
Figure 56:	A plot of root scan rate versus peak current of PHE	131
Figure 57:	SWV for the binary mixtures of AN and PHE at PPyox/Ag-AuNPs/GCE in 0.1 M LiClO <sub>4</sub> and acetonitrile, [PHE] was kept constant and [AN] was changed (i.e. [AN]: (a) 0, (b) 30, (c) 60, (d) 100, (e) 130, (f) 166, (g) 200, (h) 230, (i) 250, (j) 280, (k) 312 μM).	132
Figure 58:	A calibration plot of concentration versus peak current of AN	132
Figure 59:	SWV for the binary mixtures of AN and PHE at PPyox/Ag-AuNPs/GCE in 0.1 M LiClO <sub>4</sub> and acetonitrile, [AN] was kept constant and [PHE] was changed (i.e. [PHE]: (a) 0 (b) 30 (c) 60 (d) 100 (e) 130 (f) 166 (g) 200 (h) 230 (i) 250 (j) 280 μM).	133
Figure 60:	A calibration plot of concentration versus peak current of PHE.	134
Figure 61:	SWV for the binary mixtures of AN and PHE at PPyox/Ag-AuNPs/GCE in 0.1 M LiClO <sub>4</sub> and acetonitrile, at increasing [AN] and [PHE] (i.e. (a) 250, (b) 280, (c) 312, (d) 340, (e) 356, (f) 380 μM).	135
Figure 62:	SWV of 2.80 x 10 <sup>-4</sup> M pyrene at bare GCE, Ag-AuNPs/GCE, PPyox/GCE and PPyox/Ag-AuNPs/GCE in acetonitrile and 0.1 M LiClO <sub>4</sub>	136
Figure 63:	SWV of PPyox/Ag-AuNPs/GCE at increasing concentration of pyrene (a) 0, (b) 10, (c) 33, (d) 66, (e) 100, (f) 130, (g) 166 μM).	137



## LIST OF TABLES

TABLE	TITLE	page
Table 1:	Diagnostic tests for the electrochemical reversibility of a redox couple, carried out by cyclic voltammetry .....	52
Table 2:	The EIS parameters obtained from the circuit fitting of Figure 27 data.....	97
Table 3:	Effect of Ag-AuNPs electrode on the kinetics of $[\text{Fe}(\text{CN})_6]^{3-/4-}$ .....	98
Table 4:	CV data for bare GCE and PPy/GCE in 5 mM $\text{K}_3\text{Fe}(\text{CN})_6$ .....	104
Table 5:	CV data obtained from Figure 33 .....	107
Table 6:	Anodic current response data for the development of the sensor .....	111



## LIST OF SCHEMES

SCHEME	TITLE	Page
Scheme 1:	Research framework.....	9
Scheme 2:	Procedure of ion exchange behavior of conducting polymer.....	30
Scheme 3:	Synthesis of polypyrrole from pyrrole monomer.....	32
Scheme 4:	Overoxidation of polypyrrole.....	33
Scheme 5:	A schematic picture of an electrochemical sensor.....	45
Scheme 6:	Schematic illustration of the stepwise sensor fabrication process.....	Error! Bookmark not defined
Scheme 7:	Outline of various products expected from the oxidation of anthracene. ....	109





## LIST OF ABBREVIATIONS

AN	Anthracene
CV	Cyclic voltammetry
DNA	Deoxyribonucleic acid.
EIS	Electrochemical impedance spectroscopy
Au	Gold
GCE	Glassy carbon electrode
HMW	High molecular weight
HPLC	High performance liquid chromatography
LMW	Low molecular weight
NPs	Nanoparticles
Ag	Silver
Ag-AuNPs	Silver-gold nanoparticles
SOD	Superoxide dismutase
SWV	Square wave voltammetry
PPyox	Overoxidized-polypyrrole
PHE	Phenanthrene
PAHs	Polyaromatic hydrocarbons
PPy	Polypyrrole
Py	Pyrene
TEM	Transmission electron microscopy
US EPA	United state environmental protection agency

# CHAPTER 1

## 1.0 INTRODUCTION

### 1.1 Background.

The quality of the environment is one of the key parameters that determine the life expectancy of human beings as well as the other living organisms. Interfering with the environment by means of contaminating it affects in one way or the other the life expectancy of the living organisms. The environment is contaminated through a process called pollution which is defined as the introduction of contaminants into the environment that causes instability, disorder, harm or discomfort to the ecosystem. This can be through air, water or soil pollution. Air pollution, both indoors and outdoors, is a significant cause of health problems worldwide. Urban and rural outdoor environment contains infections, allergens, irritants and chemical toxins that reduce the quality of life and causes diseases. These pollutants shorten the life span of people. Consequently, water pollution is a great threat to the life of human beings as well as other organisms. It has been suggested to be the leading world wide cause of death and diseases and that it accounts for the death of more than 14,000 people daily [1]. This pollution occurs through the passage of domestic wastes as well as industrial wastes such as oil, grease, and volatile organic compounds into the water bodies. Moreover, soil pollution is caused by the presence of man-made chemicals or other alteration in the natural soil environment. This contamination typically arises from the rupture of underground storage tanks, application of pesticides, and percolation of contaminated surface water to subsurface strata, oil and fuel dumping, leaching of wastes from landfills or direct discharge of industrial wastes to the soil.

Since the publication of Rachel Carson's silent spring [2], there has been concern that chemicals in the environment might exert profound and deleterious effects on wildlife population, and that the human health is extricably linked to the environment. However, the most common chemicals that cause great harm to the environment are petroleum hydrocarbons, solvents and pesticides. Due to the dangers associated with the pollution of the environment, it is of paramount importance to identify the specific causes of the pollution, the pollutants, and their specific composition in the environment. This calls for the development of fast and sensitive methods for monitoring the type of pollutants and the proportional amount of the pollutants in the environment. For this reason, the development of procedures for the extraction, determination and analysis of environmental pollutants has been one of the most important objectives of global research efforts today [3]. Some of the major environmental pollutants that require constant monitoring due to their environmental toxicity are the polyaromatic hydrocarbons (PAHs). They are chemical compounds that consist of aromatic rings and do not contain heteroatom or carry substituents [4]. They occur in oil, coal, and tar deposits and are produced as by-products of fuel burning (whether fossil fuel or biomass). As pollutants, they are of great concern because some of them have been identified to be carcinogenic, mutagenic and teratogenic. They are released into the air through burning of fuel or carbon containing compounds such as wood thus acting as air pollutants. Consequently, once oil and petroleum fuel spill to the water bodies they act as sources of PAHs which pollute water and soil.

Contamination of the environment is thus a global problem [3], especially the presence of PAHs in the environment as a result of their high levels of toxicity,

persistence and environmental prevalence [5]. Thorough research has been done on the causes, methods of determining and the maximum amount of PAHs that is allowed in the environment. In connection to this, the governments and environmental scientists around the world have begun screening and controlling them so as to reduce and restrain their risk to people and the environment. In fact, recent studies have focused on developing methods for monitoring traces of PAHs [6-9]. However, these studies have been limited to 16 PAHs, designated as priority pollutants by the United States Environmental Protection Agency (US EPA) [10]. In view of this, this work aims at developing a cheap and less time consuming electroanalytical method for the determination of anthracene, phenanthrene and pyrene which are some of the carcinogenic PAHs and that have been designated to be among the priority pollutants by the United States Environmental Protection Agency (US EPA). Since PAHs are made up of benzene rings and are easily oxidized at high potentials, the method employed involves the use of an electrochemical method, in form of an electrochemical sensor based on silver-gold alloy nanoparticles/overoxidized-polypyrrole composite. The composite is used to modify glassy carbon electrode and through the application of positive potentials, the specific PAHs are oxidized at specific potentials hence making them to be identified and determined. The silver-gold alloy nanoparticles act as electro-catalysts and aid in electron transfer during the oxidation process while the overoxidized-polypyrrole possess nanopores and create room for the deposition of the nanoparticles and prevent electrode fouling [11].

## 1.2 Problem statement.

The public concern about the presence of PAHs in the environment and their possible toxic effects such as being carcinogenic, mutagenic and teratogenic calls for the development of precise, accurate, cheap and less time consuming methods for identifying and quantifying them. Majority of the methods reported for the determination of PAHs involve the use of immunoassay, gas chromatography and high performance liquid chromatography (HPLC) with UV-vis absorbance or fluorescence, and capillary electrophoresis (CE) equipped with laser-induced fluorescence. These conventional methods allow high accuracy and low detection limits. However, the drawbacks of these methods although the most accurate, are that they are expensive, time consuming, require large sample volumes as well as large amount of organic solvent with separation and extraction procedures, and must be undertaken by an analytical chemist in a dedicated analytical laboratory. Moreover, electrode fouling offers a great analytical challenge during the determination of these PAHs.

In view of these analytical challenges, the silver-gold alloy nanoparticles/overoxidized-polypyrrole composite based electrochemical sensor developed in this study provides an easy, cheap, less time consuming and electrode fouling free method for the determination of PAHs.

### 1.3 Rationale and Motivation.

As a result of the above mentioned environmental effects caused by the presence of PAHs in the environment and the regulations attached to the maximum tolerated level for PAHs in the environment, there is the need to monitor the types of PAHs and their levels (compositional proportion) in the environment. Certain guidelines have been set by certain world organizations concerning the pollutants found in water and soil such as PAHs. In drinking water, the world health organization (WHO) has recommended concentration of lower than 15 ng/L for each PAH and 700 ng/L for benzo(a)pyrene (B[a]P) [12]. However, it has been recommended that drinking water samples containing around 8 PAHs, the concentration level should be less than 200 ng/L [13]. According to Kabzinski *et al.*, [13] the concentration of PAHs in surface water range from 0.1 – 830 ng/L and should not exceed that limit. In rain and snow, the concentration of all 16 PAHs has been found to vary between 500 to 20,000 ng/L. However, the concentration of PAHs in waste water and lakes can increase more than 100 times in comparison to the recommended maximum amount of PAHs in drinking water [13]. In soils, PAHs concentration should not exceed 1 µg/g [14]. Several methods for analysis and determination of PAHs have been reported. These methods include immunoassay [15], gas chromatography [16] and high performance liquid chromatography (HPLC) using UV-vis absorbance [17-18] and capillary electrophoresis (CE) equipped with laser-induced fluorescence [19]. However, these methods are known to manifest underlying disadvantages such as complicated pretreatment, high costs, and time consuming processes. Recent studies have shown that electrochemical methods are inexpensive, simple, and effective, have a high electrochemical detection and are less time consuming [20-21]. The ability of PAHs to be electrochemically oxidized forms the basis of electrochemical detection

methods. On application of potential, the electrocatalytic oxidation of PAHs is usually accompanied by generation of current. This current is proportional to the amount of the specified PAH under investigation. Consequently, by monitoring this current, the amount of the PAH under study can be inferred.

It has been found that bare electrodes such as glassy carbon electrodes, platinum electrodes and gold electrodes were able to oxidize the monitored PAHs [22]. Roman *et al.* [22] showed that naphthalene and acenaphthalene were able to be oxidized by bare glassy carbon electrodes and platinum electrodes. However, the immobilization of nanoparticles on the surface of the electrodes has been found to increase the effective surface area of the electrodes, thus enhancing the peak current leading to an increase in their sensitivity. Consequently, the use of bimetallic nanoparticles have been reported to have higher catalytic properties compared to their corresponding monometallic nanoparticles due to their increased surface area [23]. However, a great challenge of electrode fouling is observed during the oxidation of PAHs. This calls for the use of polypyrrole polymer which prevents electrode fouling. It is worth noting that over oxidizing the polypyrrole creates some nanopores on the surface of the polymer thus creating room for the deposition of the nanoparticles [11]. Thus, the fabrication of an electrochemical sensor based on overoxidized-polypyrrole and silver-gold bimetallic alloy nanoparticles presents a novel, simple, cheap, less time consuming, electrode fouling free and environmentally friendly method of detecting the highly carcinogenic PAHs.

#### **1.4 The aims and objectives of the research.**

The project will investigate the electrocatalytic behaviour of silver-gold alloy nanoparticles and the antifouling properties of overoxidized-polypyrrole towards the oxidation of PAHs.

The objectives of the study are:

- 1) To chemically synthesize silver-gold alloy nanoparticles.
- 2) To characterize the synthesized alloy nanoparticles by UV-Visible spectroscopy, fluorescence spectroscopy, transmission electron microscopy (TEM), electrochemical impedance spectroscopy (EIS) and cyclic voltammetry (CV).
- 3) To electrochemically synthesize polypyrrole and investigate its electrochemical properties.
- 4) To electrochemically overoxidize the synthesized polypyrrole.
- 5) To develop silver-gold alloy nanoparticles/overoxidized-polypyrrole composite on glassy carbon electrode (GCE) surface.
- 6) To study the electrochemical properties of the composite.
- 7) Apply the fabricated electrochemical sensor in the detection of PAHs.

In this study, a simple cheap and less time consuming procedure for preparing silver-gold alloy nanoparticles/overoxidized-polypyrrole composite based sensor for novel detection of anthracene, phenanthrene and pyrene is described. Pyrrole monomer doped with 0.1 M LiClO<sub>4</sub> was polymerized on glassy carbon electrode (GCE) to form polypyrrole modified glassy carbon electrode (PPy/GCE). The polypyrrole was then overoxidized in 0.1 M NaOH at positive potentials (1.0 V) for 420 s. Overoxidation of

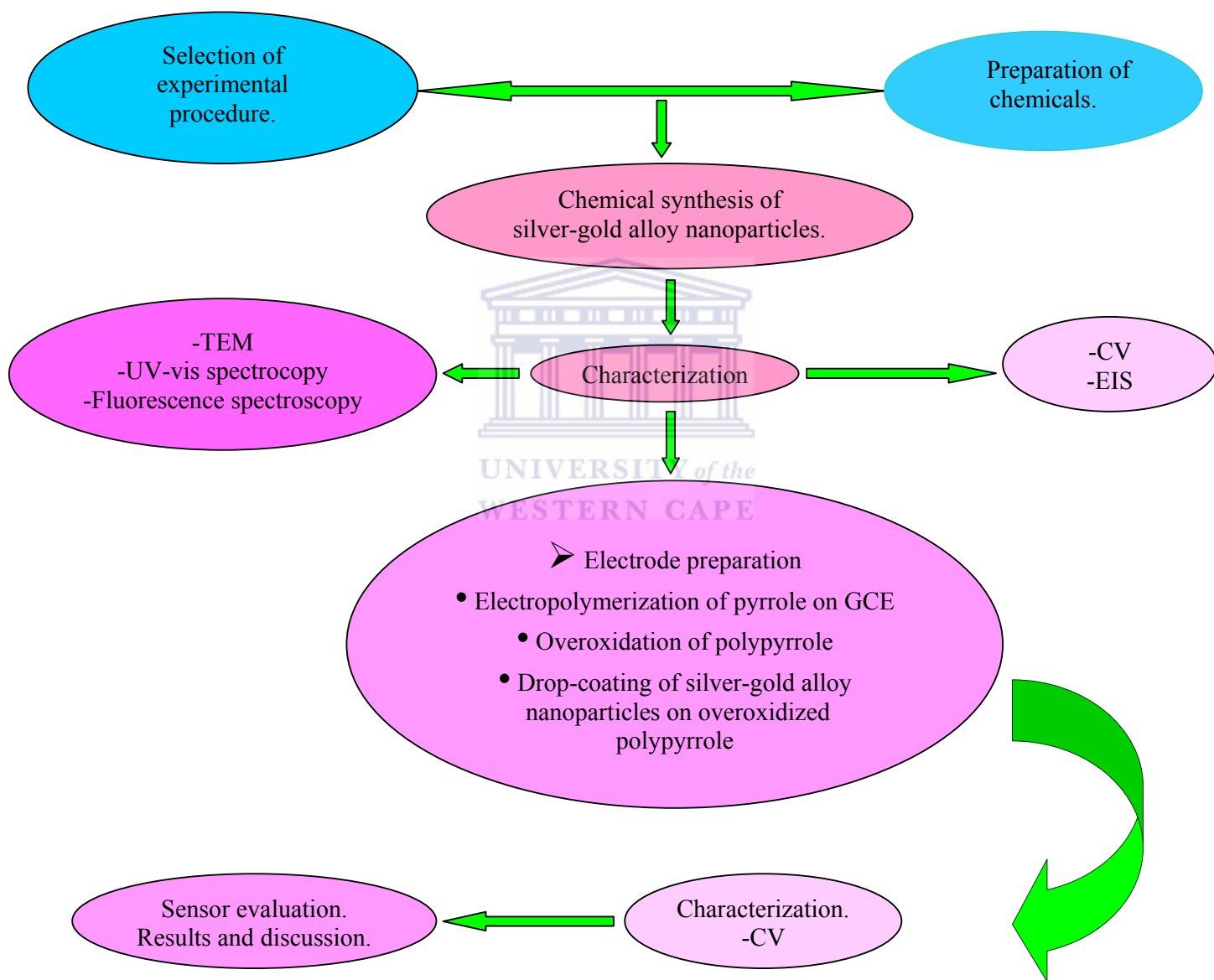


the polymer is accomplished by a loss of conjugation, electronic conductivity and dedoping with a net electronegative character imparted to the polymer film. Hence, the small doping anions ejected from the overoxidized film, creates a porous structure on the electrode. This creates room for the deposition of the nanoparticles. The immobilization of the silver-gold (1:3) alloy nanoparticles on the overoxidized-polypyrrole leads to the formation of silver-gold alloy nanoparticles/overoxidized-polypyrrole composite (PPyox/Ag-AuNPs/GCE) which is thus used as the electrochemical sensor for the detection of anthracene, phenanthrene and pyrene.



## 1.5 Research framework.

In line with the study objectives and the experimental procedure, the research framework is shown on the scheme below.

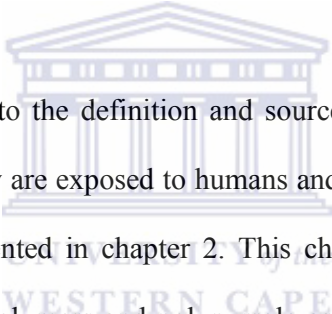


**Scheme 1. Research framework.**

## 1.6 Outline of the thesis.

The thesis will be presented as outlined briefly below:

An introduction giving various issues especially pollutants that affect human life and which require continuous monitoring are raised in this chapter. Polyaromatic hydrocarbons (PAHs) as one of the pollutants, their sources and their side effects are briefly highlighted in this chapter. Various methods used in the determination of PAHs are briefly discussed and the need for the use of electrochemical methods for the determination of PAHs is mentioned in this chapter. The objectives of this study are also stated in this chapter.



A literature review relating to the definition and sources of PAHs, their formation, properties, toxicity, how they are exposed to humans and the various methods used in their detection will be presented in chapter 2. This chapter will also cover a brief introduction to conducting polymers and polypyrrole as one of the polymers as well as the use of nanoparticles in the development of sensors. Characterization techniques, mainly cyclic voltammetry (CV), square wave voltammetry (SWV), electrochemical impedance spectroscopy (EIS), UV-visible spectroscopy, fluorescence spectroscopy, and transmission electron microscopy (TEM) will be discussed in this chapter. In chapter 3, information on the chemicals used, instrumentation and preparation procedures will be discussed. The chapters 4 and 5 will present results and discussion, chapter 4 will mainly present and discuss the characterization of the synthesized silver-gold (1:3) alloy nanoparticles, overoxidized-polypyrrole and silver-gold alloy nanoparticles/overoxidized-polypyrrole composite. Chapter 5 will present and discuss the electrochemical sensor response to some

monitored PAHs. It is also in this chapter that a detailed description of the sensor and its analytical characteristics such as stability, detection limit, linear range and reproducibility will be discussed. The final chapter, 6 will present the conclusions.



## CHAPTER 2

### 2.0 LITERATURE REVIEW.

#### 2.1 Polyaromatic hydrocarbons (PAHs).

##### 2.1.1 Definition and sources of PAHs.

Polycyclic aromatic hydrocarbons (PAHs) also known as polyarenes are a diverse group of organic compounds composed of hydrogen and carbon atoms arranged in two or more fused benzene rings. They are widespread ubiquitous environmental contaminants of anthropogenic or natural origin usually occurring in mixtures. The natural sources of PAHs include natural fires, volcanic eruptions, thermal geological reactions etc. [24]. Anthropogenic sources are the major sources of PAHs and this include fuel oil or gasoline spills, natural seeps as well as the combustion of fossil fuels such as coal, oil, and natural gas. The main source of PAHs is the incomplete combustion of coal, oil and petrol as well as in processes involving the petrochemical industries. They can also be found airborne, in the gas phase or adsorbed to airborne particles, in aqueous phases, such as groundwater, wastewater or drinking water, and adsorbed to solids in soil or sediments [25]. Crude oil and coal have also been identified as sources of PAHs. The adverse effects of PAHs are as a result of their persistence, hydrophobic character, bioaccumulation and carcinogenic properties. Hence, due to their ubiquitous distribution, PAHs detection in water and soils has arose a lot of concern and thus of ongoing interest to analytical chemists. They are emitted in the atmosphere, adsorbed to particles, and may then be transported over long distances [25]. According to Voogtp *et al.*, [26] an estimated total input of

230,000 metric tons of PAHs is released annually to the aquatic environment. This is mainly from spillage of fuels such as petroleum, oil and coal products causing a threat to the aquatic life. Djomo *et. al.* [27] showed that PAHs have adverse toxic effects on green alga and *scenedesmus subspicatus* once released into the aquatic environment.

### **2.1.2 Formation of PAHs.**

PAH is a name commonly used to refer to numerous benzene rings connected to one unit which can either be fused in a linear, angular, or clustered arrangement. The simplest example is naphthalene having two benzene rings side by side while others vary from two, three and more fused aromatic rings. The carcinogenic and mutagenic potential of some of the PAHs and their ubiquity in the environment led to the inclusion of 16 PAHs compounds in the list of priority pollutants in waste water published by the United States (US) Environmental Protection Agency (EPA) 1984 [25, 28] and later adopted by the US government in 1988. Some of the 16 US EPA priority PAHs are shown in Figure 1.

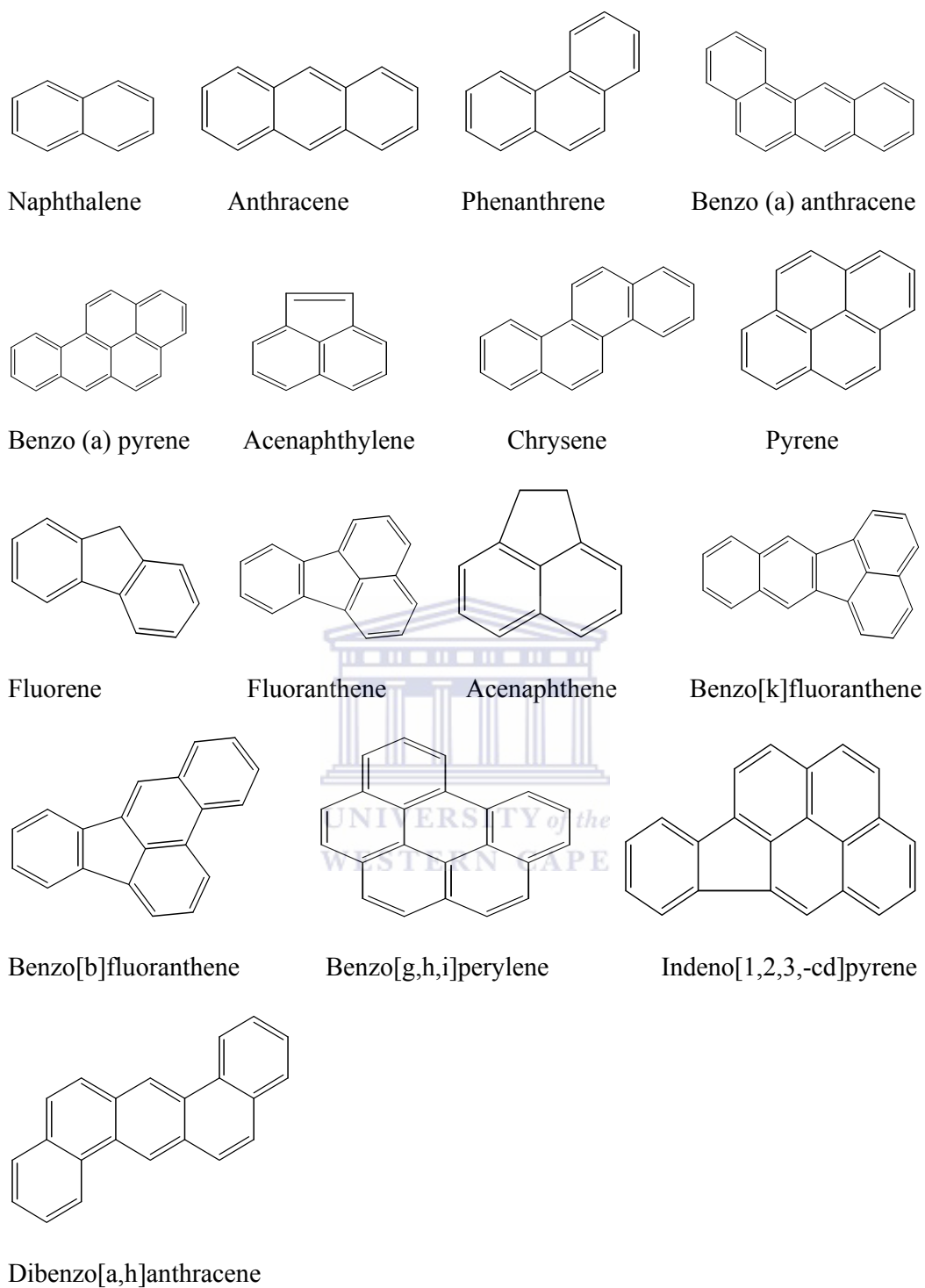


**Figure 1. The chemical structure of some common 16 US EPA priority PAHs.**

PAHs are formed during organic combustion processes without sufficient amounts of oxygen present (pyrolysis) and are found as a mixture of individual compounds [29]. The formation of PAHs can occur when parts of the fuel's polycyclic hydrocarbon backbone does not completely decompose or through high temperature processes of smaller alkanes clustering together to form aromatic compound. Due to the toxicity, persistency and environmental prevalence of PAHs [5], they have been thoroughly studied. However, these studies have been limited to the above mentioned 16 PAHs, designated as priority pollutants by the United States Environmental Protection Agency (US EPA).

### **2.1.3 Properties of PAHs.**

PAHs are grouped into two categories based on their molecular structure. Those with up to four rings and below, belong to low molecular weight (LMW) while those with more than four rings are high molecular weight (HMW). PAHs containing three or less benzene rings (LMW) have a high vapour pressure and can normally be found in the gas phase [25]. They are semi-volatile and exist in the atmosphere partly as vapors, which are highly susceptible to atmospheric degradation processes. The semi-volatile property of PAHs makes them highly mobile through out the environment via deposition and re-volatilization between air, soil, and water bodies. They are thus considered a regional pollutant. HMW PAHs are less volatile and condense on soot particles formed during combustion, are primarily associated with particles in the atmosphere and water and are less available for degradation [25]. PAHs are less oxidized in the atmosphere due to their ability to condense on particles and this enhances their transportation over long distances in the atmosphere and hence causes them to be ubiquitous in the environment. They accumulate in the environment



because they are thermodynamically stable compounds as a result of their large negative resonance energies; have low aqueous solubility, and adsorb to soil particles. Because of these reasons, PAHs do not readily undergo natural environmental processes including biodegradation. Therefore, PAHs persist for long periods under many natural conditions in the contaminated environment [30]. They are insoluble in water but readily solubilize in organic acids and solvents implying that in aqueous environment, they are found adsorbed on particulates. This is supported by Quantin *et al.*, [31] who argues that PAHs have high boiling points, are very lipophilic and are hard to dissolve in water. As a result of their hydrophobicity and recalcitrance, they accumulate in sediments in high concentrations. The low molecular weight PAHs are more water soluble and volatile than the higher molecular weight compounds since solubility of PAHs in water is inversely proportional to the number of rings they contain. For example, three-ring PAHs tend to be more water soluble than the five-ring compounds [32]. Due to their high partition coefficients and low water solubility, these compounds can strongly adsorb on to the surface of porous media, such as sediments and ground water [33-34]. In addition, the aqueous concentrations of PAHs in the contaminated environments can accumulate at higher concentrations in the presence of other organic compounds [35]. Mackay and Gschwend [35] showed that concentrations of PAHs in groundwater at a coal tar site were elevated by factors of 3-50 over purely dissolved concentration in water. These elevated concentrations of PAHs could enter into human body via food webs, and cause hazards to human health. Therefore, the investigation of concentration and distribution of PAHs in the environment provides a valuable record for clinical diagnosis, risk assessment, and the development of pre-warning system.

## 2.1.4 Characteristics of some of the monitored PAHs.

### 2.1.4.1 Phenanthrene (PHE).

Phenanthrene is a polycyclic aromatic hydrocarbon (PAH) composed of three fused benzene rings and with the chemical formula,  $C_{14}H_{10}$ . It is a colorless, crystal-like solid but can also look yellow as well as a white powder and has a bluish fluorescence. It is derived from coal tar, melts at 99 °C, boils at 340 °C and is insoluble in water but soluble in most organic solvents such as toluene, carbon tetrachloride, ether, chloroform, acetic acid, acetonitrile and benzene. It is a composite of phenol and anthracene [36] and its oxidation reactions occur at the 9 and 10 positions to form phenanthrenequinone. The structure of phenanthrene is shown in Figure 2.

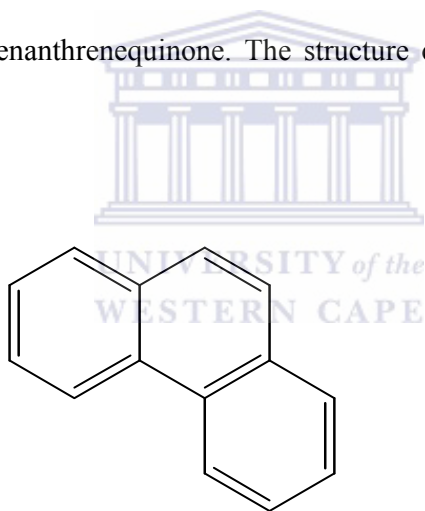
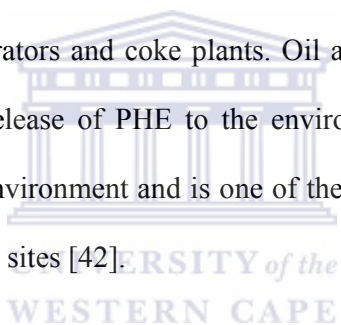


**Figure 2. Structure of phenanthrene.**

One of the most common ways through which phenanthrene gets into the body of human beings is through the breathing of contaminated air. This can be either through breathing it or working in a hazardous waste site where PAHs are disposed. Eating food or drinking water that is contaminated with PAHs can also lead to the exposure of the body to phenanthrene. Exposure to phenanthrene can also occur if one's skin

comes into contact with contaminated soil or products like soils, coal, coal tar, roofing tar or creosote where PAHs are found [37]. It has also been found that breathing cigarette and tobacco smoke, eating foods grown in contaminated soils or eating grilled meat can expose one to phenanthrene [37]. Once it gets into the body, it spreads and targets the fat tissues. The major target organs in the body include the kidneys and the liver. However, in a matter of days, it leaves the body through urine and feces [37]. It has been identified as one of the priority pollutant by the United States Environmental Protection Agency (USEPA) [38].

Other sources of PHE include incomplete combustion of fossil fuels, vehicular emissions, municipal incinerators and coke plants. Oil and petrol spillage into water bodies also results in the release of PHE to the environment [39-41]. It is widely distributed throughout the environment and is one of the most frequent and abundant PAHs found at contaminated sites [42].



#### **2.1.4.2 Anthracene (AN).**

It is a colorless solid polycyclic aromatic hydrocarbon consisting of three fused benzene rings derived from coal-tar or other residues of thermal pyrolysis. It has the chemical formula  $C_{14}H_{10}$  and has been identified in surface and drinking water, ambient air, smoke of cigarettes and cigars, foods, honey and edible aquatic organisms. This compound comes originally from both natural and anthropogenic sources involving incomplete combustion, aluminum smelting or the spillage of fossil fuel. Most people are exposed to anthracene through some of the foods they eat. Evidence indicates that anthracene is absorbed following oral and dermal exposure [43]. Oil and petrol spillage into water bodies also results in the release of anthracene

in to the environment [43]. Its determination is vital due to its acute toxicity. Its structure is shown in Figure 3.

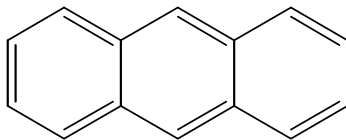


**Figure 3. Structure of anthracene**

#### **2.1.4.3 Pyrene (Py).**

Pyrene is a colorless solid and a highly toxic polycyclic aromatic hydrocarbon consisting of four fused benzene rings, resulting in a flat aromatic system. It has the chemical formula  $C_{20}H_{12}$  and is formed during incomplete combustion of organic compounds. It gets into the bodies of organisms through breathing contaminated air. Eating food and drinking water that is contaminated with PAHs may also lead to its exposure [43]. Its structure is shown in Figure 4.

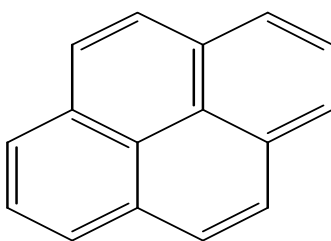


**Figure 4. Structure of pyrene**

## **2.1.5 Toxicological effects of PAHs.**

### ***2.1.5.1 Toxicity of PAHs.***

PAHs have been reported to cause a decrease in body weight, enlarge liver with cell edema and congestion of the liver parenchyma, reproductive toxicities, and destruction of oocyte and inflammation of kidney cells. Developmental toxicities such as embryo lethality, reduced fetal weight and malformations have been reported in response to benzo(a)anthracene, benzo(a)pyrene, dibenzo(a,h)anthracene and naphthalene [44]. Death in rodents has been reported to occur after short-time exposure to high doses of PAHs. It is noteworthy that, no deaths have been reported from short term occupational exposure in humans [45]. Since the environmental levels are generally much lower than the occupational exposure, it is unlikely that short-term exposures to PAHs would lead to death. Eye irritation, photophobia and skin toxicity such as dermatitis and keratosis have been demonstrated in workers occupationally exposed to PAHs. Respiratory effects, including acute and subacute inflammation and fibrosis, have also been demonstrated experimentally. A number of PAHs have been reported to cause tumors in laboratory animals that were exposed to PAHs through their food, from breathing contaminated air and when it was applied to their skin. For example, when pregnant mice ate high doses of benzo(a)pyrene, they experienced reproductive problems [46]. Other effects include damage to skin, body fluids and the immune system which help the body fight diseases and affects immunocompetence of organisms as well as the skin of animals. Moreover, PAHs have been identified to disrupt the sex hormones and possess developmental toxicity. They have effects on sperm quality in males while in females they cause reproductive dysfunctioning by the destruction of oocyte. The testis and ovaries contain rapidly proliferating cells hence

are probably particularly susceptible to damage by PAHs [46]. Benzo(a)pyrene (B[a]p) affects egg production in fish since they reduce primary oocyte numbers and plasma testosterone as well as estrogen level. They are also considered to be developmental toxicants. In animals, they are said to have the potential to induce adverse developmental effects such as pregnancy terminations, malformations, sterility in offsprings, testicular changes and immune-suppression and tumours [46].

#### **2.1.5.2 Genotoxicity of PAHs.**

Genotoxicity or mutagenicity is the ability of a foreign compound to effect a structural rearrangement in the molecular structure of a deoxyribonucleic acid (DNA) with its attendant implications. The primary focus of toxicological research on PAHs has been on genotoxicity and carcinogenicity. According to Pickering *et al.*, [46] several PAHs have shown to damage DNA and to cause mutations thus causing structural changes in the DNA. This occurs as a result of multiple metabolic transformations that take place in the PAHs. These transformations mostly lead to the formation of electrophilic derivatives capable of covalent interaction with nucleophilic centers of macromolecules, which results in mutagenicity. Moreover, a variety of chromosomal alterations such as frame shift mutations, deletion, s-phase arrest stand breakage etc may also be induced as a result of bulky adduct of PAHs to DNA bases [47]. In mammalian system, they are metabolized principally in the liver to yield both detoxification products which are more polar and excretal, and bioactivation products, which are more reactive and genotoxic. The original PAH compound does not react with DNA but they require metabolic activation and conversion to display their genotoxic properties. PAHs do not accumulate in the body but are converted to more water-soluble forms, which facilitates their subsequent

excretion from the organism [46]. However, this may lead to the formation of reactive intermediates that may react with DNA to form adduct, preventing the gene involved from functioning normally. The DNA damage may be repaired, but if the repair fails, i.e. if there is irreparable genetic damage, a mutation occurs.

### ***2.1.5.3 Carcinogenicity of PAHs.***

The interest on PAHs has been mainly due to their carcinogenic properties. PAHs comprises the largest class of chemical compounds known to be cancer- causing agents and are included in the European Union and United States Environmental Protection Agency (EAP) Priority pollutant list due to their mutagenic and carcinogenic properties [48]. Several works have been done on the carcinogenicity of these compounds [49-50]. Many of these have been found to be positive (cause cancer); some not cancer causing, may act as synergists [51]. Humans are exposed to complex mixtures of PAHs which have been implicated in inducing lung, skin, stomach and breast cancer. The carcinogenesis of PAHs is basically on their ability to bind the DNA thereby causing a series of disruptive effects that end up in tumor initiation. The aromatic hydrocarbon receptor plays a very important role in this. PAHs biological effects are actually attributed to the oxidation process that occurs during biotransformation of the mother compounds. PAH metabolites, including bay-region diol epoxides and free radical cation intermediates formed by mono-oxygenation and one-electron oxidation, respectively, are molecules that may bind to cellular DNA forming covalent DNA adducts responsible for carcinogenic process. The PAHs induced carcinogenesis is very complex and varies with individual compound [49].

### 2.1.6 Human exposure to PAHs.

Human exposure to PAHs occurs through the smoking of tobacco, inhalation of polluted air and ingestion of food and water contaminated by combustion effluents. Emissions from the combustion of coal, diesel, petrol, kerosene, wood, biomass and synthetic chemicals such as plastics also contribute to their publicity. The spillage/leakage of oil, diesel and petrol into the water bodies during the process of transportation may get their way into water bodies and affect aquatic life which may consequently affect humans. Most of the PAHs released in the environment end up being deposited in the oceans and/or subject to long range transport making them a wide spread environmental problem which affects humans directly or indirectly. The semi-volatile property of PAHs makes them highly mobile through out the environment via deposition and re-volatilization between air, soil and water bodies. It is therefore desirable in order, to put in place adequate clean up programmes for the prevention and remediation of PAHs pollution in the environment to avoid public health hazards. There are limits for work place exposure for chemicals that contain PAHs such as coal tar and mineral oil. The Occupational Safety and Health Administration (OSHA) has set a limit of 0.2 milligrams of PAHs per cubic meter of air ( $0.2 \text{ mg m}^{-3}$ ). The OSHA permissible exposure limit (PEL) for mineral oil mist that contains PAHs is  $5 \text{ mg m}^{-3}$  averaged over an 8-hour exposure period. Likewise, the National Institute for Occupational Safety and Health (NIOSH) recommends that the average workplace air levels for coal tar products should not exceed  $0.1 \text{ mg m}^{-3}$  for a 10-hour workday, within a 40-hour workweek. There are other limits for workplace exposure for compounds that contain PAHs, such as coal, coal tar, and mineral oil [52].



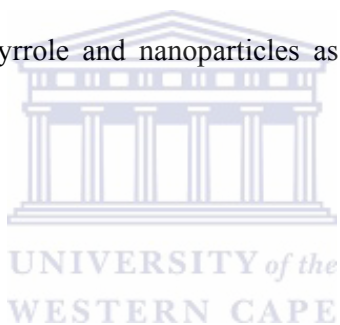
### **2.1.7 Methods used in the detection of PAHs.**

Several methods have been applied in the determination of PAHs. Some of the commonly used methods include immunoassay [15], gas chromatography [16] and high performance liquid chromatography (HPLC) with UV-vis absorbance or fluorescence [53-54] and capillary electrophoresis (CE) equipped with laser-induced fluorescence [19]. The drawback of these methods although the most accurate, are that they are expensive, time consuming, require large sample volumes as well as large amount of organic solvent with separation and extraction procedures, and must be undertaken by an analytical chemist in a dedicated analytical laboratory [55]. Moreover, the low solubility of the highly hydrophobic hydrocarbons in water and their occurrence in complex mixtures often require complex extraction, preconcentration and separation procedures for the sensitive detection of PAHs. Typical extraction methods applied are solid phase extraction (SPE), liquid-liquid extraction and supercritical fluid extractions. In addition, large amount of organic solvents used by the above techniques is environmentally unfriendly and raises concerns regarding health hazards to analysts. Most immunoassays for PAHs described in literature are enzyme linked immunosorbent assays (ELISA) [56-58], although other techniques such as radioimmunoassay (RIA) [59-60], piezoelectric immunosensor [61], capacitive immunosensor [62] and fluorescence based fiber optical immunosensors [63] have also been investigated. However, the fact that many PAHs are very similar in molecular structure, electron density and the lack of side groups makes it impossible to produce antibodies specific for only one compound [10]. This poses challenge in the application of immunoassays for determination of PAHs. These limitations can be reduced or avoided by using biosensor systems. Several biosensors including immunosensors, DNA biosensors and whole-cell

biosensors have been developed for the determination of PAHs [10, 64-67]. For example, a disposable amperometric immunosensor using screen-printed electrode was fabricated to detect low concentration of phenanthrene [10]. A soil biosensor using a recombinant bioluminescent bacterium, *Escherichia coli* GC2, and rhamnolipids, a biosurfactant, to increase the bioavailability of PAHs from the contaminated soil has been developed [65, 67]. In addition, a flow injection analysis system coupled with an evanescent wave biosensor for the detection of aromatic compounds that can intercalate with dsDNA has been reported [66]. However, these biosensors are designed for the determination of a single analyte in a sample at a time and lack the opportunity for analysis of multiple samples in the presence of multianalytes [68]. Moreover, enzymes cannot oxidize PAHs with IP values above 8 eV, an indicator that PAHs like fluorine whose IP value is above 8 eV cannot be determined [69]. Therefore, there is an ever-increasing demand for the determination of trace amounts of these substances at plant sites, water bodies and air. This calls for the development of a suitable and cost-effective analytical method that is able to carry out a rapid, simple and sensitive analysis of PAHs in environmental samples as well as able to detect more than one PAH in a sample. Electroanalytical methods are considered to be better methods for the determination of PAHs and an efficient solution to environmental problems compared to the other methods because a completely clean reagent, i.e. the electron, is utilized [10, 70-71]. However, during the determination of the PAHs using the electroanalytical methods, the problem of electrode fouling is observed which affects the stability of the methods [72].

The use of polymer-nanoparticles composite for detection of PAHs has not been reported. In this work, an electrochemical method for the determination of PAHs has

been developed by the use of overoxidized-polypyrrole and silver-gold alloy nanoparticles immobilized on the surface of the glassy carbon electrode (indicator electrode) and the modified electrode used as an electrochemical sensor to detect some PAHs. This will involve the use of a three electrode cell (glassy carbon electrode as the indicator electrode, Ag/AgCl as the reference electrode and Pt wire as the counter electrode) as will be explained in the experimental section. The polypyrrole is a conducting polymer and prevents electrode fouling thus enhancing the stability and repeatability of the method while the nanoparticles acts as electro-catalysts in the oxidation of the PAHs. The developed method is able to detect more than one PAH in a mixture of PAHs. A brief summary of the use of conducting polymers specifically polypyrrole and nanoparticles as electrode modifiers will be outlined below (2.2 and 2.3):



## 2.2 Polymers.

Researchers from different fields are in a process of combining expertise to study organic solids that poses remarkable conducting properties. Organic compounds with the ability of effectively transferring charge can be divided into three main groups namely; ion radical salts charge transfer complexes, organic species and conjugated conducting polymers. In the past two decades, a new class of polymers known as intrinsically conducting polymers or electro-active conjugated polymers has emerged. These polymers have gained popularity due to their interesting electrical and optical properties, which have previously been observed only in inorganic systems.

### 2.2.1 Conducting polymers (CPs).

The chemical bonding in conducting polymers produces one unpaired electron where there is a  $\pi$  electron per carbon atom in the backbone of the polymer. The carbon atoms are  $\pi$  bonded in a  $sp^2p_z$  configuration where the orbital of successive carbon atoms overlap providing delocalization of the electrons along the backbone of the polymer. Charge mobility is exerted along the backbone of the polymer as a result of this electron delocalization introducing properties such as electrical conductivity, low energy optical transitions, low ionization potential and high electron affinity. The  $\pi$  bonds in conducting polymers are highly susceptible to chemical or electrochemical oxidation or reduction processes. The formation of non-linear defects such as solitons, polarons and bipolarons produced during doping and polymerization of a polymer, have made a contribution to the electrical conduction in these polymer materials. An increase in electrode modification as a result of these polymers has provided new and interesting properties, which have contributed for the wide application of conducting polymers. They can either be metallic conductors or semiconductors and have been

applied in charge storage devices (batteries, capacitors), electromagnetic screens, sensors, membranes and corrosion protective coatings [73-75].

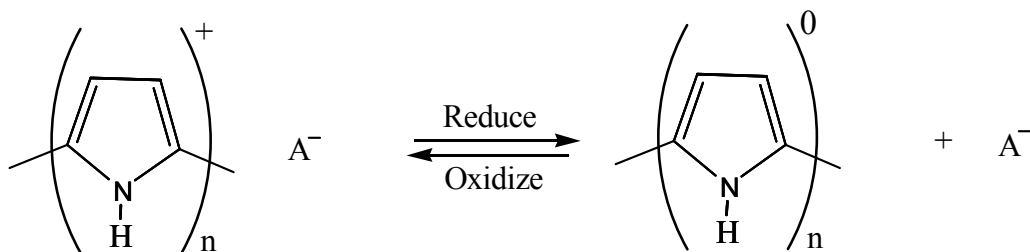
### **2.2.2 Synthesis of conducting polymers.**

There are various available methods for the synthesis of conducting polymers, with oxidative coupling of the monomer being the most widely used technique. This technique involves the formation of a cation radical followed by another coupling to produce a di-cation and the repetition then leads to the polymer [74]. Electropolymerization is normally carried out in a single cell compartment where a three-electrode configuration is employed subjected to an electrochemical solution consisting of a monomer and a supporting electrolyte (in some cases) all dissolved in an appropriate solvent which in some cases is acidic. The polymerization can be carried out either potentiostatically where the potential is kept constant with a variation of the current with time, or galvanostatically by keeping the current constant thereby monitoring the electrode potential. A three-electrode system employed during the polymerization comprises of a working electrode, a counter electrode and a reference electrode. Materials such as gold, platinum, carbon, nickel, titanium and palladium are used as working electrodes and function as support systems for the polymer films. Counter electrodes on the other hand supply the current required by the working electrode. A few commonly used counter electrodes include metallic foils of nickel, platinum and gold. Reference electrodes such as saturated calomel electrode (SCE), silver/silver chloride and mercurous sulfate are used in aqueous media [73]. Conductivity of the polymer is influenced by a number of factors including polaron length, the conjugation length, and the overall chain length and by the charge transfer to adjacent molecules. Research has proved that electrochemical synthesis is rapidly

becoming the preferred method for polymer preparation due to the simplicity and reproducibility associated with this technique. One advantage associated with the electrochemical polymerization of conducting polymers is that their reactions can be carried out at room temperature either by varying the potential or the current and with time the thickness of the film can be monitored and controlled. Besides copolymers and graft copolymers, electrochemical synthesis can be used for the generation of free standing, homogeneous and self doped films. Conducting polymers (CPs) such as polypyrrole, polythiophene, polycarbazole, polyindole and polyazulene can be synthesized using this technique [76]. However, in this work, major focus has been given to polypyrrole.

#### **2.2.2.1 Polypyrrole (PPy).**

Of all known CPs over the last 20 years, polypyrrole has appeared as the most extensively studied conducting polymer and the most frequently used because its monomer pyrrole is easily oxidized, water soluble, commercially available and the PPy posses good environmental stability, good redox properties, high electrical conductivity, simplicity of synthetic procedures and the possibility of forming homopolymers or composites with optical chemical and physical properties [77]. However, its insolubility in organic solvents hinders its processability. The electrical conductivity of conducting polymers is achieved in the film of the conducting polymers by oxidation (p-doping) or reduction (n-doping), followed respectively by the insertion of anionic or cationic species [78] according to the following procedure:



**Scheme 2. Procedure of ion exchange behavior of conducting polymer**

Due to the double bond alternation in the conjugated polymer backbone, the charged species formed upon doping are able to move along the carbon chain (delocalization) allowing electron transport and thus giving an electronically conductive material [79]. Thus, the hopping of electrons along and across the polymer chains with conjugating bonds gives PPy its electrical conductivity [77]. As a result, more positive PPy, more electron holes available, longer polymer chains and more coplanarity between interchains, are favoured for a higher conductivity performance [75].

PPy is a black powder and can be prepared by chemical or electrochemical polymerization. In the chemical polymerization process, monomers are oxidized by oxidizing agents or catalysts to produce conducting polymers while under electrochemical polymerization, PPy films are prepared by anodic electropolymerization of pyrrole in either non-aqueous or aqueous media on substrates such as glassy carbon or indium tin oxide (ITO). This can be done either through potentiostatic (constant potential), cyclic voltammetric and galvanostatic (constant current) methods. However, the principal advantage of the electrochemical method is related to the better conducting properties and long-term stability of conductivities [75]. Moreover, electrochemical polymerization provides a better

control of film thickness and morphology and cleaner polymers compared to chemical oxidation [77].

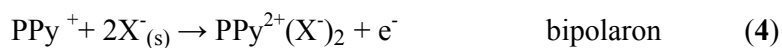
The number of electrons involved in the polypyrrole polymerization process for each monomer is approximately 2.25, one for each of the two  $\alpha$  positions to form the polymer and another one for every four monomer units to form the doped polymer. Similarly; one anion per four monomer units is incorporated during doping to maintain charge neutrality [80]. In the undoped state (pristine), neutral PPy is generally non-conducting having the aromatic and quinoid structures of which the latter posses a higher energy configuration. Generally, the redox mechanism of polypyrrole is described by one-electron transfer step; [81].



where PPy is the neutral species and  $\text{PPy}^+$  is the radical cationic species or polaron (one positive charge localized over three to four monomer units). The polaron can further be oxidized;

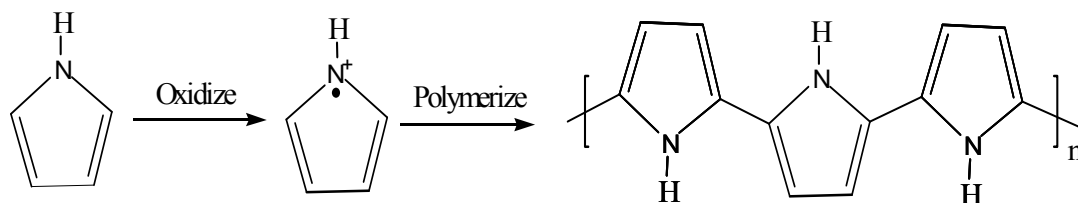


$\text{PPy}^{++}$  is the dicationic species or bipolaron (two positive charges localized over three to four monomer units). In the presence of dopant, where the dopant maintains electrical neutrality of the polymer during polymerization, the doped form (oxidized) is formed which manifest as either a polaron and/or bipolaron depending on the doping level as follows:





where  $X^-$  are anions, (the subscript  $(s)$  indicates that they are in solution phase) and PPy represents a segment of the polypyrrole chain. The synthesis of polypyrrole from solutions containing its monomer, pyrrole, may be represented by the simplified process [77]:



**Monomer**

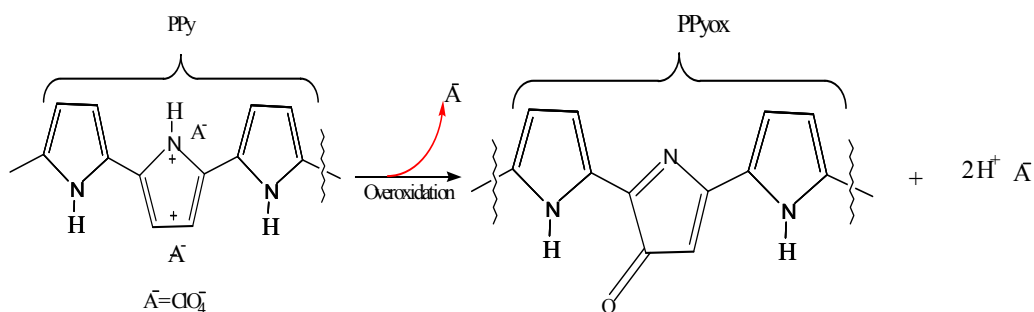
**polymer**

**Scheme 3. Synthesis of polypyrrole from pyrrole monomer.**

During electrochemical synthesis of PPy, the properties of the deposited film on the electrodes depend on the polymerization conditions. The solvent and the supporting electrolyte affect the film morphology, conductivity and mechanical behaviour. According to Said *et al.*, [77] the electropolymerization potential also affects the formation and the properties of polypyrrole films. At high positive potentials, the PPy can be overoxidized expelling the doping ions from the backbone of the polymer and thus losing its electrochemical conductivity. However, overoxidized-polypyrrole (PPyox) is an excellent material used as a matrix for deposition of metal nanoparticles, as it consists of nano-pores within the polymer film [11].

### 2.2.2.2 Overoxidation of polypyrrole.

Polypyrrole undergoes overoxidation at positive potentials, and/or at more alkaline media, and has been regarded as an undesirable degradation process, since it leads to the loss of conductivity and dedoping [11]. This means that dopant anions are expelled into the solution phase, leaving the polymer in its neutral, non-conductive state being susceptible to nucleophilic attack. Furthermore, some literature reviews have pointed out that, in aqueous solution, the PPy overoxidation potential depends on the solution pH whereby the higher the pH, the lower the overoxidation potential is. Indeed, PPy overoxidation process is more effective in basic solution (NaOH) than in NaCl solution [82]. In sodium hydroxide solution, the overoxidation of polypyrrole film proceeds faster than in pH buffer solutions because hydroxide ions in sodium hydroxide solution act as nucleophilic reactants which are stronger than anionic species present in buffer solutions [83]. During the overoxidation of pyrrole, higher density carbonyl groups such as  $>C=O$  and  $-COO^-$  are generated on the backbone of the overoxidized-polypyrrole film (PPyox-film). This is favorable for cation species (+) to be accumulated onto the film and then catalytically oxidized at the electrode. This allows favorable conditions for chemical interactions between the PPyox surface and the approaching species. The overoxidation of polypyrrole from basic solutions where the dopant ( $A^-$ ) is  $ClO_4^-$  may be represented by the simplified process:



**Scheme 4. Overoxidation of polypyrrole.**

It is noteworthy that this transformation of PPy as a result of overoxidation is accomplished by a loss of conjugation, electronic conductivity and dedoping with a net electronegative character imparted to the polymer film. Hence, the small doping anions ejected from the PPyox film, creates a porous structure on the electrode [11]. The PPy film improves selectivity, cation permselective behavior and the efficiency of PPyox in suppressing interfering electroactive species and avoiding electrode fouling [11]. The high permselectivity of overoxidized polypyrrole films allows analytes to reach the surface of electrodes easily.

For conducting polymers, the thickness of the film determines the conductivity and the permeability of the polymer film. The thinner the thickness of the overoxidized PPy film, the shorter the response time and a higher sensitivity can be achieved. This can be achieved by controlling the electropolymerization parameters such as the number of cycles used during polymerization. Thus, the thickness of the PPyox polymer can be controlled. The formation of the porous structure on the working electrode surface by the overoxidized-polypyrrole enables easy deposition of nanoparticles leading to the formation of a polymer-nanoparticles composite with antifouling properties. The deposited nanoparticles increase the rate of electron transfer and acts as electro-catalysts. Nanoparticles have found great application in the fabrication of electrodes as outlined in **2.3** below.

### **2.3 Monometallic and bimetallic nanoparticles.**

Noble metallic nanomaterials are of particular interest today because of their application in many areas. They are widely used in the development of electrochemical sensors and biosensors as described below:

#### **2.3.1 Application of nanoparticles in electrochemical sensors and biosensors.**

The unique chemical and physical properties of nanoparticles make them extremely suitable for designing new and improved sensing devices, especially electrochemical sensors and biosensors. Many kinds of nanoparticles, such as metal, bimetallic, oxide and semi-conductor nanoparticles have been used for constructing electrochemical sensors, for example, an electrochemical sensor for the determination of trace Cr(VI) was developed by the use of gold nanoparticles modified on glassy carbon electrode [84]. It has been shown that metal nanoparticles provide three important functions for electroanalysis; improved mass transport, high effective surface area and catalytic properties [85]. Due to their unique catalytic properties, they have been used as catalysts and electrocatalyst. For example, an electrochemical nitrate sensor was developed by the modification of glassy carbon electrode with Au-Fe(III) nanoparticles [86]. Silver-gold bimetallic nanoparticles immobilized on the surface of glassy carbon electrode have been used in the electrocatalytic oxidation of glucose (electrochemical glucose sensor) [87]. Biosensors have also been fabricated based on nanoparticles whereby certain enzymes have been attached on nanoparticles-modified electrodes. For example, an electrochemical biosensor has been developed by the immobilization of superoxide dismutase (SOD) on gold nanoparticles modified indium /tin oxide film coated glass [88]. Moreover, Xinhuang kang developed a novel glucose biosensor based on immobilization of glucose oxidase in chitosan on GCE

modified with gold-platinum alloy nanoparticles [89]. Hence, these nanoparticles which can either be monometallic or bimetallic play different roles in different sensing systems. They have excellent conductivity and catalytic properties which make them act as “electronic wires” to enhance the electron transfer between redox centers in proteins and electrode surfaces, and as catalysts to increase electrochemical reactions. Oxide nanoparticles are often used as labels or tracers for electrochemical analysis. According to Xiliang Luo *et al.*, [85] monometallic and bimetallic nanoparticles have several functions in electrochemical sensors and biosensors as outlined below:

#### ***2.3.1.1 Immobilization of biomolecules.***

Nanoparticles have large specific surface area and high surface free energy. This enables them to adsorb biomolecules strongly and play an important role in the immobilization of biomolecules in biosensor construction. The nanoparticles enable the biomolecules which are adsorbed on the surface of the electrodes to retain their biocompatibility. This is because they are highly compatible with the biomolecules since most of them carry charges and can electrostatically adsorb biomolecules with different charges. Besides their common electrostatic aspects, some nanoparticles can also immobilize biomolecules by other interactions. For example, gold nanoparticles have been reported to immobilize proteins through the covalent bonds formed between the gold atoms and amide groups and cysteine residues of proteins [90-91]. Other nanoparticles such as Pt, Ag, TiO<sub>2</sub>, ZrO<sub>2</sub> and bimetallic nanoparticles such as Ag-Au and Au-Pt alloy nanoparticles have also been applied in the immobilization of enzymes. Electrochemical immunosensors based on the immobilization of antigen or antibody with nanoparticles has also been extensively applied. For example, Zhuo *et*

*al.* [92] developed a reagentless amperometric immunosensor based on the immobilization of  $\alpha$ -1-fetoprotein antibody onto gold nanoparticles and the immunosensor exhibited good long-term stability. Generally, immobilization of biomolecules with certain nanoparticles can effectively increase the stability and maintain the activity of biomolecules and can be a good option for bimolecular immobilization [85].

### ***2.3.1.2 Catalysis of electrochemical reactions.***

Many nanoparticles, especially metal nanoparticles have excellent catalytic properties. The introduction of nanoparticles with catalytic effects into electrochemical sensors and biosensors can decrease overpotentials of many analytically important electrochemical reactions and even realize the reversibility of some redox reactions, which are irreversible at common unmodified electrode. For example, Ohsaka and Coworkers [93] developed an electrochemical sensor for selective detection of dopamine in the presence of ascorbic acid which was based on the catalytic effect of gold nanoparticles on the ascorbic acid oxidation. This resulted in the decrease of the oxidation overpotential of ascorbic acid and the effective separation of the oxidation potentials of ascorbic and dopamine, thus allowing the selective electrochemical detection. Several nanoparticles and bimetallic nanoparticles have been used as catalysts and electrocatalysts. For example, Tianyan *et al.* [94] prepared a highly sensitive H<sub>2</sub>O<sub>2</sub> sensor based on the modification of carbon film electrode with Pt nanoparticles. Bimetallic Ag-Au alloy nanoparticles have also been used as electrocatalyst in the electrocatalytic oxidation of glucose [87].

### ***2.3.1.3 Enhancement of electron transfer.***

Enzymes usually lack direct electrochemical communication with electrodes since the active centers are surrounded by considerably thick insulating protein shells, hence blocking the electron transfer between electrodes and the active centers. Conductivity properties of nanoparticles, mostly metal nanoparticles at nanoscale dimensions makes them suitable for enhancing the electron transfer between the active centers of enzymes and the electrodes. They act as electron transfer “mediators” or “electrical wires” e.g. Ag and Au nanoparticles have good conductivity and have been used to enhance electron transfer between proteins and electrodes [95].

### ***2.3.1.4 Labeling biomolecules.***

The labeling of biomolecules, such as antigen, antibody and DNA with nanoparticles plays an increasingly important role in developing sensitive electrochemical biosensors. Biomolecules labeled with nanoparticles can retain their bioactivity and interact with their counterparts and based on the electrochemical detection of those nanoparticles, the amount or concentration of analytes can be determined. Metal nanoparticles labels can be used in both immunosensors and DNA sensors. Gold nanoparticles are the most frequently used among all the metal nanoparticles labels available. For example Limoges's group [96] has reported a sensitive electrochemical immunosensor for goat immunoglobulin G (IgG) based on a gold nanoparticles label.

### ***2.3.1.5 Nanoparticles acting as reactant***

Nanoparticles are chemically more active than the related bulk materials due to their high surface energy. For example, MnO<sub>2</sub> is known to catalyze the decomposition of H<sub>2</sub>O<sub>2</sub>, while MnO<sub>2</sub> nanoparticles can react with H<sub>2</sub>O<sub>2</sub> directly [97]. However, the

application of the special reactivity of electrochemical sensors and biosensors has not been extensively studied.

### **2.3.2 Bimetallic nanoparticles.**

Metal nanoparticles can either be monometallic or bimetallic. Bimetallic nanoparticles are nanoparticles made up of two metal nanoparticles and have been reported to have higher catalytic properties compared to their corresponding monometallic nanoparticles due to their increased surface area [98]. There are two types of bimetallic nanoparticles namely; alloy nanoparticles and core-shell nanoparticles. The difference between the two arises from their method of preparation where bimetallic alloy nanoparticles are as a result of simultaneous reduction of the metal salts to nanoparticles while core-shell nanoparticles result from successive reduction of the more noble metal salt followed by the reduction of the less noble metal salt. The alloy nanoparticles are homogeneously distributed over the whole volume on an atomic scale; however, the core-shell metal nanoparticles constitute the core of the structure and the other one the external shell.

Bimetallic nanoparticles are of considerable interest since they possess interesting size-dependent electrical, chemical and optical properties [99]. They are of special importance in the field of catalyst, since they often exhibit better catalytic properties than their monometallic counterparts [23].



### 2.3.3 Silver-gold bimetallic alloy nanoparticles (Ag-AuNPs).

#### 2.3.3.1 Preparation methods for Ag-AuNPs.

Many methods have been reported for the synthesis of Ag-Au alloy nanoparticles. This is because Ag and Au have very similar lattice constants and are completely miscible over the entire composition [100] hence are able to form alloy nanoparticles upon reduction of their metal salts. They have been synthesized by the use of chemical and electrochemical methods. Electrochemical methods involve the reduction of their metal salts by the application of electric potential while in chemical synthesis, reducing agents are used. The use of strong reducing agents such as sodium borohydride ( $\text{NaBH}_4$ ) has been reported to yield smaller particles compared to the use of weak reducing agents such as sodium citrate which results in the production of larger particles [101]. For example, a simple co-reduction of  $\text{HAuCl}_4$  and  $\text{AgNO}_3$  with sodium citrate in aqueous solution has been reported to yield 17 to 22 nm sized alloy nanoparticles [102] while using  $\text{NaBH}_4$  as the reducing agent yielded stable Ag-Au alloy nanoparticles of 2-3 nm which were stabilized using optically transparent inorganic imogolite fibers [103]. However, the use of sodium citrate is preferred since the reductant can easily be decomposed to carbon dioxide and it is not as toxic as  $\text{NaBH}_4$ . Moreover, the sodium citrate acts as a reducing agent as well as a stabilizing agent compared to the use of  $\text{NaBH}_4$  which requires a stabilizing agent. A stabilizing agent is of great importance in the synthesis of nanoparticles to prevent agglomeration of the nanoparticles, which lowers their catalytic properties. According to Masato *et al.*, [87] electrochemical properties and the electrocatalytic property of Ag-Au alloy nanoparticles with different Ag and Au composition depends on the composition of Ag in the bimetallic alloy nanoparticles. Increasing the amount of Ag content in the

bimetallic alloy nanoparticles, would show no improved electrocatalytic reactions. Thus, a high Ag content above 70% in the bimetallic alloy nanoparticles showed low electrocatalytic properties [87]. However, Ag-Au bimetallic alloy nanoparticles with low Ag content have been observed to show improved electrocatalytic properties. Masato *et al.* showed that Ag-Au bimetallic alloy with Ag:Au atomic ratio 27:73 had higher electrocatalytic properties compared to the other Ag:Au alloy nanoparticles [87]. Aiqin Wang *et al.* [104] and Xhiang *et al.* [105] showed that Ag-Au bimetallic alloy nanoparticles portrayed better electrocatalytic properties when Ag:Au was in the ratio of 1:3 (25:75). On this basis, more focus has been on the synthesis, characterization and the application of Ag-Au with an Ag: Au atomic ratio of 25:75 (1:3).

#### **2.4 Chemical sensors.**

A chemical sensor can be defined as “ a small device that as a result of a chemical interaction or process between the analyte and the sensor device transforms chemical or biochemical information of a quantitative type into an analytically useful signal ” [106]. Chemical sensors consist of a transducer, which transforms the response into a detectable signal on modern instrumentation, and a chemically selective layer, which isolates the response of the analyte from its immediate environment. They are classified according to the property that is being determined such as; electrical, optical, mass or thermal properties and are designed to detect and respond to an analyte in the gaseous, liquid or solid state. Compared to optical, mass and thermal sensors, electrochemical sensors are highly attractive because of their remarkable detection capability, experimental simplicity and low cost. They have a leading position among the presently available sensors that have reached the commercial

stage and which have found a vast range of importance in the fields of clinical, industrial, environmental and agricultural analyses [107].

#### **2.4.1 Electrochemical sensors**

Electrochemical sensors operate by reacting with the analyte of interest and producing an electrical signal proportional to the analyte concentration. There are three types of electrochemical sensors: namely; potentiometric, conductometric and amperometric sensors.

##### ***2.4.1.1 Potentiometric sensors.***

Potentiometric sensors have found the most widespread practical applicability since early 1930's due to their simplicity, familiarity and cost. They involve the establishment of a local equilibrium at the sensor surface, where either of the electrode or membrane potential is measured, and information about the composition of the sample is obtained from the potential difference between reference electrode and the indicator electrodes [107]. Basically, in potentiometric sensors, the potential difference between the reference electrode and the indicator electrode is measured without polarizing the electrochemical cell, that is, very small current is allowed. The reference electrode is required to provide a constant half-cell potential. The indicator electrode develops a variable potential depending on the activity or concentration of a specific analyte in solution. The change in potential is related to the concentration of the analyte in a logarithmic manner [108]. Potentiometric devices can be categorized into three basic types:

- i) Ion-selective electrodes (ISE)
- ii) Coated wire electrodes (CWE)

iii) Field effect transistors (FET).

The ion-selective electrode is an indicator electrode capable of selectively measuring the activity of a particular ionic species. In classic configuration, ISE are mainly membrane-based devices, consisting of permselective ion-conducting materials, which separate the sample from the inside of the electrode. One of the electrodes is the working electrode whose potential is determined by its environment while the second electrode is a reference electrode whose potential is fixed by a solution containing the ion of interest at a constant activity. Since the potential of the reference electrode is constant, the value of the potential difference (cell potential) can be related to the concentration of the dissolved ions.

Under classical CWE design, a conductor is directly coated with an appropriate ion-selective polymer (usually poly(vinyl chloride), poly (vinylbenzyl chloride) or poly(acrylic acid)) to form an electrode system that is sensitive to electrolyte concentration. The design eliminates the need for a reference electrode.

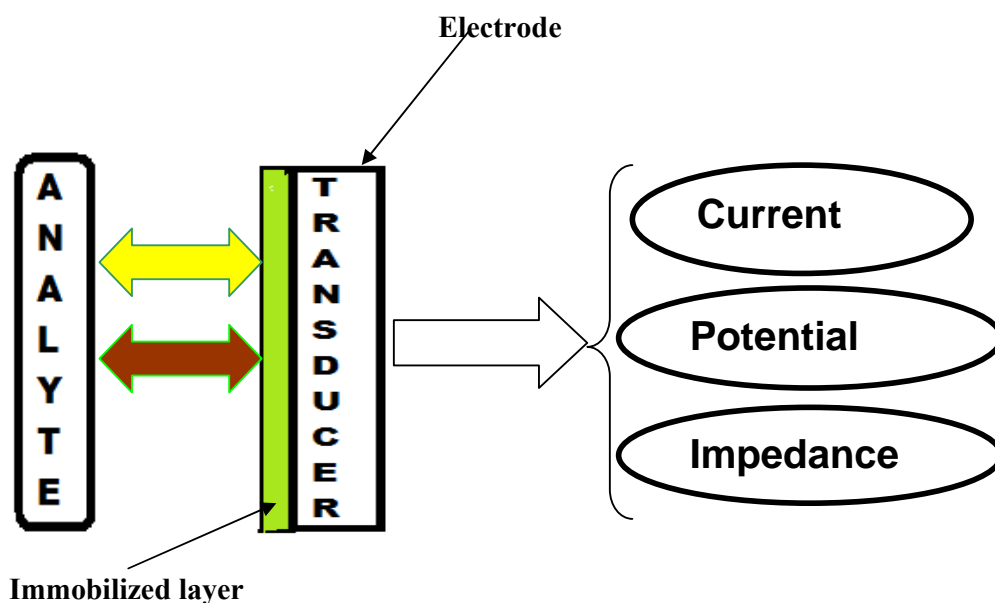
The field effect transistor (FET) is a solid-state device that exhibits high input impedance and low- output impedance hence capable of monitoring charge build up on the ion sensing membrane. Polymer matrix (electrode modifiers) of the potentiometric sensors can be altered by the immobilization of biological/biomedical materials leading to the development of potentiometric biosensors [107].

#### **2.4.1.2 Conductometric sensors.**

These are sensors that depend on changes of electric conductivity of a film or a bulk material whose conductivity is affected by the analyte present. Conductometric sensors are cheap, simple and no reference electrodes are needed. Analytes are determined based on the measurement of conductivity.

#### **2.4.1.3 Amperometric sensors.**

Amperometry is a method of electrochemical analysis in which the signal of interest is a current that is linearly dependent upon the concentration of the analyte. As certain chemical species are oxidized or reduced (redox reactions) at inert metal electrodes, electrons are transferred from the analyte to the working electrodes or to the analyte from the electrode. The direction of electron flow of electrons depends upon the properties of the analyte and can be controlled by the electric potential applied to the working electrode [108]. The basic instrumentation of these sensors requires controlled-potential equipment and the electrochemical cell consists of three – electrode cell; namely, working electrode, reference electrode and counter electrode. The working electrode is the electrode at which the reaction of interest occurs, the reference electrode provides a stable potential compared to the working electrode while an inert conducting material (e.g. platinum, graphite) is used as the counter electrode (auxiliary electrode). A supporting electrolyte is required in controlled-potential experiments to eliminate electro migration effects, decrease the resistance of the solution and maintain the ionic strength constant. The working principle of an electrochemical sensor is described below (scheme 5):



**Scheme 5: A schematic picture of an electrochemical sensor.**

The analyte molecules interact with the immobilized layer interface (e.g. polymers, nanoparticles, enzymes etc) in a lock and key mechanism to generate an electrical signal through the chosen transducer. The generated signal is amplified and monitored with an artificial intelligence such as computer hardware/software to produce measurable analytical signal. The signal can be in the form of current, potential or impedance. Furthermore, it is possible to change the properties of the sensor by changing parameters (e.g. sensing material or temperature) during manufacturing or operation of the sensor in order to improve selectivity and sensitivity. If the signal is in the form of current, the current can be measured at a fixed potential or potential difference across an electrochemical cell is scanned from one preset value to another and the cell current is recorded as a function of the applied potential. The rate of flow of electrons is proportional to the analyte concentration. The working electrode can be modified with different materials such as polymers, nanoparticles or composites of

polymers and nanoparticles etc to increase its sensitivity and reduce electrode fouling of reduced or oxidized species.

## **2.5 Characterization techniques.**

### **2.5.1 Electroanalytical techniques.**

Electrochemistry affords some of the most sensitive and informative analytical techniques in the chemists arsenal. Electroanalytical methods such as cyclic voltammetry, stripping voltammetry, differential pulse polarography, square wave and chronoamperometry complements other analytical techniques such as chromatography and spectroscopy and are not only capable of assaying trace concentrations of an electroactive analyte, but also supply useful information concerning its physical and chemical properties. Electrochemical methods of analysis include all methods of analysis that measure current, potential and resistance and relate them to analyte concentration. Quantities such as oxidation potentials, diffusion coefficients, electron transfer rates, and electron transfer numbers are readily obtained using electroanalytical methods, and are difficult to obtain using other techniques. Arguably, the most popular electroanalytical techniques are cyclic voltammetry and square wave. This section describes the basic components of the modern electroanalytical system, the principles of cyclic voltammetry and square wave voltammetry.

#### ***2.5.1.1 Basic components of an electroanalytical system.***

The basic components of a modern electroanalytical system for voltammetric measurements are a potentiostat, a computer, and the electrochemical cell. The role of

the potentiostat is to apply accurate and controlled potential and monitor the current produced. The electrochemical cell, where the electrochemical measurements are carried out, consists of a working (indicator) electrode, reference electrode, and counter (auxiliary) electrode. The working electrode is where the reaction or transfers of interest take place hence usually referred to as the indicator electrode. In this three-electrode system, voltage is carefully regulated between the working and reference electrodes, while the current passes between the working and the counter electrode. It is noteworthy that at no time does current pass through the reference electrode; this is ensured by the use of a potentiostat. The arrangement of the three electrodes in an electrochemical cell is presented in Figure 5 and described below:

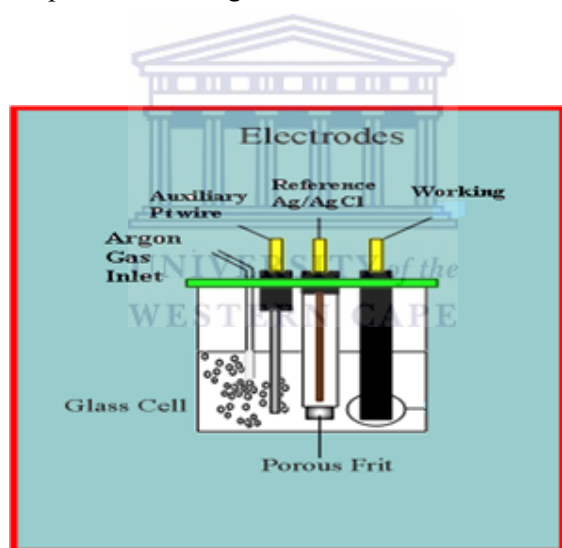


**Figure 5. Schematic representation of an electrochemical cell consisting of three electrodes.**

**Electrochemical cell and Reagents-** The arrangement of the electrodes within the cell is important. The reference electrode is placed close to the working electrode and located between the working and the auxiliary electrode. The cell material depends on the application, usually a glass beaker or a glass cell is used which has a close fitting



lid containing ports for electrodes and a purging line. If the reaction being investigated involves a potential sweep in the negative direction then the reduction of oxygen may interfere. To avoid this, the solution is deoxygenated, usually achieved by purging the solution with an inert gas such as nitrogen, argon or helium prior to analysis, and blanketing the solution with the gas during analysis. Electrolyte solutions are combinations of solvent and supporting electrolyte. The choice of the electrolyte solution depends on the application. In general, the solution must be conducting, chemically and electrochemically inert. It should not contribute to any chemical reactions and must not undergo any electrochemical reaction. The most common electrolyte solution is water with an added salt or buffer. In some studies usually organic electrode processes, the system may be non-aqueous. Acetonitrile or dimethyl sulphoxide (DMSO) are common organic solvents. Supporting electrolytes added to aid in conductivity include tetrabutylammonium hexafluorophosphate, tetrabutylammonium tetrafluorophosphate (TBAPF<sub>4</sub>), lithium perchlorate etc.

**Electrodes-** As with electrolyte solution, the cell geometry, and potential waveform applied and the choice of electrode depends on the application. The choice of the working or indicator electrode is of great importance. The shape of the electrode is important, in terms of its size or any modification to the surface. The common electrodes used are:

**i) Working electrode (indicator electrode)** - this is the electrode at which the redox of the analyte or the electrochemical phenomena investigated takes place. The commonly used materials for working electrodes include platinum, gold and glassy carbon. The ideal characteristics of an indicator electrode are a wide potential range, low resistance and a reproducible surface.

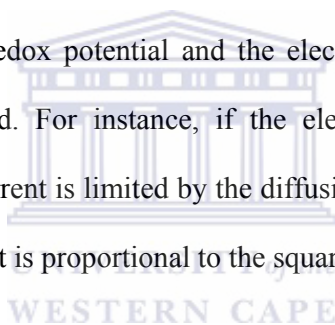
**ii) Reference electrode-** this is the electrode with a constant and a known potential. Its potential is taken as the reference, against which the potentials of the other electrodes are measured. The commonly used reference electrodes for aqueous solutions are the saturated calomel electrode (SCE) and silver/silver chloride (Ag/AgCl).

**iii) Counter electrode (auxiliary electrode)** - It acts as a sink for electrons so that current can be passed from the external circuit through the cell. Reactions occurring at the counter electrode surface are unimportant as long as it conducts current well. In most cases the counter electrode consists of a metallic foil or thin platinum wire, although gold and sometimes graphite may be used.

#### **2.5.1.2 Cyclic voltammetry (CV).**

Cyclic voltammetry is a widely used electroanalytical technique that uses microelectrodes and unstirred solution so that measured current is limited by the analyte diffusion at the electrode surface. It has wide applications in the study of redox processes, electrochemical properties of analytes in solution and for understanding reaction intermediates as well as for obtaining the stability of reaction products [109]. The technique works by varying some applied potential at a working electrode at some scan rate ( $\nu$ ) in both forward and reverse direction while monitoring the current. The resultant trace of current against potential is termed as a voltammogram. During cyclic voltammetry measurement, the potential is ramped from an initial potential,  $E_i$  to a more negative or positive potential but, at the end of the linear sweep, the direction of the potential scan is reversed, usually stopping at the initial potential,  $E_i$  (or it may commence an additional cycle) [110]. The potential is usually measured between the reference electrode and the working electrode and the

current is measured between the working electrode and the counter electrode (auxiliary electrode). This data is then plotted as current versus potential as shown in Figure 6. The forward scan produces a current peak for any analyte that can be reduced or oxidized depending on the initial scan direction over the range of potential scanned. The current increases as the current reaches the reduction potential of the analyte, but then decreases as the concentration of the analyte is depleted close to the electrode surface. If the redox couple is reversible, then reversing the applied potential makes it reach a potential that re-oxidizes the product formed in the first reduction reaction, thus producing a current of reverse polarity from the forward scan. The oxidation peak usually has the same shape as that of the reduction peak. As a result, the information about the redox potential and the electrochemical reaction rates of compounds can be obtained. For instance, if the electron transfer is fast at the electrode surface and the current is limited by the diffusion of species to the electrode surface, then the peak current is proportional to the square root of the scan rate ( $v^{1/2}$ ).



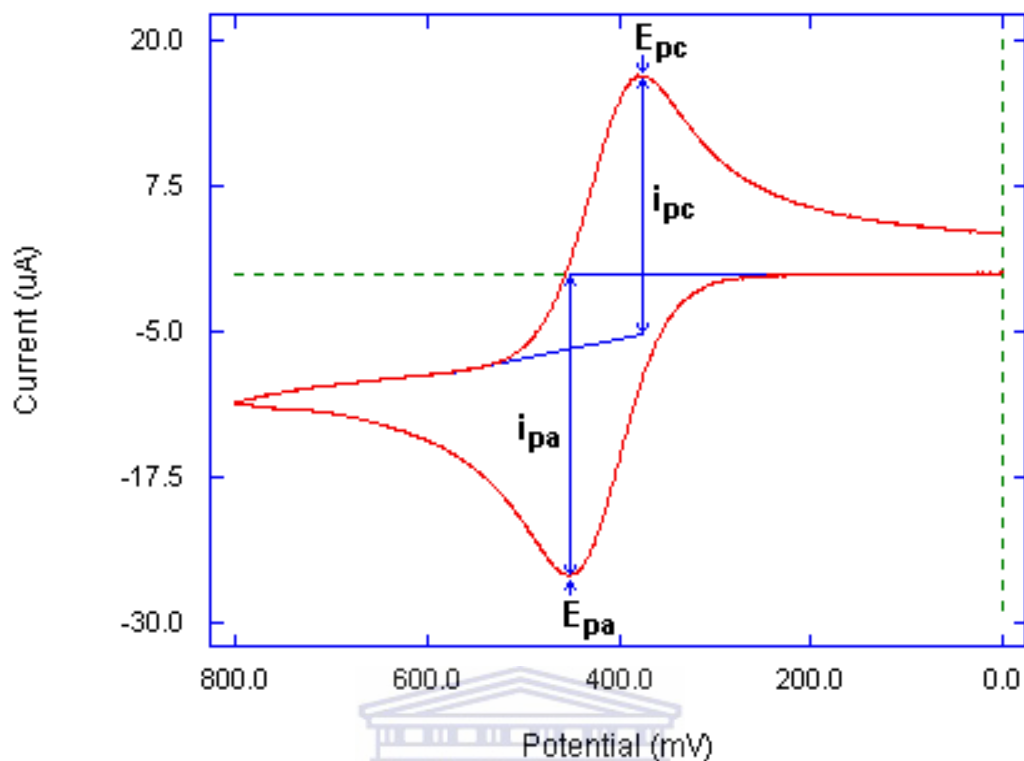


**Figure 6. A typical cyclic voltammogram**

Important parameters are usually obtained from cyclic voltammograms for analysis of redox properties of an electroactive sample. These parameters include peak potentials ( $E_{pc}$ ,  $E_{pa}$ ) and peak currents ( $I_{pc}$ ,  $I_{pa}$ ) of the cathodic and anodic peaks, respectively. Consequently, important information about the sample under investigation can be obtained from the above peak parameters. This includes whether the electrochemical process displayed by the sample is reversible, irreversible or quasi-reversible. It also gives an insight into how fast the electron process is, relative to other processes such as diffusion. For instance, if the electron transfer is fast relative to the diffusion of electroactive species from the bulk solution at the surface of the electrode, the reaction is said to be electrochemically reversible and the peak separation ( $\Delta E_p$ ) is given by equation 5 below;

$$\Delta E_p = |E_{pa} - E_{pc}| = 2.303 RT / nF \quad (5)$$

Where  $\Delta E_p$  is the peak separation (V),  $E_{pa}$  is the anodic peak potential (V),  $E_{pc}$  is the cathodic peak potential (V),  $n$  is the number of electrons,  $F$  is the Faraday constant (96 486 C mol<sup>-1</sup>),  $R$  is the gas constant (8.314 J mol<sup>-1</sup> K<sup>-1</sup>) and  $T$  is the absolute temperature of the system (298 K). The number of electrons ( $n$ ) involved in the electrochemical process can be estimated from the above equation. Thus, for a reversible redox reaction at 25 °C (298 K) with  $n$  electrons,  $\Delta E_p$  should be 0.0592/ $n$  V or about 60 mV for one electron. In practice, this value is difficult to attain because of cell resistance. Irreversibility due to a slow electron transfer rate results in  $\Delta E_p > 0.0592/n$  V, possibly, greater than 70 mV for a one-electron reaction [111]. The diagnostic tests for electro-reversibility are listed in Table 1.

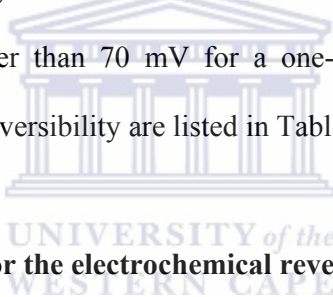


**Table 1: Diagnostic tests for the electrochemical reversibility of a redox couple, carried out by cyclic voltammetry.**

1.  $I_{pc} = I_{pa}$
2. The peak potentials,  $E_{pc}$  and  $E_{pa}$ , are independent of the scan rate ( $\nu$ )
3. The formal potential ( $E^{\circ}$ ) is positioned mid-way between  $E_{pc}$  and  $E_{pa}$ , so
 
$$E^{\circ} = (E_{pa} + E_{pc}) / 2.$$
4.  $I_p$  is proportional to  $\nu^{1/2}$
5. The separation between  $E_{pc}$  and  $E_{pa}$  is 59 mV/ $n$  for an  $n$ -electron couple (i.e.  $\Delta E_p = |E_{pa} - E_{pc}| = 0.0592/n$  V).

For reversible reaction, the concentration is related to peak current by the Randles-Sevcik equation (at 25 °C) [109-110].

$$I_p = 2.69 \times 10^5 n^{3/2} A D^{1/2} \nu^{1/2} C_0 \quad (6)$$

Where  $I_p$  is the peak current in amperes,  $\nu$  is the rate at which the potential is swept in  $V s^{-1}$ ,  $A$  is the electrode area ( $cm^2$ ),  $n$  is the number of electrons transferred,  $D$  is the diffusion coefficient ( $cm^2 s^{-1}$ ),  $p_a$  is peak anodic,  $p_c$  is the peak cathodic and  $C_0$  is the concentration in  $mol cm^{-3}$ . Several voltammograms performed at different scan rates can lead to preparation of several linear plots whose slopes could give further information about the redox properties of the sample in question. For, instance, when the peak current is plotted against the square root of the scan rate, the slope of the linear plot can be used to estimate the diffusion coefficient according to the Randles-Sevcik, equation (6) shown above. When plotted, the log of peak current versus the log of scan rate gives a linear plot whose slope distinguishes between diffusion controlled peaks, adsorption peaks or even a mixture of the two. A plot of the  $\log I_p$  versus  $\log \nu$  is linear, with a slope of 0.5 for diffusion peak and a slope of 1 for an adsorption peak. Intermediate values of the slope are sometimes observed, suggesting a “mixed” diffusion-adsorption peak [111].

In some cases, the sample to be characterized may be deposited on the surface of the electrode (chemically modified electrodes). In such cases, one can estimate the surface concentration of the adsorbed material by the use of the Brown-Anson equation model;

$$I_p = \frac{n^2 F^2 \Gamma^* A \nu}{4RT} \quad (7)$$

Where  $I_p$ ,  $n$ ,  $F$ ,  $A$ ,  $R$ ,  $v$  and  $T$  are explained in equations 5 and 6 and  $\Gamma^*$  is the surface concentration of the adsorbed species of the electrode modifier.

Although cyclic voltammetry is very widely used for the initial redox characterization of a molecule (i.e., the redox potentials, and the stability of the different oxidations state) and for qualitative investigation of chemical reactions that accompany electron transfer, there are a number of disadvantages inherent in this technique which includes:

- i) The effects of slow heterogeneous electron transfer and chemical reactions cannot be separated if both of these effects are present, then the rate constants for these processes can only be calculated using simulations methods.
- ii) There is a background charging current throughout the experiment of magnitude  $vC_{dl}$  (where  $C_{dl}$  is the capacitance of the interface at the working electrode). This restricts the detection limit to about  $10^{-5}$  M. In addition, the ratio of the peak faradaic current to the charging current decreases with increasing  $v$  ( $I_p$  is proportional to  $v^{1/2}$ ) [112].

In spite of these limitations, cyclic voltammetry is very suited for a wide range of applications and is one of the standard techniques used in characterization.

### **2.5.1.3 Square wave voltammetry (SWV).**

This technique involves the application of square wave modulation to a constant or nearly constant dc potential, and the current generated is sampled at the end of successive half cycles of the square wave. Three currents are generated i.e. forward current from the forward pulse ( $I_f$ ), the reverse current from the reverse pulse ( $I_r$ ) and that for the net current ( $I_d$ ) which are then plotted against the potential on the

corresponding staircase tread. The net current ( $I_d$ ) is obtained by the difference between the forward and the reverse current ( $I_f - I_r$ ) and is centered on the redox potential. The net current serves better analytical usage than the forward and reverse currents because it increases the discrimination against the charging current, since any residual charging current is subtracted out. Figure 7 shows the SWV containing the forward, reverse and net currents. The net current is larger than that of the forward and reverse current since it is the difference between them [113]. The peak height is directly proportional to the concentration of the electroactive species and detection limit as low as  $10^{-8}$  is possible.

SWV has many advantages over cyclic voltammetry such as much faster scan times (high scanning speed), excellent sensitivity, the rejection of background current, high signal to noise ratio and applicability to a wider range of electrode materials and systems [114-115]. Square wave voltammetry can play very important role in the characterization of electroactive species with poor, overlapping or ill-formed redox signals in cyclic voltammetry by producing individual sharp peaks [113]. It can also be applied in study of the electrode kinetics with regard to preceding, following or catalytic homogeneous chemical reactions and determination of some species at trace levels.



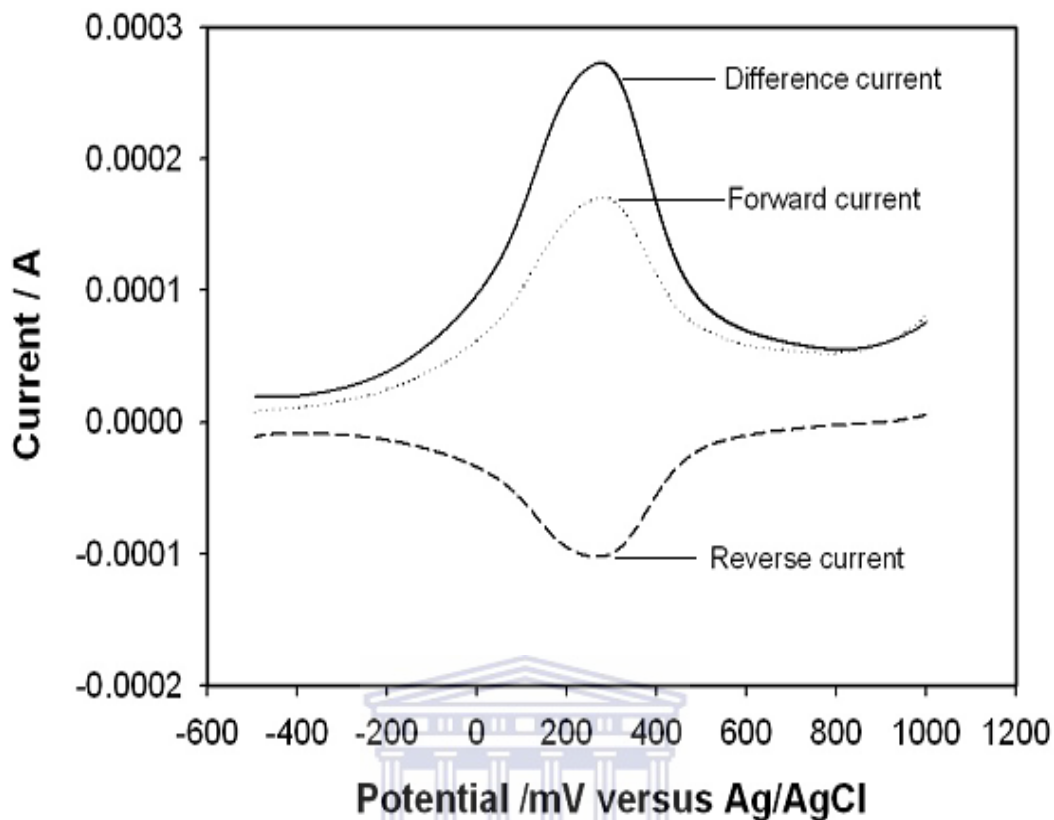


**Figure 7: A typical SWV containing the forward, reverse and difference currents.**

Consequently, the difference ( $I_d$ ) is larger than each individual component in the region of the peak that is centered on the half-wave potential because  $I_f$  and  $I_r$  have opposite signs. This difference effectively cancels the capacitive currents and thus higher scan rates are possible without background current interferences. This makes SWV a useful tool in kinetic study.

## 2.5.2 Spectroscopic techniques

### 2.5.2.1 *Electrochemical impedance spectroscopy (EIS).*

In cyclic voltammetry and other dynamic electroanalysis, an applied potential is either constant (potentiostatic) or changing (potentiodynamic) when ramped at a constant rate of  $v = dE/dt$  [110]. However, in impedance, a small perturbing potential is applied across a cell or sample and changes in a cyclic sinusoidal manner and generates a current resulting from the overpotential ( $\eta$ ) caused by the small displacement of the potential from the equilibrium value. Over a time scale, the averaged over potential is zero. Because the potential is only perturbing, it has the advantage of minimizing the concentration change after the experiment. The induced current alternates because the voltage changes in a cyclic manner, and hence the term alternating current (AC). The term impedance is therefore a measure of the ability of a circuit to resist the flow of an alternating current (AC) [115]. It is synonymous to resistance ( $R$ ) used in direct current (DC), which is defined by Ohm's law (equation 8) as the ratio between voltage ( $E$ ) and current ( $I$ ) [109-110].

$$R = \frac{E}{I} \quad (8)$$

EIS is an excellent, non-destructive, accurate and rapid insitu technique for examining processes occurring at the electrode surface. During a controlled-potential EIS experiment, the electrochemical cell is held at equilibrium at a fixed DC potential, and a small amplitude (5–10 mV) AC wave form is superimposed on the DC potential to generate a response from the equilibrium position. The response to the applied perturbation, which is generally sinusoidal, can differ in phase and amplitude from the

applied signal. This response is measured in terms of the AC impedance or the complex impedance,  $Z^*$  (overall or complete impedance), of the system, which permits analysis of electrode process in relation to diffusion, kinetics, double layer, coupled homogeneous reactions, etc [116]. The complex impedance ( $Z^*$ ) is made up of a resistive or real part  $Z'$ , attributable to resistors (in phase with the applied voltage), and a reactive or imaginary part  $Z''$ , attributable to the contributions of capacitors. This is related to the resistance ( $R$ ), reactance ( $X$ ) and capacitance ( $C$ ) by the equation:

$$Z^* = R - jX \quad (9)$$

where  $X = 1/\omega C$  and  $\omega = 2 \pi f$ .  $R$  is the resistance measured in Ohms ( $\Omega$ ),  $X$  is the reactance,  $C$  the capacitance measured in Farads ( $F$ ),  $\omega$  the applied angular frequency measured in  $\text{rad s}^{-1}$  and  $f$  is the frequency in Hertz (Hz) [109]. Notational representation of this in terms of  $Z'$  and  $Z''$  is given by:

$$Z^* = Z' - jZ'' \text{ where } j = \sqrt{-1} \quad (10)$$

Because  $Z^*$  is defined by the complex term,  $j$ , which determines the contribution of  $Z''$  to  $Z^*$ , the term complex impedance is often used. For a pure resistor that is not having any capacitance, its resistance when determined with a continuous current (DC) is  $R$  because its impedance is frequency independent,  $Z^* = Z' = R$ .

The experimental data collected from an impedance experiment is often presented as Nyquist plot of  $Z'$  (usually positive x-axis corresponds to the real impedance), versus

$Z''$  (usually, the positive y-axis correspond to  $-Z''$ ), over a wide frequency range (normally 100 kHz to 0.1 Hz). The Nyquist plot of impedance spectra includes a semicircle portion and a linear portion, with the former at higher frequencies corresponding to the electron transfer process and the latter at lower frequencies corresponding to the diffusion process. The electron transfer resistance ( $R_{ct}$ ) at the electrode surface is equal to the semicircle diameter, which can be used to describe the interface properties of the electrode [117].

Another way of presenting impedance data is a bode plot in which the logarithm of the absolute value of  $Z'$  and the phase ( $\phi$ ) are plotted against the logarithm of the frequency ( $f$ ) [118]. This can be plotted together or separately. Nyquist plots are more commonly displayed for historical reasons, the data is however often poorly resolved (particularly at high frequencies), and the explicit frequency dependence is not displayed in the plot. In contrast, the bode plot directly displays the frequency dependence; in addition, the data is well resolved at all frequencies, since a logarithmic frequency scale is used. When the frequency of the AC waveform is varied over a wide range of frequency (ca about  $10^{-4}$  and  $> 10^6$  Hz), the impedance obtained for the system is a function of the operating frequency. Spectra of the resulting impedance at different frequencies do reveal the different electrochemical kinetics involved in the system. While dipolar properties are manifest at the high frequency regions, bulk and surface properties will be evident at intermediate and low frequencies respectively [118]. The total impedance of a system is determined by the impedances of the various components of the electrochemical cell; for example, electron transfer kinetics, diffusion and passivating layers. The relative contribution of the various components typically varies with frequency; for example, electron transfer

kinetics may dominate at high frequencies, whereas diffusion may dominate at lower frequencies [118].

Measuring impedance over a wide frequency range allows processes with different time scales such as electron transfer, mass transport and chemical reaction to be detected within the same experiment. Impedance data is commonly analyzed by fitting it to an equivalent circuit model. The frequently used circuit, called the Randles equivalent circuit is composed of different elements such as resistors, capacitors, and inductors joined in series or in parallel. Figure 8 shows the impedance diagram for the real impedance (x-axis) and imaginary impedance (y-axis) with low frequency data being on the right side of the plot and higher frequencies are on the left [118].

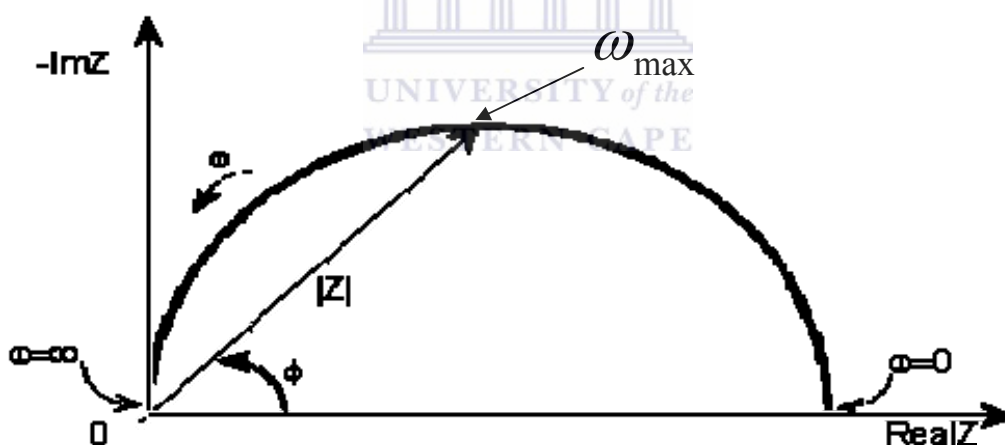


**Figure 8. A typical impedance diagram**

A typical Nyquist plot for the impedance data is shown in Figure 9. The semicircular shape is characteristic of a single "time constant".

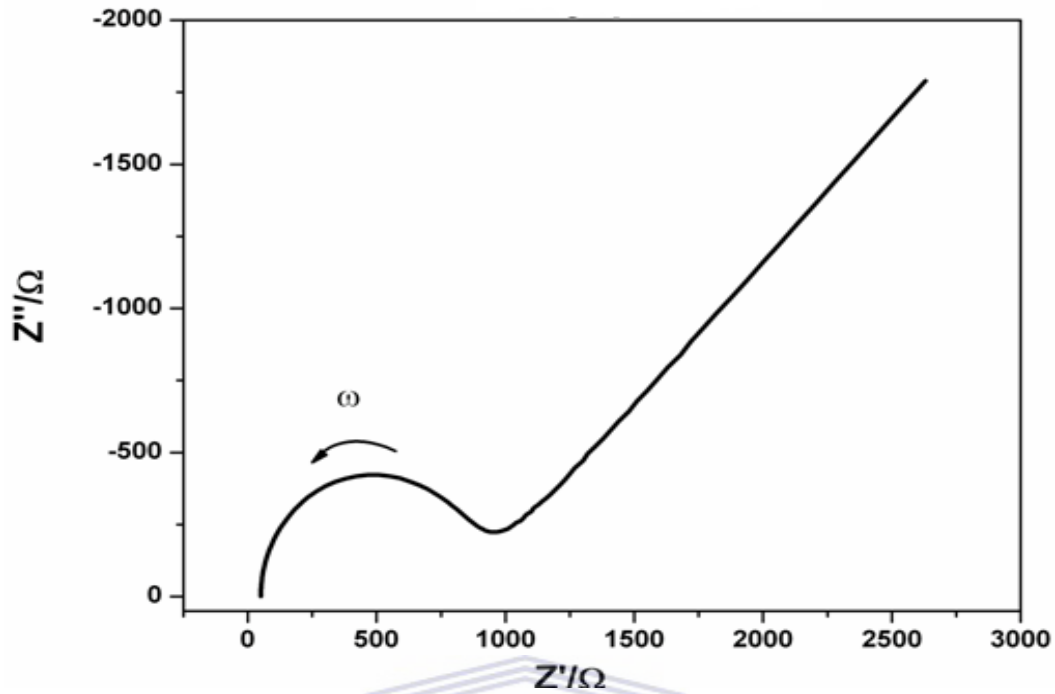


**Figure 9. A typical Nyquist plot.**

EIS is a useful tool in studying the kinetics of electrochemical reactions. Redox reactions usually involve charge transfer kinetics and mass transfer. The slower of these two determines the rate of the reaction. The mass transfer in EIS is limited to diffusion (concentration gradient) by the steady state condition. Figure 10 shows the Nyquist plot indicating the kinetically controlled (higher frequency) and the mass controlled (low frequency) parts of the plot.

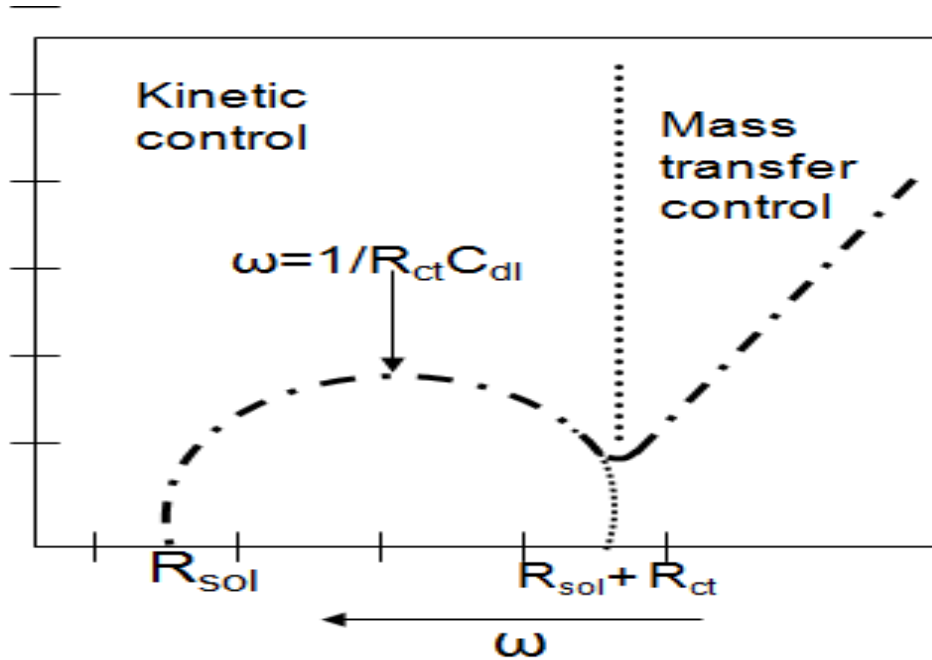


Figure 10. A typical Nyquist plot showing some kinetic parameters.

From  $\omega_{\max}$  (frequency at maximum imaginary impedance of the semicircle) useful kinetic parameters such as double layer capacitance ( $C_{dl}$ ), (obtained using equation 11), time constant (cycle life)  $\tau$ , (calculated using equation 12), exchange current  $I_0$ , (Calculated using equation 13) and heterogeneous rate constant  $K_{et}$  (calculated using equation 14) can be evaluated:

$$\omega_{\max} = \frac{1}{R_{ct} C_{dl}} \quad (11)$$

$$\tau = R_{ct} C_{dl} \quad (12)$$

$$I_0 = \frac{RT}{nFR_{ct}} \quad (13)$$

$$K_{et} = \frac{I_0}{nFAC_0} \quad (14)$$

where  $\omega_{\max} = 2 \pi f$ ,  $R_s$  is the solution resistance,  $R_{ct}$  is the charge transfer resistance,  $C_{dl}$  is the double layer capacitance,  $R$  is the gas constant ( $8.314 \text{ J K}^{-1} \text{ mol}^{-1}$ ),  $F$  is the Faradays constant ( $96\,486 \text{ C mol}^{-1}$ ),  $n$  is the number of electrons,  $\tau$  is the time constant or cycle life (relates to the time required for the proton to completely move across the electrolyte layer from one side to the other),  $I_0$  is the exchange current (relates to rate constant to electron transfer at zero overpotential),  $C_0$  is the concentration ( $\text{mol cm}^{-3}$ ) and  $k_{ct}$  is the heterogeneous rate constant.

A representative plot of frequency as x-axis versus logarithm of real impedance as  $y_1$ -axis, and phase angle as  $y_2$ -axis called bode plot is presented in Figure 11 and 12. Bode plot is a plot of log magnitude of impedance and phase angle versus log of frequency [115].

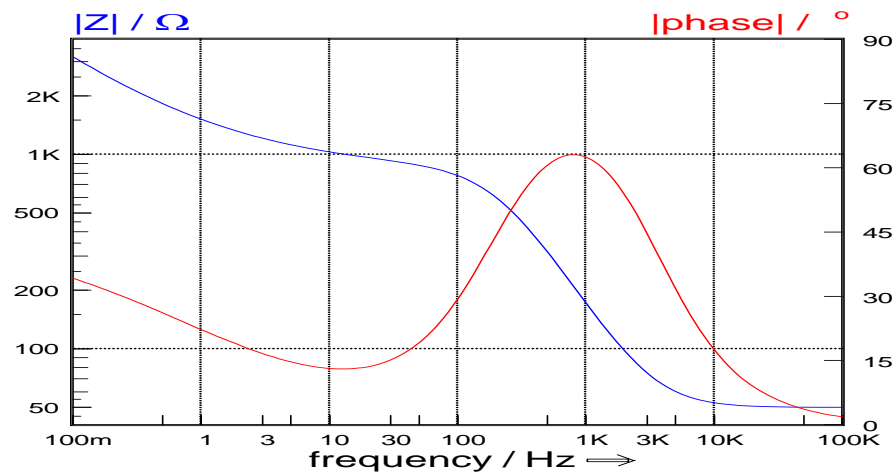


**Figure 11. A typical bode plot showing variation of impedance and phase angle with changes in frequency.**



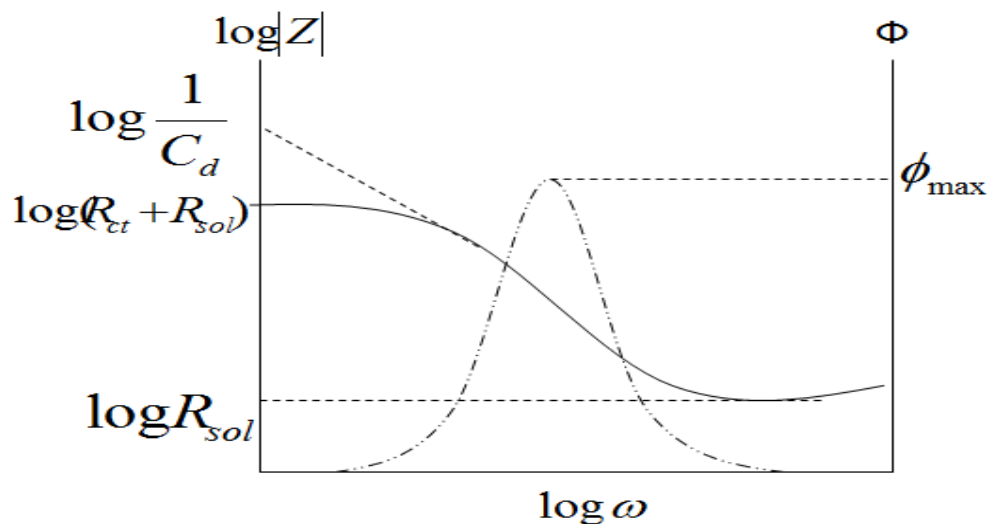


Figure 12. A bode plot showing some kinetic parameters.

The bode plot gives direct information on the frequency and phase angle. The frequency at maximum phase is a useful parameter in determining the double layer capacitance using equation 15:

$$\omega_{\phi_{\max}} = \frac{(1 + R_{ct} / R_{sol})}{R_{ct} C_{dl}} \quad (15)$$

The commonly used Randles equivalent circuit for fitting of the impedance data is shown in Figure 13.

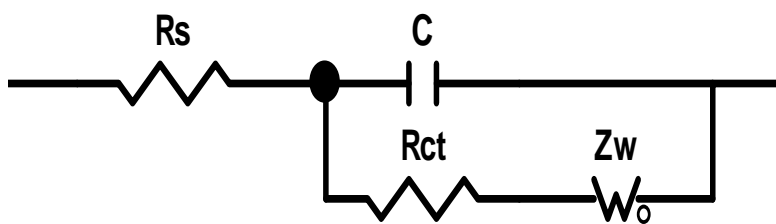


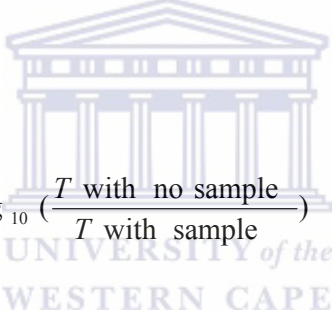
Figure 13. Randles equivalent circuit for a simple electrochemical cell.

$C$  is capacitance which is the ability of an electrochemical system to store or retain charge and  $Z_w$  is the Warburg impedance associated with the resistance as a result of the diffusion of ions across the electrode/electrolyte interface. Thus, EIS can give

useful information of the impedance changes on the electrode surface before and after modification.

### 2.5.2.2 *UV-visible spectroscopy*

It is a spectroscopic technique that involves the spectroscopy of photons in the UV-visible region. It uses light in the visible and adjacent (ultraviolet (UV) and near infrared (NIR) ranges). In UV-visible spectroscopy, one can monitor the colour of a material and current at the same time. The colour monitored is the wavelength at which the maximum of the absorption band (s) occurs,  $\lambda_{\max}$ , together with the absorbance at each of these wavelengths. The optical absorbance,  $Abs$ , is defined according to the equation:


$$Abs = \log_{10} \left( \frac{T \text{ with no sample}}{T \text{ with sample}} \right) \quad (16)$$

where  $T$  is the transmittance of light following its passage through the cell. Any changes in the absorbance relates to the amount of electroactive material as converted by the flow of current. The absorption spectrum tells us the nature of the material generated. It is a major technique that is used in the quantitative determination of solutions of transition metal ions and highly conjugated compounds. For example, if a material absorbs UV-visible light, then we can monitor its concentration using Beer-Lambert relationship;

$$Abs = \epsilon C_0 l \quad (17)$$

where the absorbance is determined at fixed wavelength  $\lambda$ ,  $\epsilon$  is the extinction coefficient (cited at the same value of  $\lambda$ ), and  $l$  is the optical pathlength. If the magnitude of the extinction coefficient at  $\lambda$  is known, then the amount of analyte ( $C_0$ ) can be quantified simply by determining the optical absorbance and inserting the values into equation (17).

Most of the analytical techniques are not particularly useful for telling us what ‘something’ is, but are excellent at telling us how much of that ‘something’ is present, or has been formed or has been changed. However, UV-visible spectroscopy is one of the best ways of identifying an analyte. This is because each specific analyte absorbs energy in the form of photons at different wavelengths [110]. Hence, one is able to identify a certain analyte by the application of UV-vis spectroscopy. It is a complementary technique to fluorescence spectroscopy in that it deals with transitions from the ground state to the excited state while fluorescence spectroscopy measures transitions from excited state to the ground state [119].

### ***2.5.2.3 Fluorescence spectroscopy.***

Fluorescence is the emission of visible light by a substance that has absorbed light of a different wavelength while spectroscopy is the study of the any measurement of a quantity as function of either wavelength or frequency. Thus, fluorescence spectroscopy can be defined as a type of electromagnetic spectroscopy which analyzes fluorescence from a sample. It involves using a beam of light, usually ultraviolet light that excites the electrons in molecules of certain compounds and causes them to emit light of a lower energy, typically, but not necessarily, visible light. Since molecules have various states called energy levels, fluorescence

spectroscopy is primarily concerned with electronic and vibrational states. The species being examined are first excited, by absorbing a photon, from its ground electronic state to one of the various vibrational states in the excited electronic state. Collisions with other molecules cause the excited molecule to lose vibrational energy until it reaches the lowest vibrational state of the excited electronic state. The molecules then drop down to one of the various vibrational levels of the ground electronic state again, emitting a photon in the process. As molecules drop down into any of the several vibrational levels in the ground state, the emitted photons will have different energies, and thus frequencies. Therefore, by analyzing the different frequencies of light emitted in fluorescence spectroscopy, along with their relative intensities, the structure of the different vibrational levels can be determined. It can be noted that, in a typical experiment, the different frequencies of fluorescent light emitted by a sample are measured, holding the excitation light at a constant wavelength. This is called an emission spectrum. The emission spectrum provides information for both qualitative and quantitative analysis. Fluorescence spectroscopy is an important investigational tool in many areas of analytical science, due to its extremely high sensitivity and selectivity [120].

### **2.5.3 Other techniques**

#### ***2.5.3.1 Transmission electron microscopy (TEM).***

Transmission electron microscopy (TEM) is a microscopic technique whereby a beam of electrons is transmitted through an ultra thin specimen, interacting with the specimen as it passes through. An image is formed from the interaction of the electrons transmitted through the specimen; the image is magnified and focused onto

an imaging device, such as a fluorescent screen on a layer of photographic film, or to be detected by a sensor such as a CCD camera. Transmission electron microscopes are capable of imaging at a significantly higher resolution than light microscopes, owing to the small de Broglie wavelength of electrons. This enables the instrument's user to examine fine detail-even as small as a single column of atoms, which is tens of thousands times smaller than the smallest resolvable object in a light microscope. TEM forms a major analysis method in a range of scientific fields, in both physical and biological sciences. TEMs find application in cancer research, virology, materials science as well as pollution and semiconductor research. Through the use of TEM, one can view the finest structures.



## CHAPTER 3

### 3.0 EXPERIMENTAL SECTION

#### 3.1 Introduction

This chapter describes the general experimental procedures for the chemical synthesis of Ag-Au alloy nanoparticles, characterization of the synthesized alloy nanoparticles; electrochemical synthesis and overoxidation of nanostructured polypyrrole. The fabrication of an electrochemical sensor based on Ag-Au alloy nanoparticles/overoxidized-polypyrrole composite and its application in the determination of selected polycyclic aromatic hydrocarbons (PAHs) will also be discussed.

#### 3.2 Reagents and materials

The reagents and materials used in this study included: Pyrrole (Py) (99%), Hydrogen tetrachloroaurate(III) trihydrate ( $\text{HAuCl}_4 \cdot 3\text{H}_2\text{O}$ ), trisodium citrate ( $\text{Na}_3\text{C}_6\text{H}_5\text{O}_7$ ) (99%), silver nitrate ( $\text{AgNO}_3$ ) (99%), anthracene (99%), phenanthrene (99%), pyrene (99%), Lithium perchlorate ( $\text{LiClO}_4$ ) (99.99%) and acetonitrile (HPLC grade). They were obtained from Sigma-Aldrich and were of analytical grade. Phosphate buffer solution (PBS), 0.1 M, pH 7.0 was prepared from anhydrous disodium hydrogen phosphate ( $\text{Na}_2\text{HPO}_4$ ) and sodium dihydrogen phosphate ( $\text{NaH}_2\text{PO}_4$ ). Deionized water (18.2 M $\Omega$ ) purified by a milli-Q<sup>TM</sup> system (Millipore) was used for aqueous solution preparations. Analytical grade argon (Afrox, South Africa) was used to degas the system. Pyrrole was purified twice by distillation under the protection of high purity nitrogen and then kept in a refrigerator when not in use.

### 3.3 Instrumentation.

All electrochemical experiments were carried out using a BAS 50B electrochemical analyzer from Bioanalytical systems inc. (West Lafayette, IN) with conventional three- electrode system consisting of glassy carbon electrode (GCE) as the working electrode ( $A = 0.071 \text{ cm}^2$ ), platinum wire as the auxiliary electrode and Ag/AgCl (3 M NaCl) as the reference electrode. All experimental solutions were purged with high purity argon gas and blanketed with argon atmosphere during measurements. The experiments were carried out at controlled room temperature ( $25 \text{ }^\circ\text{C}$ ). UV-Vis spectra measurements were recorded over a range of 350-700 nm using  $3 \text{ cm}^3$  quartz cuvettes with Nicolette Evolution 100 Spectrometer (Thermo Electron Corporation, UK). Transmission electron microscopy (TEM) images were acquired using a Tecnai G<sup>2</sup> F<sub>2</sub>O X-Twin MAT. TEM characterizations were performed by placing a drop of the solution on a carbon coated copper grid and dried under electric bulb for 30 min. Fluorescence spectra measurements were obtained by the use of the NanoLog<sup>TM</sup> HORIBA JOBINYVON machine. Electrochemical impedance spectra (EIS) measurements were performed using VoltaLab PGL 402 from Radiometer Analytical (Lyon , France) in a solution containing 0.1 M KCl and  $\text{Fe}(\text{CN})_6^{3-/4-}$  and plotted in the form of complex plane diagrams (Nyquist plots) with a frequency range of 100 KHz to 0.1 Hz. The amplitude of the applied sine wave potential was 10 mV, whereas the ambient applied dc potential was set at the formal potential (184 mV) which was obtained from the CV experiment of the  $[\text{Fe}(\text{CN})_6]^{3-/4-}$  redox probe. Alumina micro powder and polishing pads were obtained from Buehler, IL, USA and were used for polishing the GCE.

### 3.4 Preparation of silver, gold and silver-gold alloy nanoparticles.

Silver nanoparticles (AgNPs) were synthesized by the reduction of AgNO<sub>3</sub> with trisodium citrate according to procedures described by Fang *et al.* [121] and Asta *et al.* [122]. Briefly, 50 mL of 1.0 mM AgNO<sub>3</sub> solution was heated to boiling in an Erlenmeyer flask. To this solution, 5 mL of 1% C<sub>6</sub>H<sub>5</sub>O<sub>7</sub>Na<sub>3</sub> was added dropwise (0.5 g of C<sub>6</sub>H<sub>5</sub>O<sub>7</sub>Na<sub>3</sub> was dissolved in 50 mL of distilled water in order to prepare 1% C<sub>6</sub>H<sub>5</sub>O<sub>7</sub>Na<sub>3</sub> solution). During the process, the solution was mixed vigorously by the use of a magnetic stirrer. The solution was heated until a pale yellow colour was observed. It was then removed from the heating surface and stirred until it cooled to room temperature. The mechanism of the reaction can be expressed as follows; [122].



Gold nanoparticles (AuNPs) were prepared through the reduction of 1.0 mM HAuCl<sub>4</sub> using sodium citrate as the reducing agent. 20 mL of 1.0 mM HAuCl<sub>4</sub> solution was added to a 50 mL Erlenmeyer flask on a stirring hot plate. A magnetic stirrer was added into the solution and the solution heated to boil. To the boiling solution, 2 mL of 1% solution of sodium citrate, (C<sub>6</sub>H<sub>5</sub>O<sub>7</sub>Na<sub>3</sub>) was added. Gold sol gradually formed as the citrate reduced Au<sup>3+</sup> to Au<sup>0</sup>. The solution was heated until a deep red colour was observed [123].

Silver-gold alloy nanoparticles (Ag-AuNPs) were synthesized via a previously reported procedure [102]. 49 mL of water was added into a 100 mL round bottomed flask. 0.5 mL 2% (w/v) sodium citrate was added into the flask of water and the



reaction mixture heated to 92 °C. 0.5 mL of a mixture of 10 mM H<sub>2</sub>AuCl<sub>4</sub> and 10 mM AgNO<sub>3</sub> solution was added into the reaction mixture and the temperature regulated between 90 °C and 92 °C and refluxed for 1 hour. The volume of the mixture was adjusted so as to prepare Ag-Au nanoparticles with Ag/Au ratio of 1:3 by mixing 0.125 mL of 10 mM AgNO<sub>3</sub> and 0.375 mL of 10 mM H<sub>2</sub>AuCl<sub>4</sub>. After refluxing the mixture at temperature between 90 °C and 92 °C for 1 hour, a colour change was observed in the solution (dark red) indicating the formation of nanoparticles according to the hallmarks reported in the literature [124].

### **3.5 Preparation of glassy carbon electrode (GCE) with nanoparticles.**

For the preparation of electrodes for electrochemical measurements, GCE was polished repeatedly with 1.0, 0.3, and 0.05 μm alumina slurries respectively and then rinsed thoroughly with distilled water followed by sonication in ethanol and water respectively. 4 μL solutions of already synthesized Ag-Au (1:3) alloy nanoparticles were drop-coated onto the surface of a thoroughly polished GCE and left to dry at room temperature and it is henceforth denoted as Ag-AuNPs/GCE. Ag-modified and Au-modified electrodes were as well prepared by drop-evaporation over the bare GCE, and each henceforth denoted as AgNPs/GCE and AuNPs/GCE, respectively.

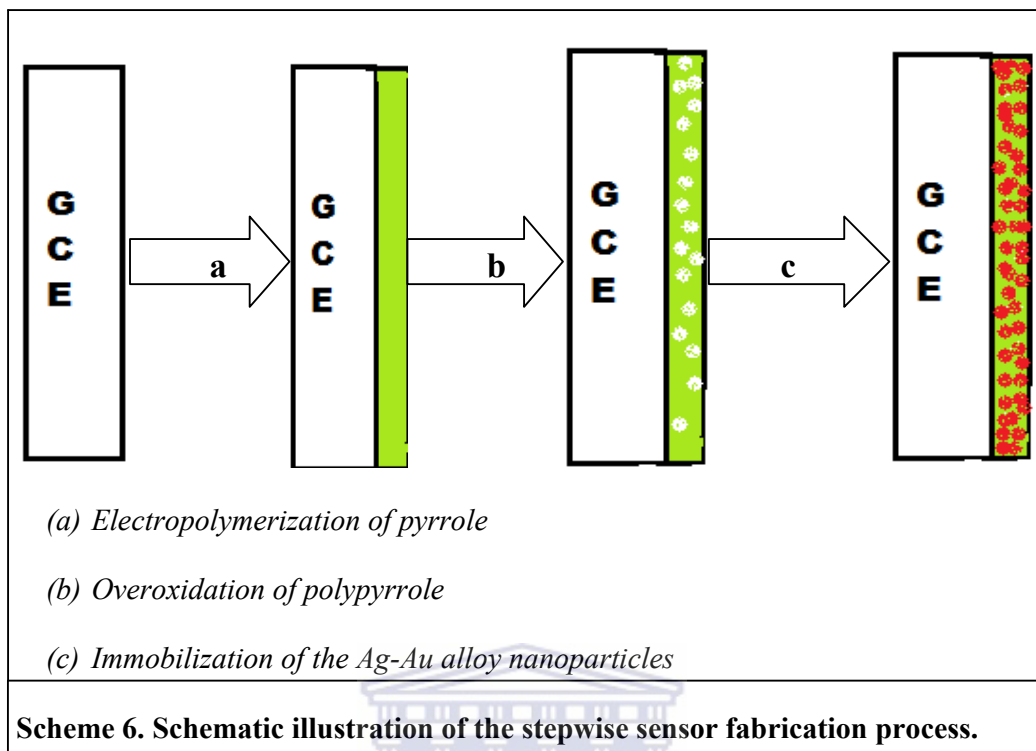
### **3.6 Preparation of overoxidized-polypyrrole polymer on GCE (PPyox/GCE).**

Prior to modification, the bare GCE was polished to a mirror finish as described in 3.5. Electrochemical polymerization of pyrrole was carried out in 0.1 M LiClO<sub>4</sub> solution containing 0.1 M pyrrole by cycling the potential from -400 to 700 mV at a scan rate of 50 mV s<sup>-1</sup> for 10 cycles. Before applying potential to the above polymerization solution, the solution was degassed by bubbling argon gas through for

15 min and then maintained oxygen free by keeping a blanket of argon above the solution. It is during this electropolymerization process that polypyrrole polymer was electrodeposited on the surface of the electrode. The electrode was then removed from the solution and rinsed with water to remove any traces of monomers. This modified electrode was denoted as PPy/GCE. The polypyrrole modified electrode (PPy/GCE) was then transferred into 0.1 M NaOH solution for potentiometric electrochemical overoxidation of the conductive polypyrrole film at +1.0 V for 420 s. The obtained modified electrode was thoroughly rinsed with de-ionized water and was denoted as PPyox/GCE which was kept in readiness for either characterization or immobilization of the nanoparticles.

### **3.7. Fabrication of overoxidized-polypyrrole/Ag-AuNPs composite (PPyox/Ag-AuNPs).**

In order to incorporate the intermetallic nanoparticles, 4  $\mu$ L solution of already synthesized Ag-Au alloy nanoparticles were drop-coated on the PPyox/GCE and allowed to dry at room temperature. The modified electrode was taken out and rinsed with water, and henceforth denoted as PPyox/Ag-AuNPs/GCE. The PPyox/Ag-AuNPs/GCE was ready for use as an electrochemical sensor for the detection of anthracene, phenanthrene and pyrene. In this work, the PPyox/Ag-AuNPs/GCE will thus be referred to as an electrochemical sensor. A schematic illustration of the stepwise electrochemical sensor fabrication process is shown below in scheme 6.



### 3.8 Electrochemical characterization.

UNIVERSITY of the  
WESTERN CAPE

#### 3.8.1 Characterization of the nanoparticles.

A three electrode system was used for electrochemical characterization of the synthesized nanoparticles. GCE modified with nanoparticles was used as the working electrode, platinum wire as the auxiliary electrode and Ag/AgCl (3 M NaCl) as the reference electrode. The characterization solutions used contained 3 mL of 0.1 M LiClO<sub>4</sub> and 3 mL of 0.1 M phosphate buffer pH 7 which were added into an electrochemical cell and degassed for about 5 min using argon gas. Cyclic voltammogram (CV) of Ag-AuNPs/GCE in the above solutions was achieved by scanning between -0.6 V and +1.0 V at a scan rate of 50 mV s<sup>-1</sup> as well as at different

scan rates: 20, 40, 60, 80 and 100 mV s<sup>-1</sup>. For control experiments, AgNPs/GCE and AuNPs/GCE were also characterized using the same procedure.

### **3.8.2 Characterization of polypyrrole (PPy).**

In order to investigate the electrochemistry of the prepared polypyrrole, a three electrode system was used for electrochemical characterization as described in 3.8.1 with PPy/GCE as the working electrode. The characterization of the polypyrrole was done in 0.1 M LiClO<sub>4</sub> by cathodic scanning from 500 mV to -1000 mV at different scan rates. Consequently, it was also necessary to confirm whether the synthesized polypyrrole was overoxidized before overoxidizing it in 0.1 M NaOH. This was done by testing the electrical conductivity of the polypyrrole. This was investigated by characterizing the polymer in 5 mM K<sub>3</sub>Fe(CN)<sub>6</sub> redox probe by potential scanning from +600 mV to -200 mV at a scan rate of 50 mV s<sup>-1</sup>.



### **3.8.3 Characterization of PPyox/GCE and PPyox/Ag-AuNPs/GCE.**

The catalytic properties of the Ag-Au alloy nanoparticles deposited on the PPyox/GCE were studied by performing an electrochemical characterization using cyclic voltammetry. A three electrode system was used for the electrochemical characterization of PPyox/GCE and PPyox/Ag-AuNPs/GCE as described in 3.8.1 using PPyox/GCE and PPyox/Ag-AuNPs/GCE as the working electrodes, respectively. This was investigated in 5 mM K<sub>3</sub>Fe(CN)<sub>6</sub> redox probe as described in 3.8.2.

### **3.9 Electrochemical sensor measurements.**

#### **3.9.1 Choice of suitable solvent and supporting electrolyte.**

Most PAHs are insoluble in water hence a suitable organic solvent is necessary to completely dissolve them. The choice of solvents is determined by several factors, including conductance, solubility of electrolyte and electroactive substance and the reactivity with electrolytic products. In Fry and Britton's handy review of solvents and electrolytes [125], acetonitrile, ethanol, methanol, and methylene chloride are recommended as good oxidative (anodic) electrochemical solvents, while dimethylformamide (DMF) and dimethyl sulfoxide (DMSO) are suggested for reductive (cathodic) electrochemistry. Acetonitrile ( $\text{CH}_3\text{CN}$ ) was chosen as a suitable solvent since it was found to dissolve most of the PAHs and has been reported to have a relatively high dielectric constant, has the ability to dissolve electrolytes, its relatively non-toxic and portrays good electrochemical properties. Since, acetonitrile is a non-aqueous electrolyte, a suitable supporting electrolyte was necessary to enhance conductivity, minimize double-layer and migration currents. Lithium perchlorate ( $\text{LiClO}_4$ ) was chosen as the supporting electrolyte based on its solubility in acetonitrile and its inertness towards the electroactive species (PAHs). However, most PAHs are found in waste water hence the need to introduce water in the acetonitrile. In this work, water was introduced in to the acetonitrile by preparing a solution of acetonitrile and water in the ratio 80:20 (acetonitrile: water). This mixture of acetonitrile and water was used as the solvent in all sensor applications and will thus be referred to as acetonitrile.

### 3.9.2 Preparation and analysis of the PAHs.

5 mM of standard solutions of anthracene, phenanthrene and pyrene were prepared as follows: 0.022 g, 0.022 g and 0.025 g of anthracene, phenanthrene and pyrene were dissolved each in about 15 cm<sup>3</sup> of acetonitrile (to achieve solubility), respectively, and later made up to 25cm<sup>3</sup> solutions in distilled water with continuous stirring for about 30 min. The solutions were kept in brown bottles. From these stock solutions, aliquots (in  $\mu\text{L}$ ) were drawn and added to the cell and used for sensor development. The cell for electrocatalytic oxidation of the PAHs consisted of the PPyox/Ag-Au nanoparticles modified glassy carbon electrode (working electrode), platinum counter electrode and Ag/AgCl (3 M NaCl) reference electrode. A 3 mL test solution consisting of acetonitrile (acetonitrile: water = 80:20) and 0.1 M LiClO<sub>4</sub> was degassed with argon for about 10 min before the experiment. A blanket of argon was kept during the experiment to maintain an oxygen free solution. Both cyclic voltammetry and square wave voltammetry were used for the characterization of the modified electrode and the determination of the electrode response to the monitored PAHs. The potential at which anthracene was oxidized was also determined for further steady state amperometric measurements. For the steady state measurements of anthracene, a constant potential of +1181 mV was used which was obtained from CV measurements. The amperometric measurements were achieved as follows: The degassed acetonitrile and 0.1 M LiClO<sub>4</sub> solution was excited at a constant potential of +1181 mV and the current was initially allowed to attain a steady state. The first 3.0  $\mu\text{M}$  of anthracene was then injected into the cell. The increase in the catalytic current was then monitored and allowed to attain steady state, then followed by another addition of 3.0  $\mu\text{M}$  anthracene. This was repeated until no further increase in catalytic current was observed after addition of anthracene. The solution was kept oxygen free

by use of argon gas and was constantly stirred at 300 rotations per min (300 rpm) using a magnetic stirrer. After each sensor experiment, the electrode was washed in de-ionized water and kept in 0.1 M LiClO<sub>4</sub> for successive measurements in order to establish the lifetime of the sensor.

### **3.9.3 Interferences studies.**

Several substances suspected to interfere with the detection of PAHs were investigated by the developed electrochemical sensor. These substances include inorganic substances such as Na<sup>+</sup>, Cu<sup>2+</sup>, Fe<sup>2+</sup>, Mn<sup>2+</sup>, Cl<sup>-</sup>, SO<sub>4</sub><sup>2-</sup>, NO<sub>3</sub><sup>-</sup> and NO<sub>2</sub><sup>-</sup> [126]. Solutions containing 0.1 M of each of these substances were prepared. A mixture of these solutions was prepared and mixed with a similar concentration of the PAH at a ratio of 1:1. SWV measurements were carried out on the resulting mixtures. The catalytic current emanating from the mixture solution of interferences and the PAHs was compared to that of a similar concentration of standard PAHs alone. Expressed as a ratio of  $I(\text{PAH} + \text{suspected interference}) / I(\text{PAH})$  and converted into percentage, the value obtained was used to assess the level of possible interference by the investigated substances.

## CHAPTER 4

### 4.0 RESULTS AND DISCUSSION 1

#### 4.1 Characterization of Ag-AuNPs.

##### 4.1.1 UV-visible spectroscopy.

The formation of silver-gold alloy nanoparticles (Ag:Au = 1:3) by simultaneous reduction of gold and silver ions was confirmed by the use of UV-visible spectroscopy. Figure 14 shows the visible absorption spectra of silver, gold, silver-gold bimetallic alloy nanoparticles and a mixture of silver and gold nanoparticles. Absorption maximum for silver nanoparticles (**curve a**) and gold nanoparticles (**curve c**) were observed at 415 nm and 525 nm, respectively. The Ag-Au bimetallic alloy nanoparticles showed an absorption peak at 504 nm (**curve b**). The appearance of single absorption peaks at 504 nm which was between 525 nm and 400 nm shows that Ag-Au alloy nanoparticles were formed [102, 127].



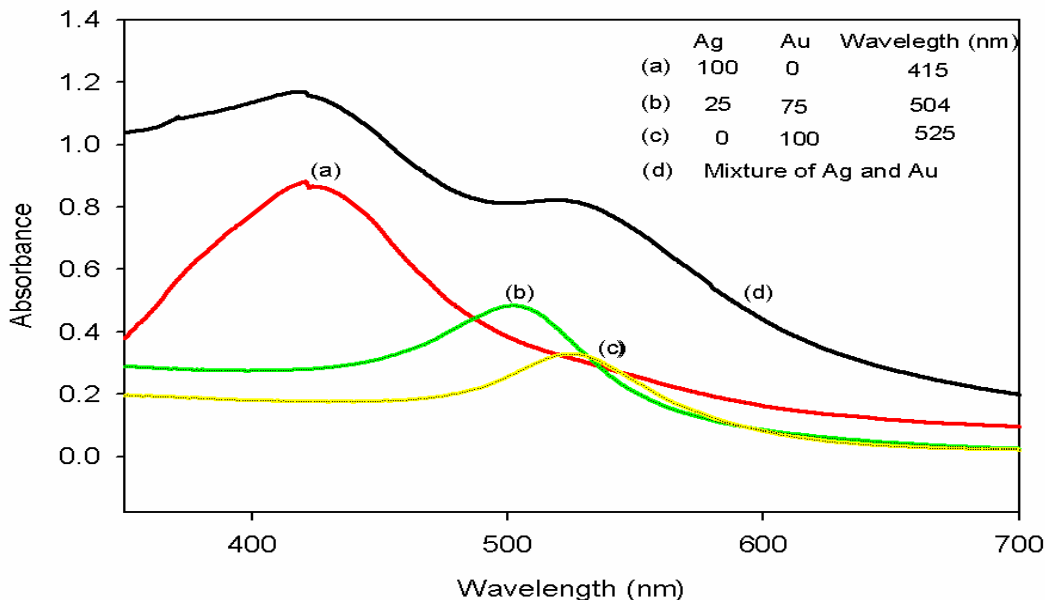


**Figure 14. UV-visible absorption spectra of Ag (curve a), Au (curve c), Ag-Au (1:3) alloy nanoparticles (curve b) and a mixture of pure Ag and Au nanoparticles (curve d).**

When pure gold and silver nanoparticles were mixed physically, two absorption peaks were observed (**curve d**) corresponding to the individual metal nanoparticles. However, only one absorption peak was observed (**curve b**) for the solution of the bimetallic alloy nanoparticles. This is a confirmation that the synthesized nanoparticles were alloys and not mixture of elemental nano-particles as described by Pal *et al.* [128]. The formation of core-shell bimetallic nanoparticles was ruled out since core-shell nanoparticles exhibit two absorption peaks whose relative intensities depend on the thickness of the shell [124]. The alloy formation can be attributed to similar lattice constants of 0.408 and 0.409 nm, respectively, for gold and silver. This small difference in lattice constants being smaller than the amplitude of thermal vibrations of atoms has already been hypothesized to favor alloy formation even at the nanometer scale [129].

A second set of spectroscopic experiment was carried out to establish that the nanoparticles were well stable on storing at room temperature for a long time. Figure 15 shows the visible spectra of solution containing Ag (curve a), Au (curve c) and Ag-Au (1:3) alloy nanoparticles (curve b) after storage for 4 months at 25 °C. The above nanoparticles stored in an air –sealed bottle at a temperature of 25 °C were found to be very stable, since no apparent change was observed by UV-visible absorption spectra even after about 4 months.

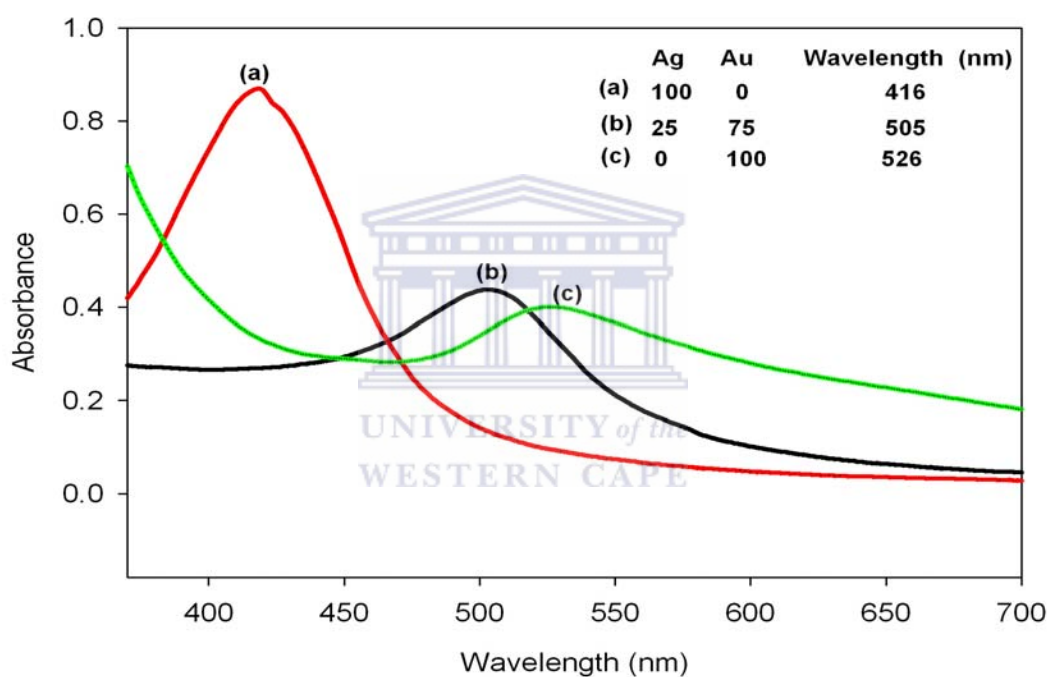


**Figure 15. UV-visible absorption spectra of Ag (curve a), Au (curve c) and Ag-Au (1:3) alloy nanoparticles (curve b) after 4 months storage at 25 °C.**

A plot of wavelength against mole fraction of one of the monometallic nanoparticles in the alloy at increasing concentration is ideally known to obey a linear fashion. However, core-shell nanoparticles do not show such a relationship [127]. To confirm this, Ag-Au alloy nanoparticles with different molar ratios were thus synthesized. Figure 16 shows UV-visible spectra of the Ag-Au alloy nanoparticles with different

molar ratio of Ag and Au (Ag/Au ratio, 1:0, 3:1, 1:1, 1:3, 1:9, 0:1). The monometallic Ag and Au nanoparticles showed one characteristic peak at 415 nm (Figure 16 curve a) and 525 (Figure 16 curve f), respectively, both consistent with previous results [102]. A change in wavelength was observed with increasing amount of gold content in the alloy. All the single absorption peaks for the alloy nanoparticles were located at intermediate wavelengths between the absorption peaks of Ag nanoparticles and Au nanoparticles showing that Ag-Au alloy nanoparticles were formed.

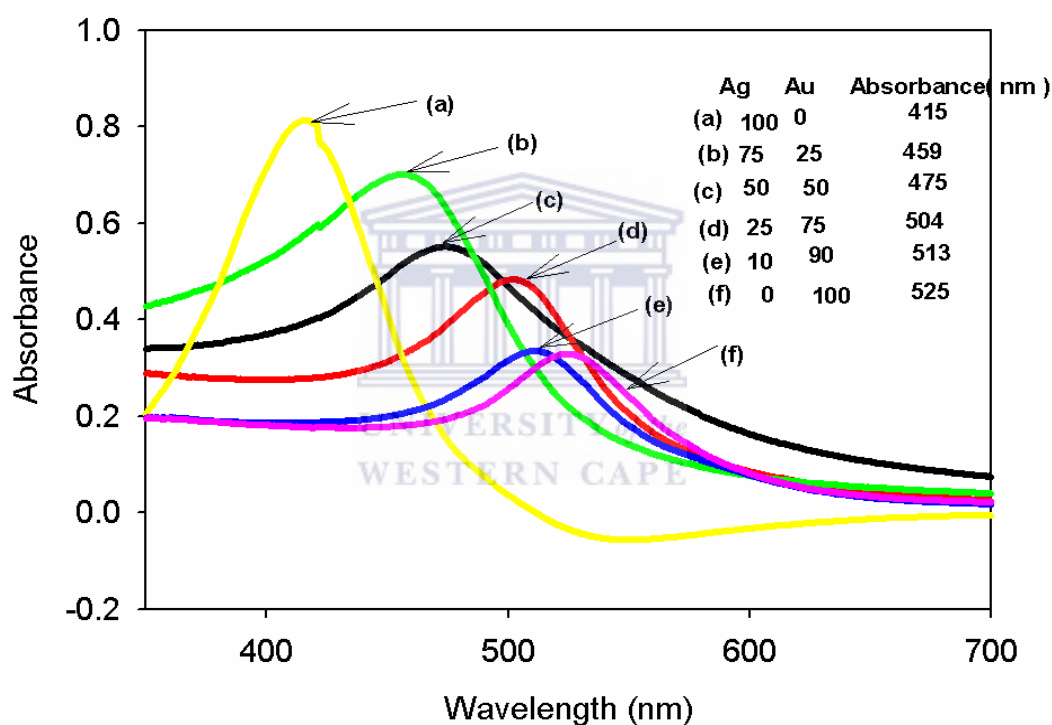


**Figure 16. UV-visible absorption spectra of Ag-Au alloy nanoparticles with various molar ratios of Ag and Au.**

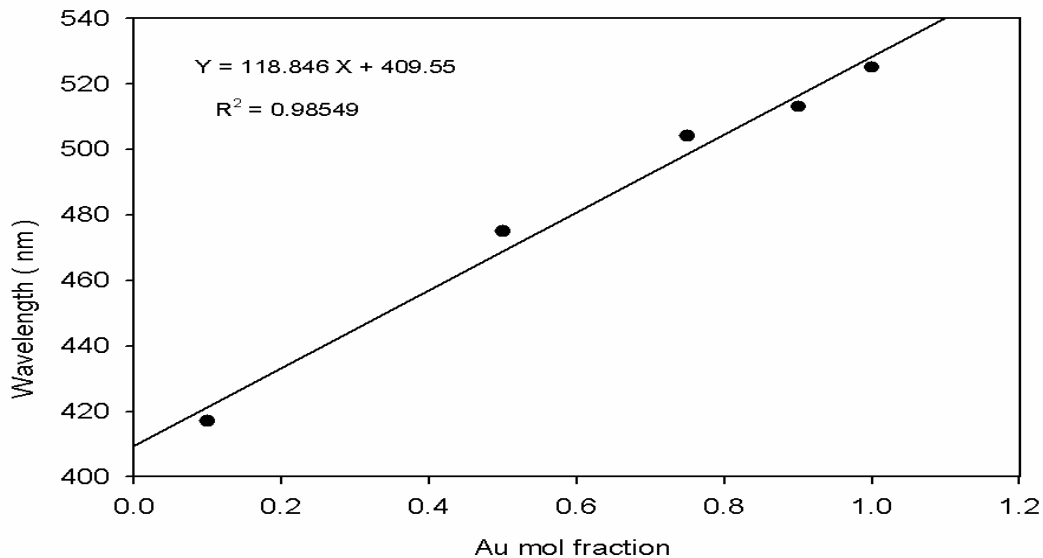


**Figure 17. A plot of the wavelength corresponding to the maximum absorbance for varying mole fractions of Ag-Au alloy nanoparticles.**

In Figure 17, it is observed that there is a linear relationship between the absorption peak position ( $\lambda$  max) values and the Au-mole ratio. According to Raveendran *et al.*, and the Murray's report [130], this linear relationship is attributed to the formation of homogeneous alloy nanoparticles rather than core-shell. It has also been supported by Jian Zhu using the Drude model and quasi-static theory [127].

The optical properties of these alloy nanoparticles vary with their composition, which is seen from the digital photographs in Figure 18. The colour of the colloidal solution changes from yellow to deep red with increasing gold content which could be visually detected as a progressive change in the colour.

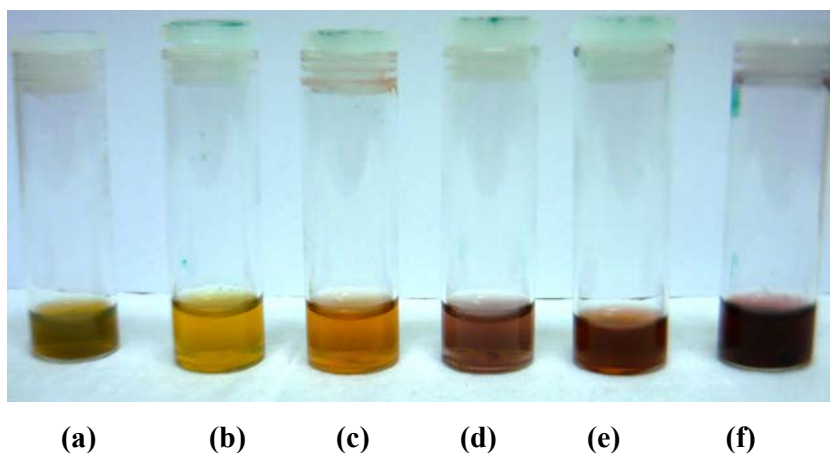


**Figure 18. Digital photographs of Au, Ag and Ag-Au alloy (Au mole fraction: (a) 0, (b) 0.1, (c) 0.5, (d) 0.75, (e) 0.9 and (f) 1) nanoparticles.**

#### **4.1.2 Fluorescence properties of Ag-AuNPs.**

The characteristic fluorescence property of silver-gold bimetallic alloy nanoparticles was observed by measuring fluorescence emission spectra as shown in Figure 19. The emission spectrum (fluorescence band) for pure Au nanoparticles was observed at 606 nm when excitation was carried out at 525 nm (**curve d**) while Ag-Au (1:3) bimetallic alloy nanoparticles showed a fluorescence band at 562 nm when excitation was carried out at 504 nm (**curve b**). The concentration of the gold content and silver content in the alloy composition was varied and the spectra were recorded for each case (see Figure 19) which correlates well with previous reports [102]. It is worth noting that with silver content above 50% in the alloy, we were not able to observe any emission spectra even after exciting the alloy at their respective  $\lambda_{\max}$  values.

The fluorescence properties of silver and gold nanoparticles have been attributed to electronic transitions between the highest valence d-band and conductance sp-band. [131]. The d-band electrons of the noble metal nanoparticles absorb the incident

photon energy and promote to higher electronic states in the sp-band. The electron-hole pair recombines non-radioactively through electron-photon scattering process but then may combine radioactively giving rise to the observed fluorescence [128]. So, as the Au content in the alloy increases, the energy gap between valence and conduction band decreases and as a result, the emission peaks of the alloy nanoparticles showed an increase in wavelength [102]. Thus, the Ag-Au bimetallic alloys were confirmed to have been formed.

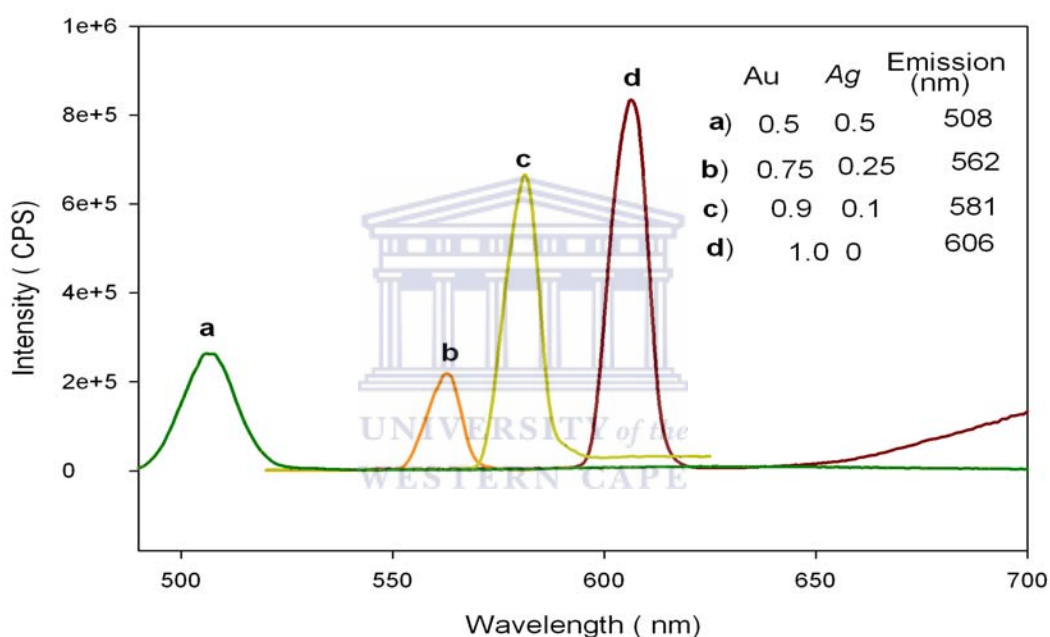


**Figure 19. Emission spectra of Au and Ag-Au alloy (Au mole fraction: (a) 0.5, (b) 0.75, (c) 0.9 and (d) 1) nanoparticles with varying Au mole fraction.**

#### **4.1.3 Transmission electron microscopy (TEM).**

In the present work, spherical Ag-Au alloy nanoparticles were synthesized by reduction of  $\text{HAuCl}_4$  and  $\text{AgNO}_3$  by the use of sodium citrate as the reducing agent as well as the capping agent. Sodium citrate molecules which are negatively charged were adsorbed on the surface of the nanoparticles causing repulsion of the nanoparticles against each and hence stabilizing the alloy nanoparticles by preventing

them from aggregating. Samples of the prepared alloy nanoparticles (molar ratio Ag: Au =1:3) were characterized by TEM. Figure 20 shows the TEM images of Ag-Au bimetallic alloy nanoparticles, Ag nanoparticles and Au nanoparticles. From the particle size distribution it is observed that, particle sizes in the range of ca 20-30 nm, 30-40 nm and 20-30 nm were observed for Ag-Au alloy, Ag and Au nanoparticles, respectively.

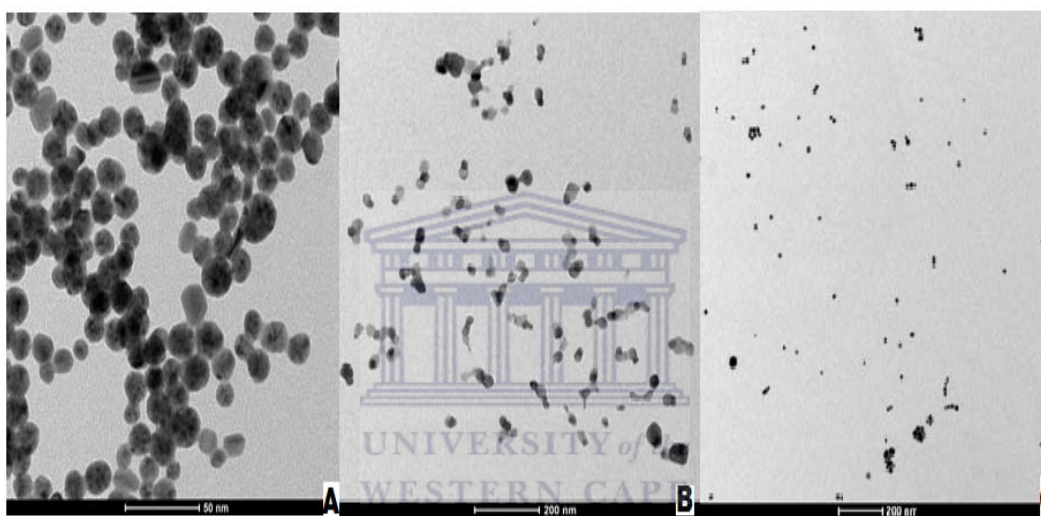


**Figure 20. TEM images of (a) Ag-Au (1:3) bimetallic alloy nanoparticles, (b) pure Ag nanoparticles and (c) pure Au nanoparticles.**

#### **4.1.4 Electrochemical characterization of Ag-AuNPs.**

##### ***4.1.4.1 Characterization in neutral medium.***

The synthesized Ag-Au (1:3) bimetallic alloy nanoparticles were also characterized by the use of cyclic voltammetric technique. Cyclic voltammetry (CV) of Ag-AuNPs/GCE was carried out in degassed phosphate buffer solution (0.1 M PBS, pH 7) solution at a scan rate of  $50 \text{ mV s}^{-1}$ . Similarly, AgNPs/GCE and AuNPs/GCE were

characterized respectively, using the same procedure as shown in Figure 21 a, b and c.

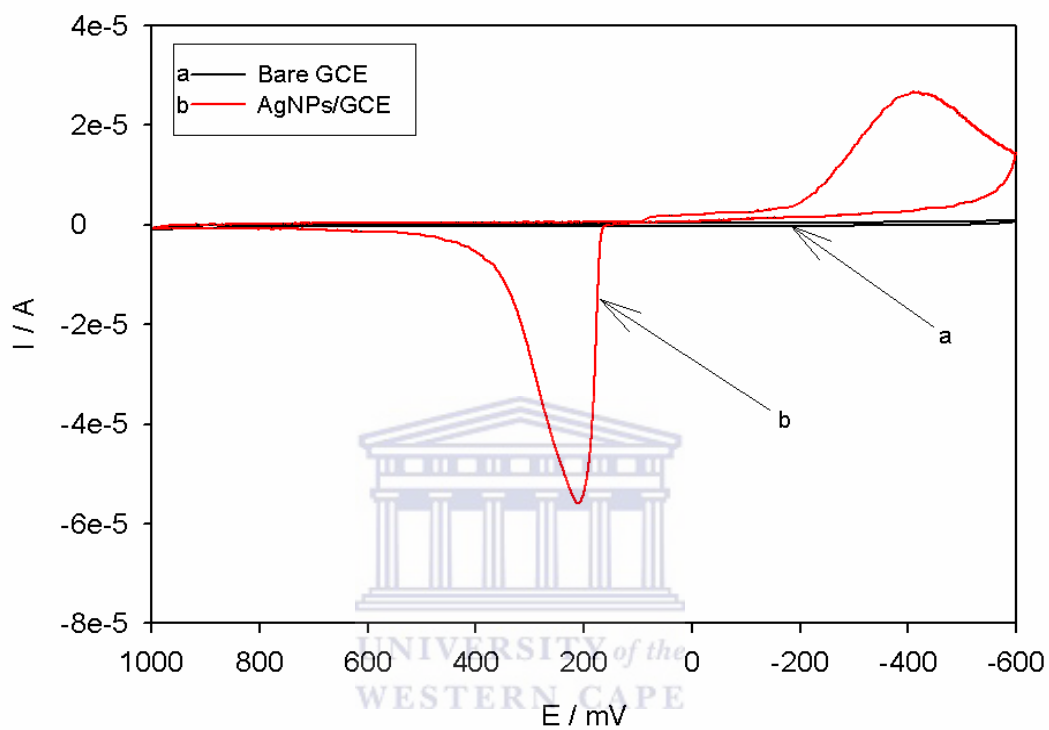


**Figure 21a.** Cyclic voltammogram of bare GCE (curve a) and AgNPs/GCE (curve b) in 0.1 M PBS pH 7: Scan rate  $50 \text{ mV s}^{-1}$ .



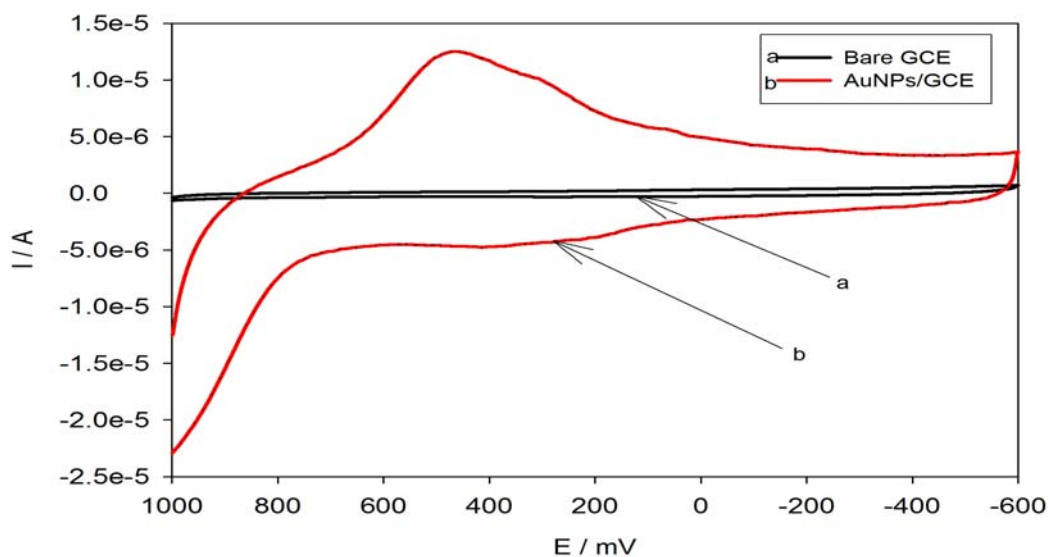


**Figure 21b.** Cyclic voltammogram of bare GCE (curve a) and AuNPs/GCE (curve b) in 0.1 M PBS pH 7: Scan rate  $50 \text{ mV s}^{-1}$ .

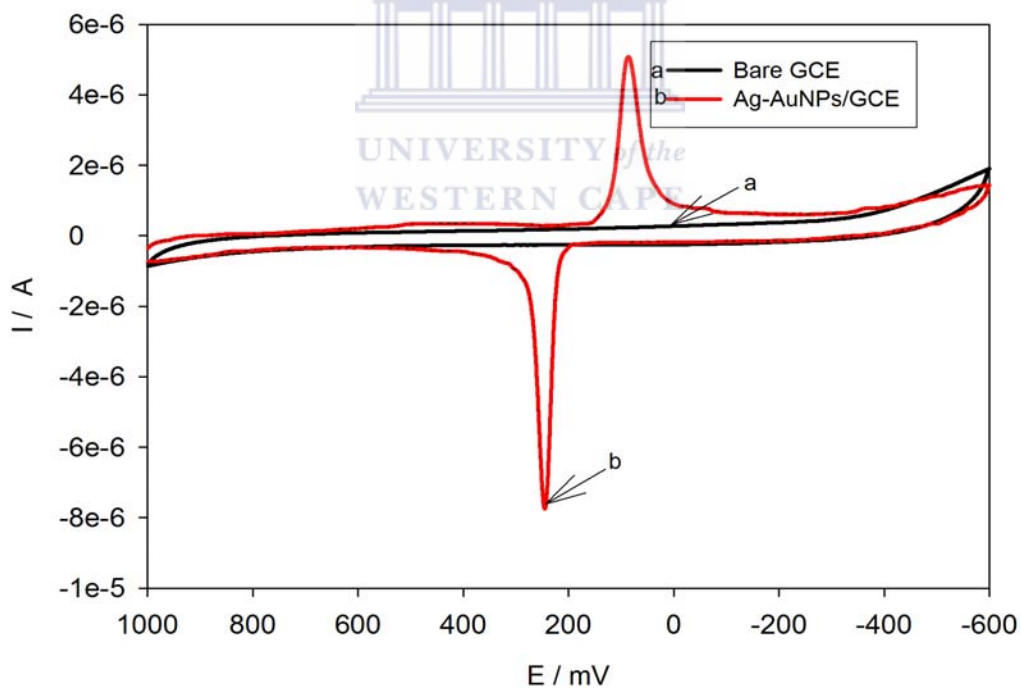


**Figure 21c.** Cyclic voltammogram of bare GCE (curve a) and Ag-AuNPs/GCE (curve b) in 0.1 M PBS pH 7: Scan rate  $50 \text{ mV s}^{-1}$ .

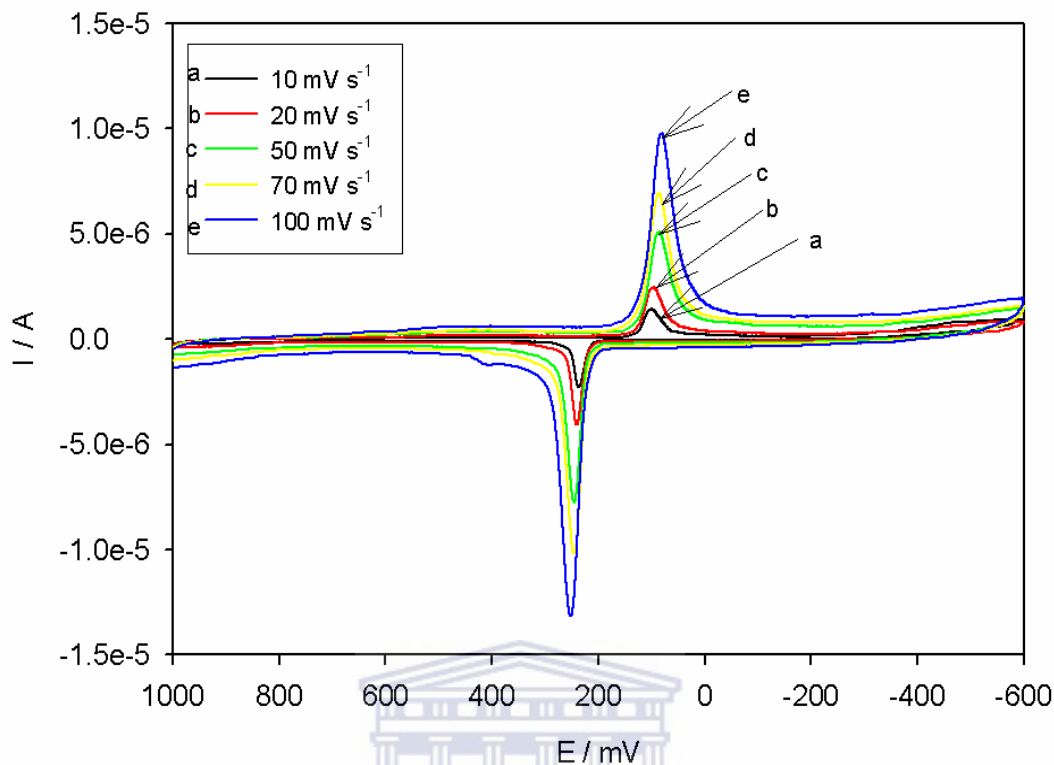


**Figure 22. Cyclic voltammograms of Ag-AuNPs/GCE in 0.1M PBS pH 7 at different scan rates.**

Large oxidation and reduction peaks of Ag nanoparticles were observed at -414 mV and 209 mV (corresponding to the Ag/Ag<sup>+</sup> redox couple), respectively (see Figure 21 a). The Au nanoparticles-modified electrodes also showed a broad anodic peak and reduction peak corresponding to the oxidation and reduction of Au at a potential range of 0 to 700 mV (Figure 21 b). For the Ag-AuNPs/GCE, a reduction peak was observed around 86 mV while an anodic peak was observed at 245 mV (Figure 21 c). It is interesting to note that, for the Ag-Au alloy nanoparticles, only one reduction and one oxidation peak was observed. This showed that the Ag-Au alloy nanoparticles were composed of atomically mixed Ag and Au atoms and not composed of Ag and Au metal domains. Increasing the scan rate showed an increase in the peak current as

shown in Figure 22. Further characterizations of the modified AgNPs/GCE, AuNPs/GCE and Ag-AuNPs/GCE electrodes were done using 0.1 M LiClO<sub>4</sub> as shown in Figure 23 a, b and c. Similar results were obtained even when 0.1 M LiClO<sub>4</sub> was used instead of 0.1 M PBS pH 7. This strongly supports that the synthesized Ag-Au nanoparticles were relatively homogeneous forming alloy nanoparticles.

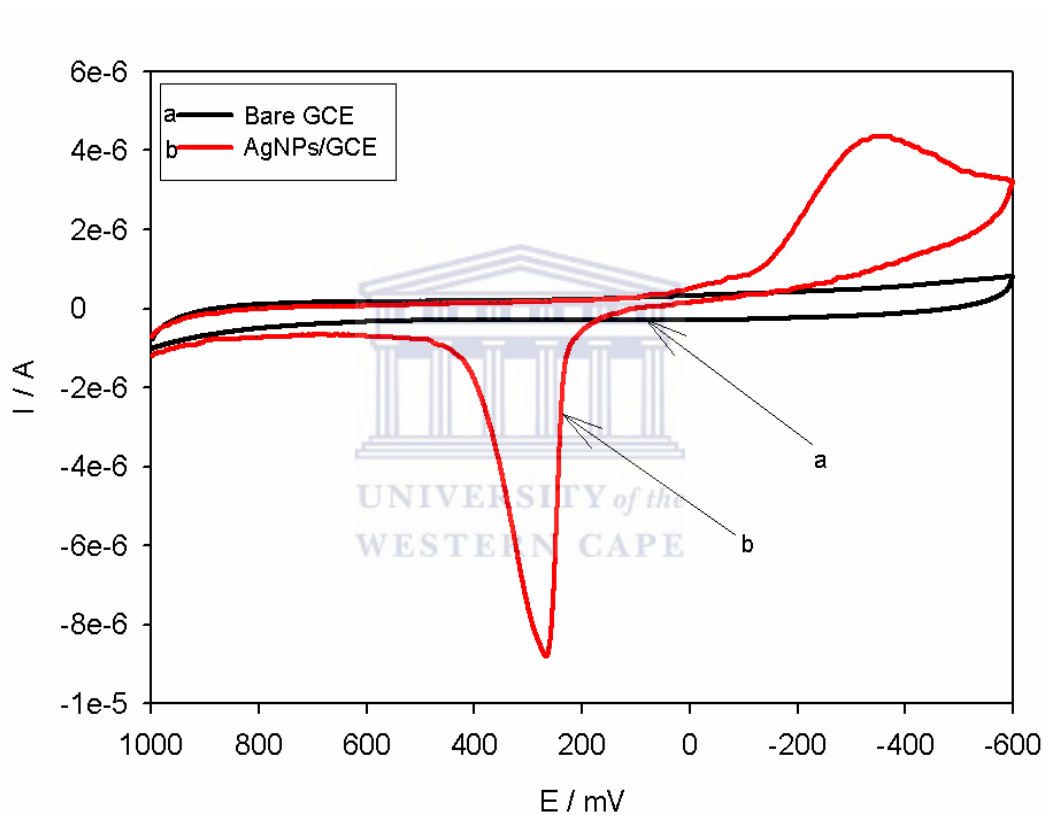


**Figure 23a.** Cyclic voltammogram of bare GCE (curve a) and AgNPs/GCE (curve b) in 0.1M LiClO<sub>4</sub>: Scan rate 50 mV s<sup>-1</sup>.

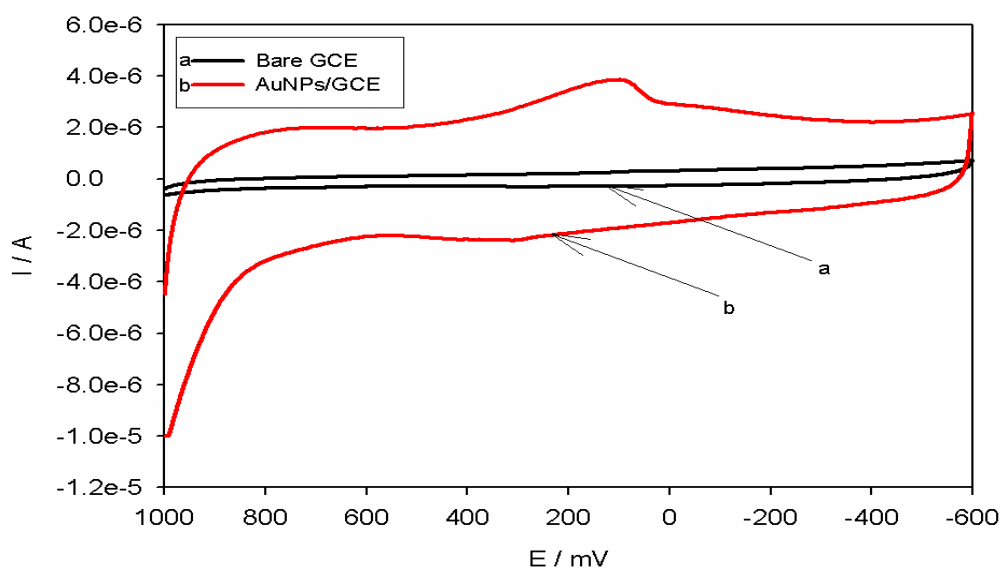


**Figure 23b.** Cyclic voltammogram of bare GCE (curve a) and AuNPs/GCE (curve b) in 0.1M LiClO<sub>4</sub>: Scan rate 50 mV s<sup>-1</sup>.

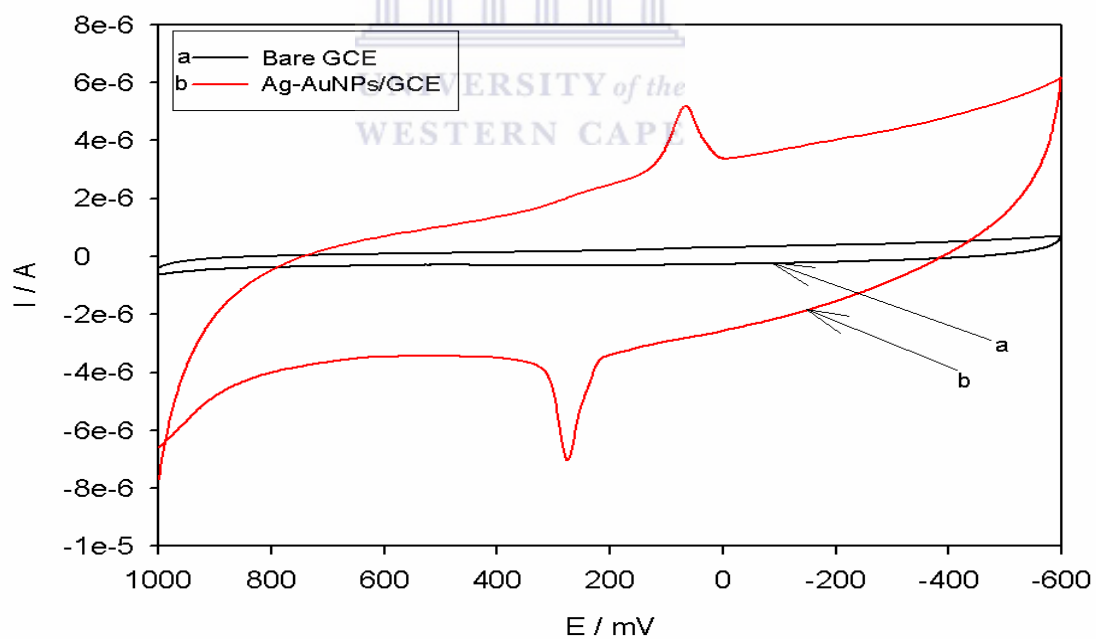


**Figure 23c.** Cyclic voltammogram of bare GCE (curve a) Ag-AuNPs/GCE (curve b) in 0.1M LiClO<sub>4</sub>: Scan rate 50 mV s<sup>-1</sup>.

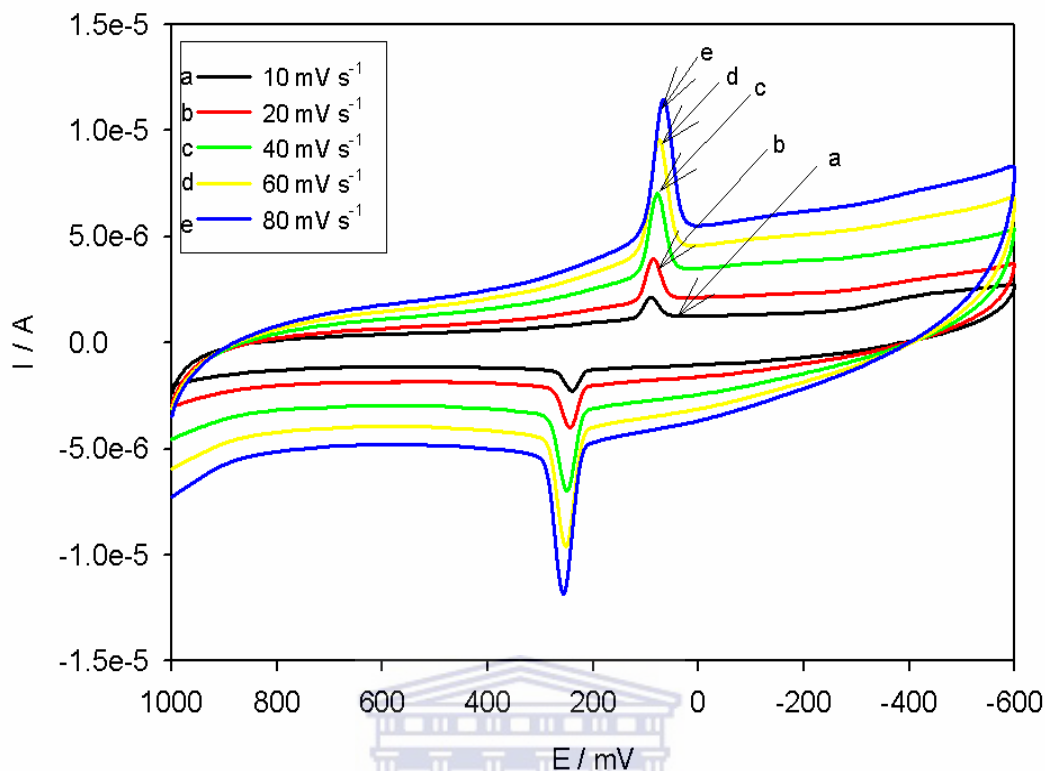


**Figure 24. Cyclic voltammograms of Ag-AuNPs/GCE in 0.1M LiClO<sub>4</sub> at different scan rates.**

The effect of potential scan rate was investigated as shown in Figure 24. The oxidation peak current ( $I_{pa}$ ) against the scan rate ( $\nu$ ) was linear over the range of 10-80  $\text{mV s}^{-1}$  as shown in Figure 25. The linear regression equation was obtained as  $I_{pa}/\text{A} = -3.2695 \times 10^{-7} - 8.45488 \times 10^{-8} \nu / (\text{mV s}^{-1})$  with a correlation coefficient ( $r^2$ ) of 0.9980. This indicated that the electrode process was redox reaction of surface adsorbed species.

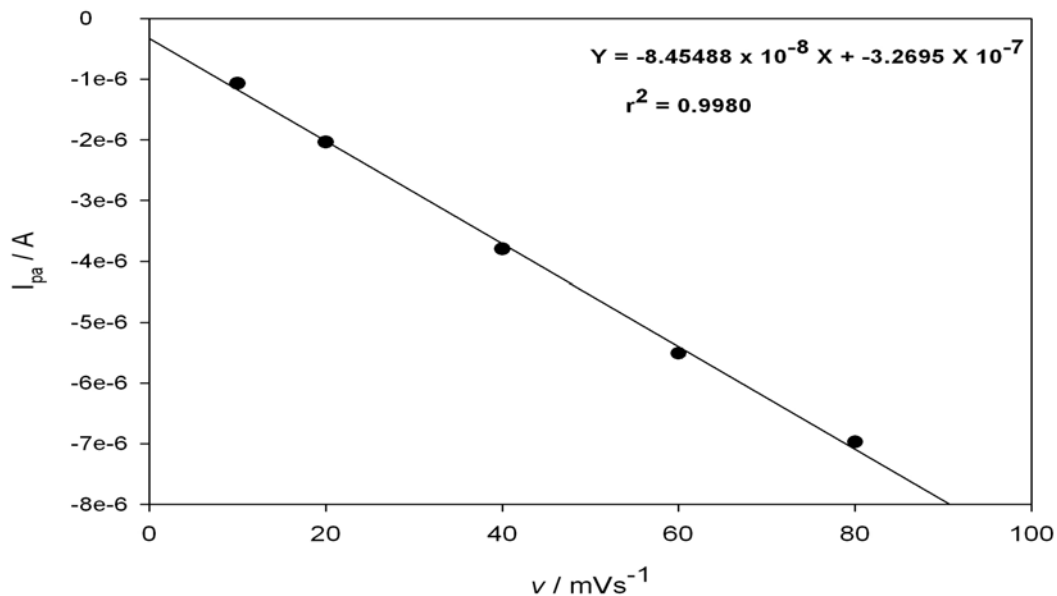


**Figure 25. A plot of scan rate versus anodic peak current.**

#### 4.1.4.2. Characterization in the presence of $\text{K}_3\text{Fe}(\text{CN})_6$ redox probe.

Cyclic voltammetry of the ferricyanide system is a convenient and valuable tool to monitor the electrochemical characteristics of the surface of modified electrodes. CV of the modified electrode was recorded (Figure 26) in the presence of  $\text{K}_3\text{Fe}(\text{CN})_6$  (5 mM) in aq. KCl (0.1 M) at a scan rate of  $50 \text{ mV s}^{-1}$ .

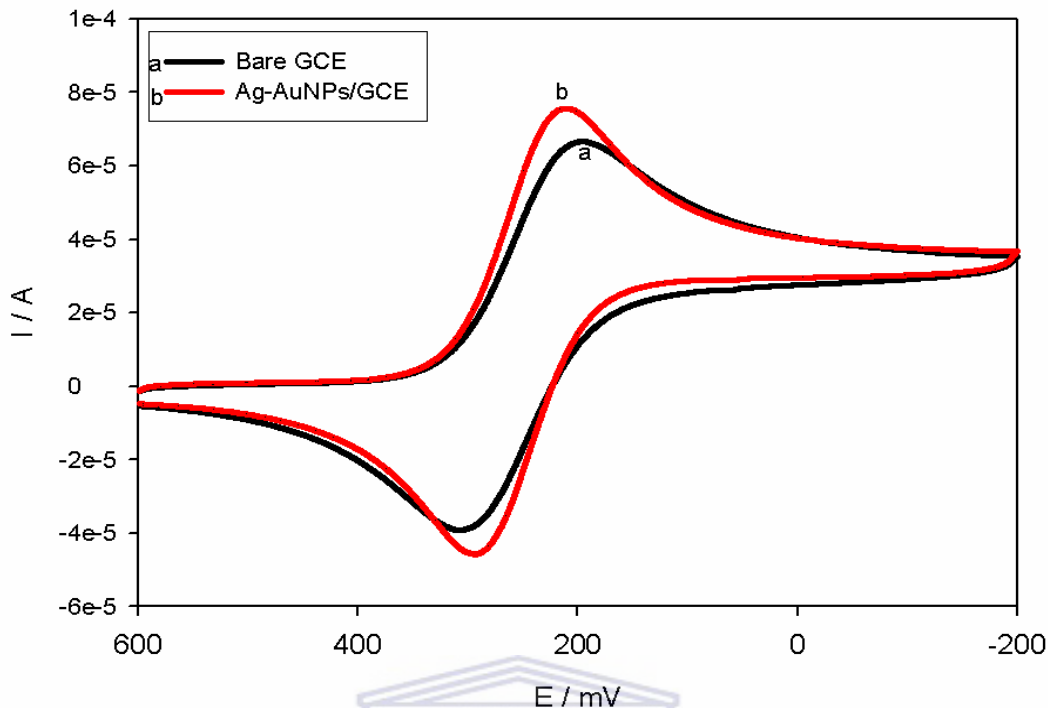


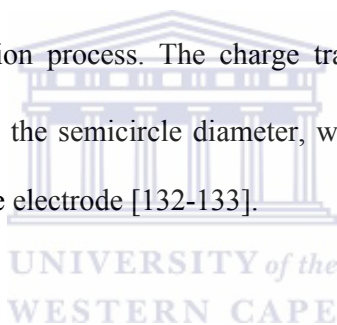
**Figure 26.** CVs of bare GCE (curve a) and Ag-AuNPs/GCE (curve b) in 5 mM  $K_3Fe(CN)_6$  solution containing 0.1 M KCl. Scan rate : 50 mV s<sup>-1</sup>.

The CVs of  $K_3Fe(CN)_6$  as an electrochemical probe at the bare GCE and the modified electrode are shown in Figure 26. At the bare GCE, the cathodic peak and anodic peaks of this redox probe were observed at 196 mV and 307 mV, respectively (see **Curve a**). However at the Ag-AuNPs/GCE these peaks occurred at 210 mV and 292 mV, respectively (see **Curve b**). The respective formal potentials were therefore 251.5 mV and 251.0 mV. Hence, in comparison with the CV at bare GCE, a moderate enhancement of about 12% of the redox peak current was observed at the Ag-Au bimetallic alloy nanoparticles modified electrode. The reason was that Ag-Au alloy nanoparticles with large surface area and good conductivity could act as tiny conduction centers which facilitate the transfer of electrons. Consequently, the modified electrode showed a marked decrease in peak-to-peak separation (i.e.,  $\Delta E_p =$

82 mV), compared to that measured in case of the bare GCE ( $\Delta E_p = 111$  mV). This can be attributed to the presence of the nanoparticles which enhanced faster electron transfer.

#### ***4.1.4.3. Impedimetric characterization of Ag-AuNPs/GCE.***

The preparation process of electrodes was also monitored by electrochemical impedance spectroscopy (EIS), which is an effective method for probing the features of the surface of modified electrodes. The Nyquist plot of impedance spectra includes a semicircle portion and a linear portion, with the former at higher frequencies corresponding to the electron transfer process and the latter at lower frequencies corresponding to the diffusion process. The charge transfer resistance ( $R_{ct}$ ) at the electrode surface is equal to the semicircle diameter, which can be used to describe the interface properties of the electrode [132-133].





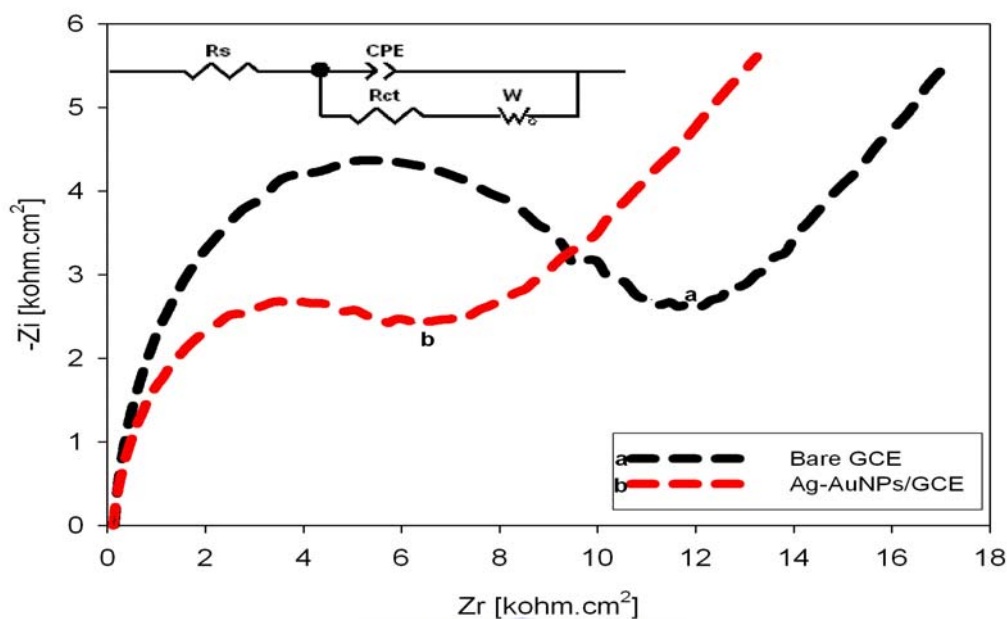


**Figure 27.** Nyquist plots of the EIS recorded in the presence of  $K_4[Fe(CN)_6]/K_3[Fe(CN)_6]$  (1:1) containing aq. KCl (0.1 M) for the bare GCE (curve a) and Ag-AuNPs/GCE (curve b).

UNIVERSITY of the  
WESTERN CAPE

From Figure 27, the charge transfer resistance ( $R_{ct}$ ) of Ag-AuNPs/GCE was lower ( $R_{ct} = 4674 \Omega$ ) with a decrease of 49% (curve b) compared to the bare GCE (curve a) which had an  $R_{ct}$  of  $9125 \Omega$  indicating that the Ag-Au alloy nanoparticles have good conductivity and played an important role in accelerating the transfer of electrons. This agrees well with the results presented in Figure 26.

The impedance parameters (table 2) were obtained by fitting using the inset equivalent circuit and the fitting errors were less than 2%.  $R_s$  is the solution resistance,  $R_{ct}$  is the charge transfer resistance, and CPE (constant phase element) is a distributive element that models the double layer capacitance owing to surface

inhomogeneity and  $Z_w$  ( $\omega$ ) measures mass transport. The  $\text{Fe}(\text{CN})_6^{3-/4-}$  redox probe exhibited kinetic control and diffusion controlled electrochemistry at high and low frequency respectively at the Ag-AuNPs and GCE interface.

**Table 2. The EIS parameters obtained from the circuit fitting of Figure 27 data.**

Circuit element	$R_s$ ( $\Omega$ )	$R_{ct}$ ( $\Omega$ )	CPE ( $nF$ )	$Z_w$ ( $k \Omega s^{1/2}$ )
Bare GCE	146.5	9125	932.23	377.35
Ag-AuNPs/GCE	127.2	4674	911.44	355.69

From  $\omega_{\max}$  (frequency at maximum imaginary impedance of the semicircle), useful kinetic parameters of  $\text{Fe}^{2+} \leftrightarrow \text{Fe}^{3+} + e^-$  electron transfer such as time constant (cycle life)  $\tau$ , exchange current  $I_0$ , and heterogeneous rate constant  $k_{et}$  [134-135] were calculated from equations (11,12,13, and 14) and shown in table 3.

$$\omega_{\max} = \frac{1}{R_{ct} C_{dl}} \quad (11)$$

$$\tau = R_{ct} C_{dl} \quad (12)$$

$$I_0 = \frac{RT}{nFR_{ct}} \quad (13)$$

$$K_{et} = \frac{I_0}{nFAC_0} \quad (14)$$

Where  $\omega_{\max} = 2 \pi f$ ,  $C_{dl}$  is the double layer capacitance,  $R = 8.314 \text{ J K}^{-1} \text{ mol}^{-1}$ ,  $F = 96486 \text{ C mol}^{-1}$ ,  $n = 1$ ,  $C_0$  is the concentration of  $[\text{Fe}(\text{CN})_6]^{3-/4-} = 5 \times 10^{-6} \text{ mol cm}^{-3}$ . The maximum frequency values ( $f$ ) were taken from Figure 27 (15.82 Hz and 8.85 Hz for Ag-AuNPs/GCE and bare GCE, respectively).

**Table 3. Effect of Ag-AuNPs electrode on the kinetics of  $[\text{Fe}(\text{CN})_6]^{3-/4-}$** 

Kinetic parameters	Bare GCE	Ag-AuNPs/GCE
$\omega_{\text{max}} (\text{rad s}^{-1})$	55.61	99.43
$\tau (\text{s rad}^{-1})$	$1.798 \times 10^{-2}$	$1.005 \times 10^{-2}$
$I_0 (\text{A})$	$2.814 \times 10^{-6}$	$5.493 \times 10^{-6}$
$k_{\text{et}} (\text{cm s}^{-1})$	$8.215 \times 10^{-5}$	$1.604 \times 10^{-4}$

From table 3,  $I_0$  values for the electron transfer reaction of  $\text{Fe}(\text{CN})_6^{3-/4-}$  on bare GCE and Ag-AuNPs/GCE are  $2.814 \times 10^{-6}$  A and  $5.4938 \times 10^{-6}$  A, respectively. A higher exchange current, which means increase in the rate of electron transfer, was observed at the modified GCE. This increase in electron transfer (increase in reaction rate) can be attributed to the catalytic effect of the nanoparticles. The kinetics of  $[\text{Fe}(\text{CN})_6]^{3-/4-}$  increased by an order of magnitude at the Ag-AuNPs/GCE// $[\text{Fe}(\text{CN})_6]^{3-/4-}$  interface. It can thus be inferred that the Ag-AuNPs/GCE catalyzed the redox reaction of  $[\text{Fe}(\text{CN})_6]^{3-/4-}$ .

The surface coverage ( $\theta$ ) of the nanoparticles on the GCE surface was calculated from equation (18) [136].

$$\theta = 1 - \frac{R_{\text{ct}}^{\text{Ag-AuNPs/GCE}}}{R_{\text{ct}}^{\text{bare GCE}}} \quad (18)$$

Based on the above equation and the  $R_{\text{ct}}$  values in table 2, Ag-Au alloy nanoparticles had a surface coverage of 0.4877 (48.77%) on the GCE. This may be improved if the amount of nanoparticles drop-coated is optimized.

## 4.2 Synthesis and Characterization of PPy/GCE

Figure 28 shows the cyclic voltammogram of 0.1M pyrrole in 0.1 M LiClO<sub>4</sub> on GCE at a scan rate of 50 mV s<sup>-1</sup> for 10 cycles. The deposition of a polymer was observed to occur at the GCE due to the increase in current with each successive sweep.

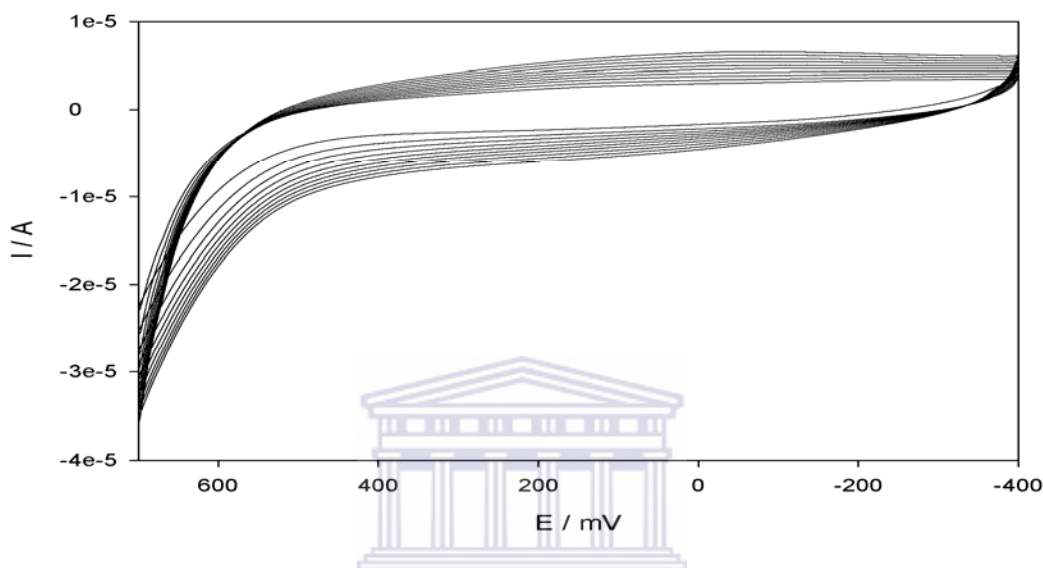
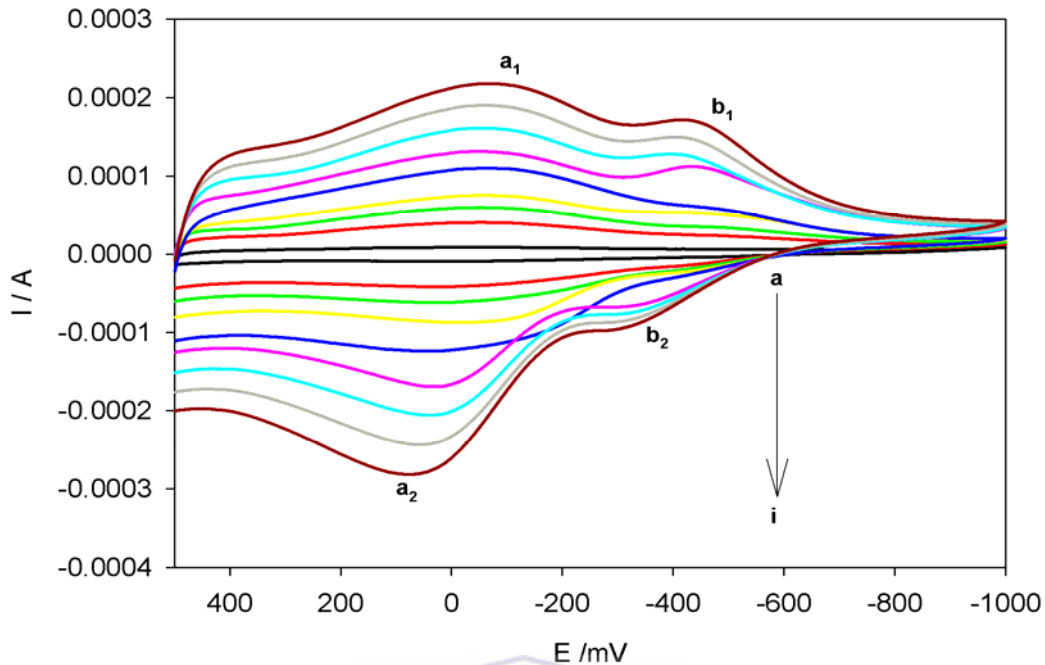


Figure 28. Polymerization of pyrrole in 0.1 M LiClO<sub>4</sub> at a scan rate of 50 mV s<sup>-1</sup>.

### 4.2.1 Characterization of PPy/GCE in 0.1 M LiClO<sub>4</sub>.

CV is very often used to characterize conducting polymer films. This is the method of choice for studying the reversibility of electron transfer because the oxidation and reduction can be monitored in the form of a current –potential diagram. Cyclic voltammetry results of PPy indicated the existence of two redox couples **a<sub>1</sub>/a<sub>2</sub>** and **b<sub>1</sub>/b<sub>2</sub>**. The multiscan voltammogram of the PPy-modified GC electrode in 0.1 M LiClO<sub>4</sub> is shown in Figure 29. Both peak potentials and corresponding peak currents varied, which showed that the polymer was electroactive and diffusion of electrons was taking place along the polymer chain [137]



**Figure 29** Multiscan voltammograms of PPy characterization in 0.1 M LiClO<sub>4</sub> at different scan rates: (a) 10 mV s<sup>-1</sup>; (b) 50 mV s<sup>-1</sup>; (c) 75 mV s<sup>-1</sup>; (d) 100 mV s<sup>-1</sup>; (e) 150 mV s<sup>-1</sup>; (f) 200 mV s<sup>-1</sup>; (g) 250 mV s<sup>-1</sup>; (h) 300 mV s<sup>-1</sup>; (i) 350 mV s<sup>-1</sup>. (initial potential: 500 mV).

The linear dependence of peak currents of cathodic peak  $I$  (Figure 29 peak  $a_1$ ) on the scan rate (Figure 30) indicated that we have a thin film of surface-bound conducting electroactive polymer, undergoing rapid reversible electron transfer reaction [137].

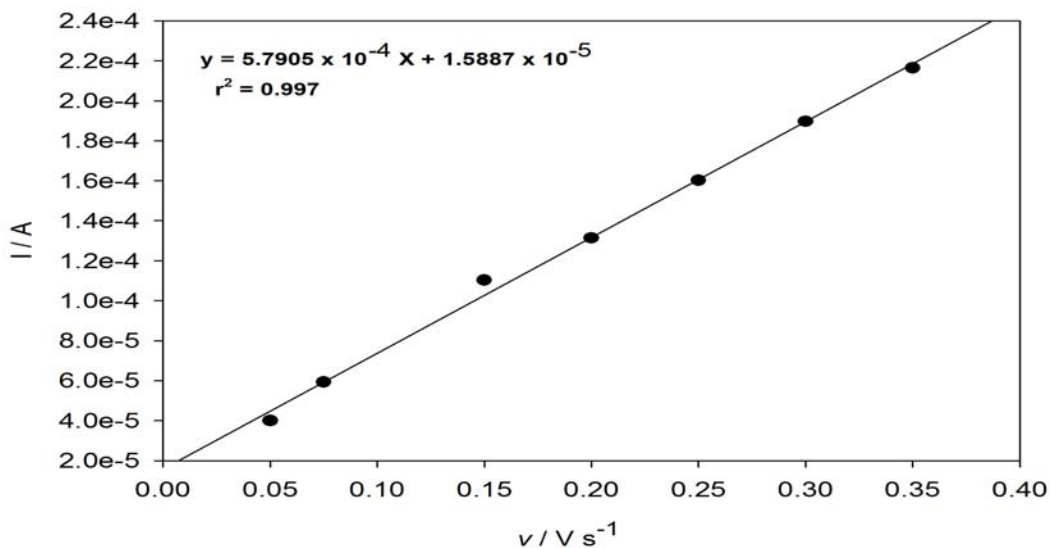


**Figure 30. A plot of current versus scan rate.**

The oxidation or reduction of polypyrrole requires two simultaneous processes: (i) the transfer of electrons either from or to polypyrrole and (ii) the diffusion of the counterion, or in some cases the diffusion of the cation into or out of the polypyrrole film to maintain charge neutrality. The redox mechanism of polypyrrole is described by one-electron transfer step;



where PPy is the neutral species and  $PPy^+$  is the radical cationic species or polaron (one positive charge localized over three to four monomer units). The polaron can further be oxidized;



where  $PPy^{++}$  is the dicationic species or bipolaron (two positive charges localized over three to four monomer units). This explains the existence of two reduction peaks in the PPy; one strong (Figure 29 curve a<sub>1</sub>) and the other weak (Figure 29 curve b<sub>1</sub>) when characterized in 0.1 M LiClO<sub>4</sub>. On the cathodic scan, the dicationic species

(PPy<sup>++</sup>) was reduced to the radical cationic species (PPy<sup>+</sup>) which is responsible for peak **a<sub>1</sub>** (Figure 29 **a<sub>1</sub>**) while the radical cationic species was further reduced to the neutral PPy species (Figure 29 peak **b<sub>1</sub>**). During reverse scanning (anodic scan), the neutral species PPy was oxidized to the dicationic species or bipolaron (PPy<sup>++</sup>) denoted by peak **a<sub>2</sub>** (Figure 29 peak **a<sub>2</sub>**). This is in line with previously reported works [81]. However, at high scan rates a second oxidation peak occurred (Figure 29 peak **b<sub>2</sub>**) as a result of the oxidation of the polaron (cationic species, PPy<sup>+</sup>) to bipolaron (dicationic species, PPy<sup>++</sup>). It is worth noting that, both cationic species (polaron) and dicationic species (bipolarons) were present in the film containing lithium perchlorate. Lithium perchlorate was used as a dopant to enhance electrical neutrality during polymerization. The surface concentration of the PPy film on the surface of the GC electrode,  $\Gamma_{\text{ppy}}^*$  was estimated from a plot of  $I_p$  against  $\nu$  in accordance with the Brown–Anson model [109] using the equation:

$$I_p = \frac{n^2 F^2 \Gamma_{\text{ppy}}^* A \nu}{4RT} \quad (19)$$

where  $n$  represents the number of electrons transferred (2),  $F$  is the faraday constant (96,584 C mol<sup>-1</sup>),  $\Gamma_{\text{ppy}}^*$  is the surface concentration of the PPy film (mol cm<sup>-2</sup>),  $A$  is the surface area of the electrode (0.071 cm<sup>2</sup>),  $\nu$  is the scan rate (V s<sup>-1</sup>),  $R$  is the gas constant (8.314 J (mol K)<sup>-1</sup> and  $T$  is the absolute temperature of the system (298 K). The surface concentration of PPy film,  $\Gamma_{\text{ppy}}^*$  was estimated to be 2.166 x 10<sup>-9</sup> mol cm<sup>-2</sup>. This was in agreement with the values found in literature [115]. On increasing the scan rate, the magnitude of the peak current increased. However, the peak potentials

shifted to more positive potentials and became broad. This shows that the peak currents are diffusion-controlled [137].

To test for the electrical conductivity of the conducting polymer and to confirm whether the polymer was overoxidized during polymerization, PPy-modified electrode was characterized in 5 mM  $\text{K}_3\text{Fe}(\text{CN})_6$  redox probe. The PPy/GCE showed a higher peak current enhancement compared to the bare GCE. This is because PPy is a good conducting polymer and hence allowed electrons to flow faster from the solution to the electrode resulting to a high peak height (Figure 31). The data obtained from Figure 31 was recorded in table 4.

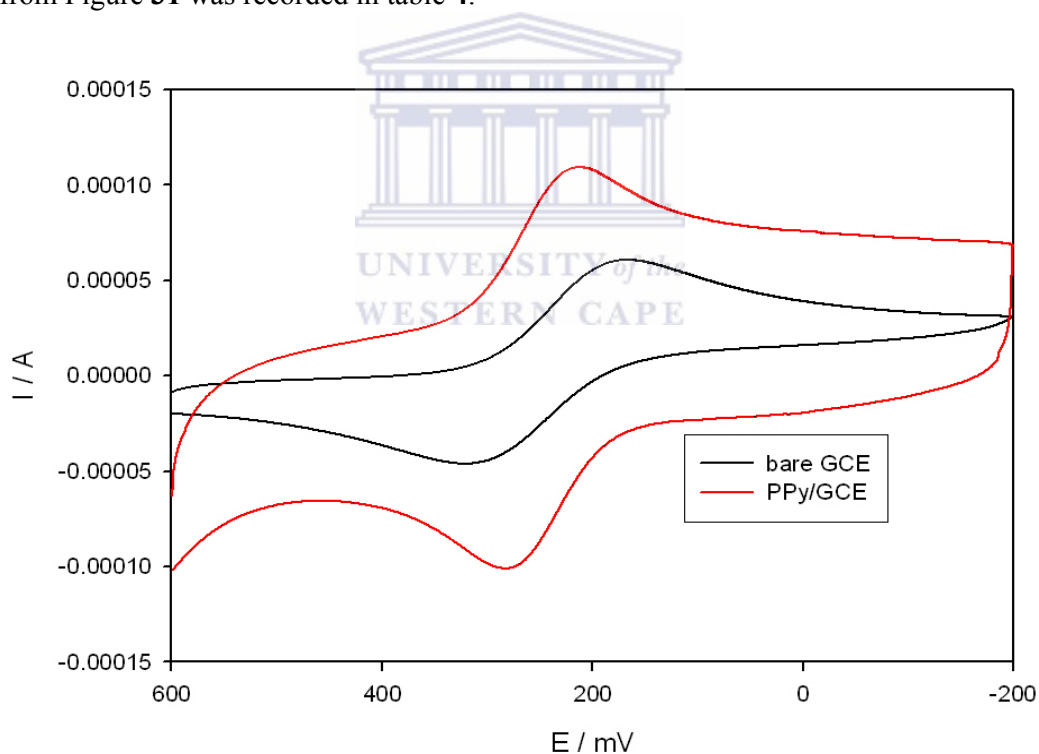


**Figure 31. Cyclic Voltammograms of bare GCE and PPy/GCE in 5 mM  $\text{K}_3\text{Fe}(\text{CN})_6$  at a scan rate of  $50 \text{ mV s}^{-1}$ .**



**Table 4. CV data for bare GCE and PPy/GCE in 5 mM K<sub>3</sub>Fe(CN)<sub>6</sub>.**

Electrode	$E_{pa}$ (mV)	$E_{pc}$ (mV)	$I_{pa}$ (A)	$I_{pc}$ (A)	$E^{o'}$ (mV)	$\Delta E_p$ (mV)
Bare GCE	317	170	$-5.53 \times 10^{-5}$	$5.70 \times 10^{-5}$	243.5	147
PPy/GCE	282	218	$-7.23 \times 10^{-5}$	$6.99 \times 10^{-5}$	250.0	64

The peak to peak separations ( $\Delta E_p$ ) were 147 mV and 64 mV at the bare GCE and PPy/GCE respectively as shown in table 4. The results indicate that the presence of the conducting PPy polymer increased the electroactive surface area of the electrodes and enhanced faster electron transfer between the solution and the electrode compared to the bare GCE as depicted by the increase in current and the decrease in peak separation. Thus PPy has been shown to be a good conducting polymer. Based on the conductivity of the electrodeposited PPy polymer, the possibility of the polymer being over-oxidized was ruled out since overoxidized PPy is a non-conducting polymer [11]. It was therefore of great importance to overoxidize the PPy.

### 4.3 Overoxidation of polypyrrole.

PPy was overoxidized in 0.1 M NaOH at a potential of 1.0 V for 420 s as shown in Figure 32. The overoxidation is indicated by the slow decay of the current after reaching a maximum as reported by Kaplin *et al.* [81].

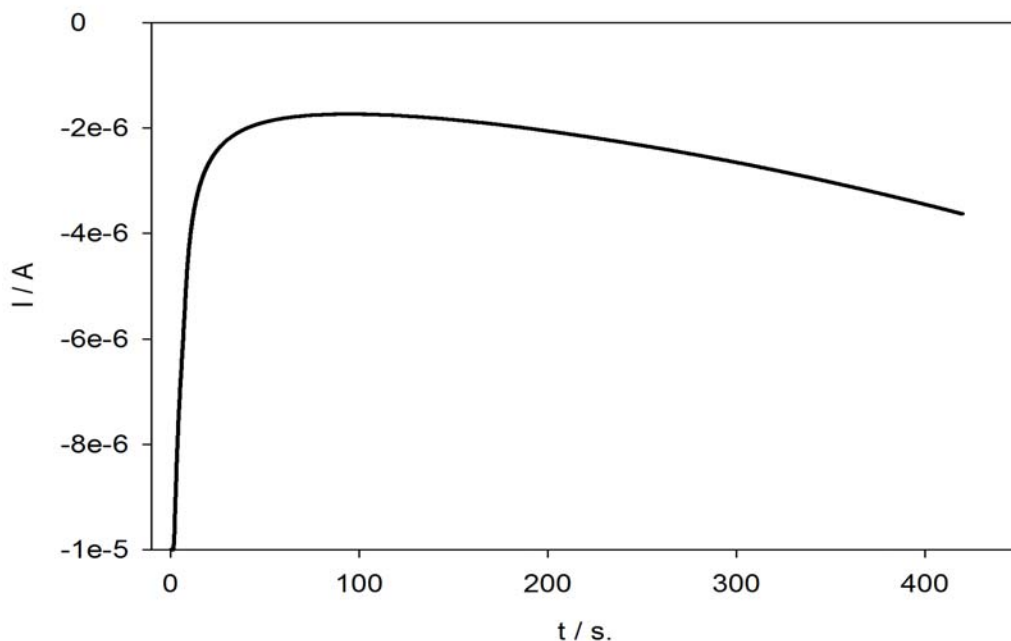


**Figure 32. Overoxidation of PPy in 0.1 M NaOH for 420 s.**

The overoxidized polypyrrole has porous structures thus allows the accumulation of nanoparticles. Ag-Au alloy nanoparticles were immobilized on the overoxidized PPy modified electrode and denoted as PPyox/Ag-AuNPs/GCE and was characterized in  $K_3Fe(CN)_6$  as a probe to test its electrical conductivity and to confirm whether the PPy polymer was overoxidized and investigate the catalytic effect of the deposited nanoparticles as shown in section 4.4.

#### **4.4 Electrochemical characterization of PPyox/Ag-AuNPs/GCE.**

PPyox is prepared by oxidizing PPy to a higher oxidation state after which it becomes susceptible to nucleophilic attack [83]. This process usually results in the addition of carbonyl functionality to the pyrrolic rings with a consequent loss of conjugation and hence the loss inherent electronic conductivity [83, 138]. A PPyox film behaves like a non-conducting polymer on an electrode (GCE in this case) and blocks electron

transfer. Hence, our observation (Figure 33, **curve a**) of lower peak currents and a larger peak to peak separation ( $\Delta E_p = 173$  mV) indicated that there was slower electron transfer compared to that recorded with the bare GCE (Figure 33 **curve b**,  $\Delta E_p = 111$  mV). Moreover, the film is negatively charged with a large loss of electroactivity [139-140]. The negative charge of the layer should be unfavorable for the approaching of ferricyanide anions. However, the purpose of the overoxidizing the PPy was to exploit the fact that this process results in a polymer with pores on its surface, which creates a better condition for the attachment of nanoparticles [11]. According to the cyclic voltammograms of the  $K_3Fe(CN)_6^{3-/4-}$  redox probe shown in Figure 33, after deposition of the Ag-Au alloy nanoparticles in the presence of electrodeposited PPyox-film on the GCE's surface (**curve c**), the peak current was enhanced by 25% and the peak-to-peak separation ( $\Delta E_p = 82$  mV) was reduced by 91 mV when compared to the CV recorded with PPyox film-modified electrode without the Ag-Au NPs. Relative to the bare GCE, the increased surface roughness and the newly induced surface functional groups and micro/nano catchment sites of the PPyox/GCE might have enhanced the loading of the nanoparticles and, thus, created significant change in the surface area and the kinetics involved. The data obtained from Figure 33 were recorded in table 5.

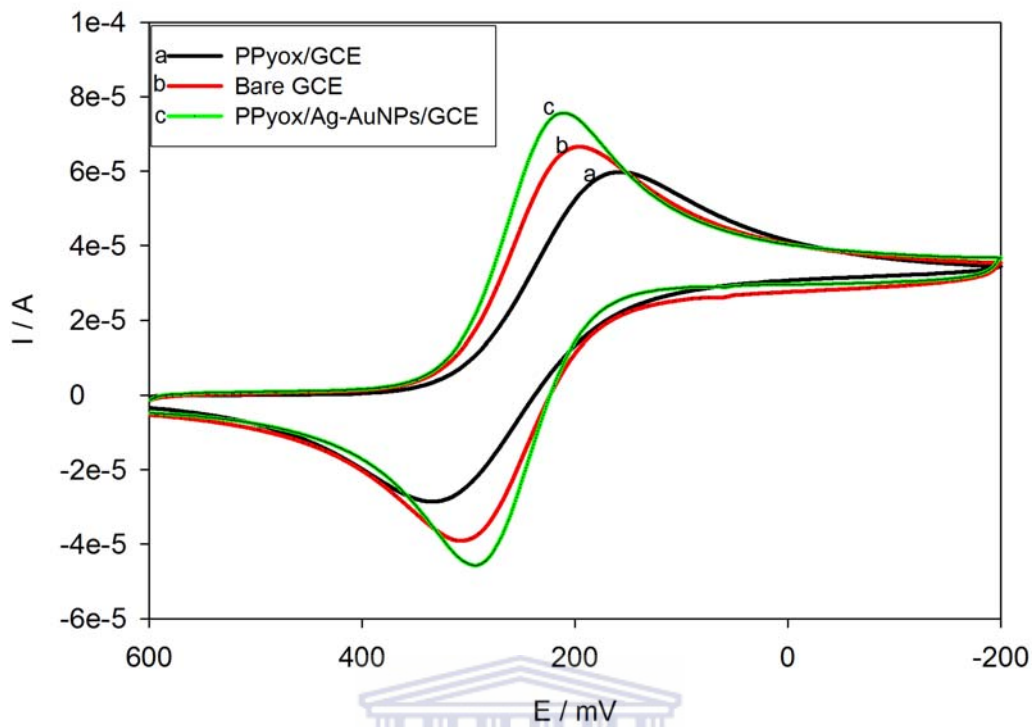


Figure 33. CVs recorded with PPyox/GCE (curve a), bare GCE (curve b) and PPyox/Ag-AuNPs/GCE (curve c) in the presence of  $K_3Fe(CN)_6$  (5 mM) in aq. KCl (0.1 M): Scan rate  $50 \text{ mV s}^{-1}$ .

Table 5. CV data obtained from Figure 33.

Electrode	$E_{pa}$ (mV)	$E_{pc}$ (mV)	$I_{pa}$ (A)	$I_{pc}$ (A)	$\Delta E_p$ (mV)	$E^{o'}$ (mV)
Bare GCE	307	196	$-6.230 \times 10^{-5}$	$6.440 \times 10^{-5}$	111	251.5
PPyox/GCE	331	158	$-5.403 \times 10^{-5}$	$5.901 \times 10^{-5}$	173	244.5
PPyox/Ag-AuNPs/GCE	293	211	$-7.372 \times 10^{-5}$	$7.360 \times 10^{-5}$	82	252.0

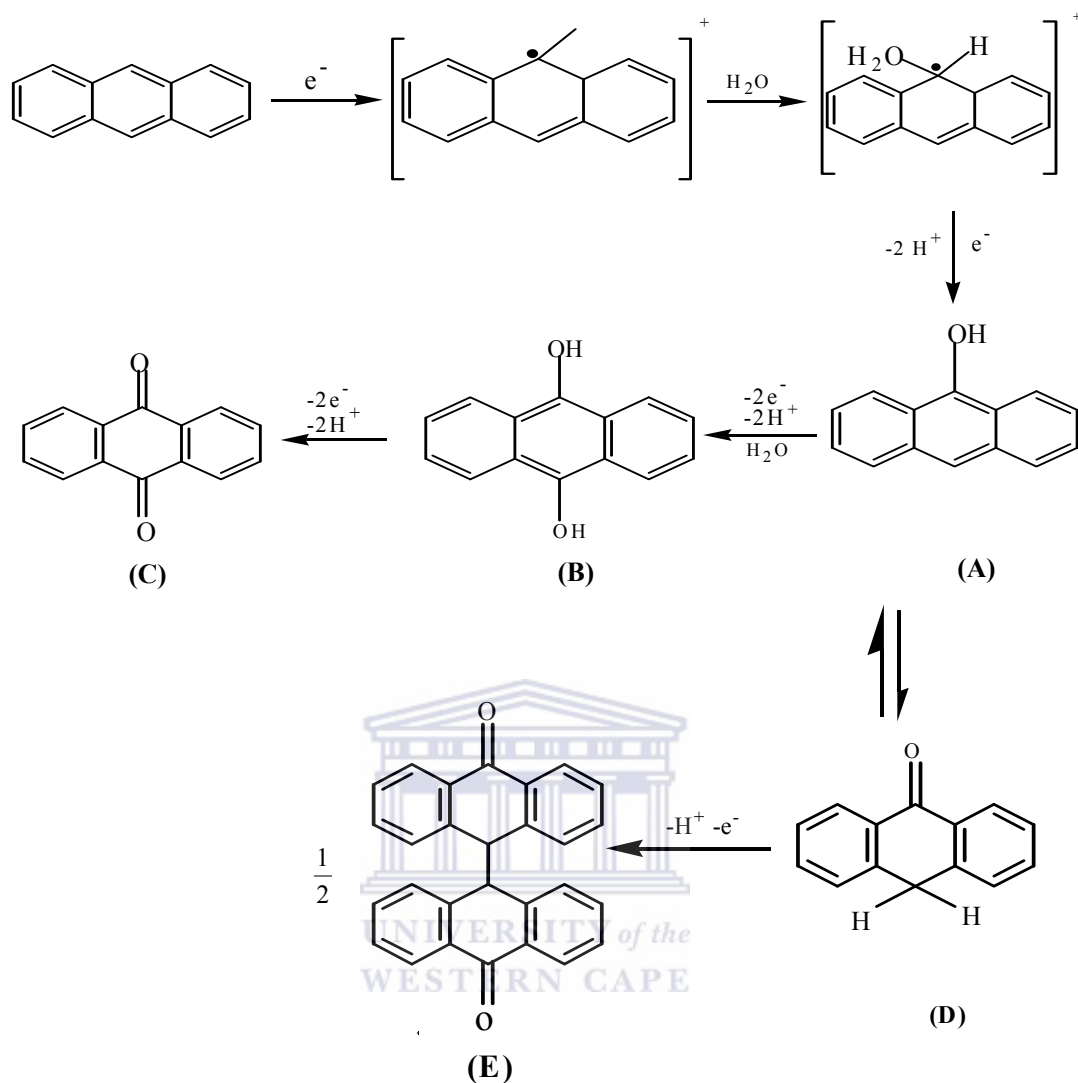
## CHAPTER 5

### 5.0 RESULTS AND DISCUSSION 2

#### 5.1 Response of the electrochemical sensor on some monitored PAHs.

##### 5.1.1 Electrocatalytic oxidation of anthracene (AN).

Experiments on the electrocatalytic oxidation of anthracene were investigated using different modified electrodes in acetonitrile with LiClO<sub>4</sub> as the supporting electrolyte. The electrochemical processes observed at all electrodes were only for the oxidation of anthracene. The following discussion is based on their cyclic voltammetric responses (see Figure 34) to anthracene ( $3.56 \times 10^{-4}$  M) dissolved in the above solution. The anodic peak around 1200 mV for anthracene was not associated with the cathodic peak. This irreversible behaviour suggested that anthracene was oxidized and then reacted to form a new product (anthraquinone) [72]. Scheme 7 shows some of the expected products from oxidation of anthracene. Hydrolysis of the radical even in the most anhydrous solutions is likely. If hydrolysis occurs before dimerisation and is followed by further oxidation and loss of protons, 9-anthranol (**A**) would be produced. Rapid keto-enol equilibrium is established and greatly favours the keto isomer, 9-anthrone (**D**), which is easily oxidized thus forming bianthrone (**E**). If a second hydrolysis occurs before keto-enol tautomerisation, then the product, 9,10-dihydroxyanthracene (**B**) would be produced, which can be readily oxidized to anthraquinone (**C**) [141]. According to Christopher *et al.*, [141] anthraquinone is the most likely product formed when little addition of water is added to acetonitrile.



**Scheme 7. Outline of various products expected from the oxidation of anthracene.**

From Figure 34, PPyox/Ag-Au alloy nanoparticles modified electrode showed an anodic peak current which was observed to be 84% higher than that for the bare electrode (Figure 34, curve f). However, the AgNps/GCE, AuNps/GCE, Ag-AuNps/GCE and PPyox/GCE exhibited peak enhancement of 4.69%, 15.27%, 28.88% and 70% respectively compared to the bare GCE (Figure 34).

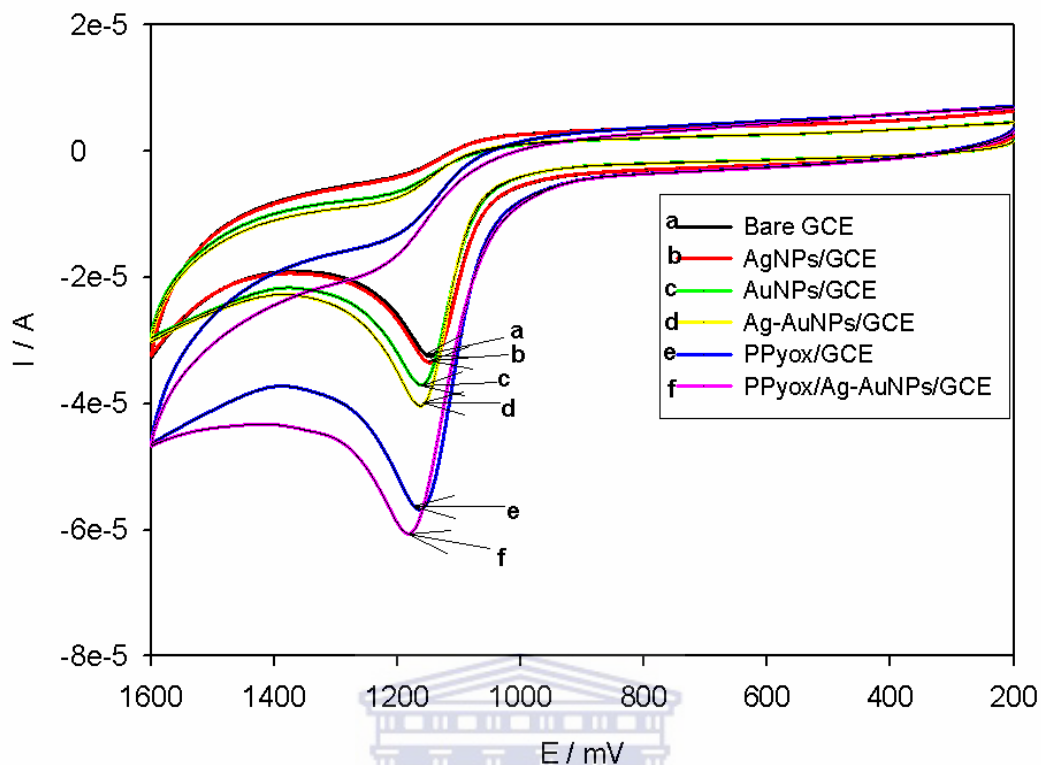


**Figure 34.** CV of  $3.56 \times 10^{-4}$  M anthracene at bare GCE (curve a), AgNPs/GCE (curve b), AuNPs/GCE (curve c), Ag-AuNPs/GCE (curve d), PPyox/GCE (curve e) and PPyox/Ag-AuNPs/GCE (curve f) in acetonitrile and 0.1 M LiClO<sub>4</sub>; Scan rate 100 mV s<sup>-1</sup>.

The better electrocatalytic performance of the AgNPs/GCE, AuNPs/GCE and Ag-AuNPs/GCE to the oxidation of anthracene as shown by their higher amperometric responses compared to the bare GCE might be attributed to the presence of nanoparticles on GCE. According to Figure 34, the electrode which was modified with the bimetallic alloy nanoparticles (curve d) exhibited higher catalytic properties compared to the monometallic nanoparticles modified electrodes (curve b and c). A similar observation was reported in the literature [142]. However, the contribution of modifying the GCE with PPyox (curve e) was most dominant as the PPyox/GCE

alone exhibited about 70% increase in the anodic peak compared to the bare electrode. On deposition of the bimetallic Ag-Au nanoparticles over the PPyox/GCE, the anodic peak was observed to slightly increase to about 84% as shown by the response of the PPyox/Ag-AuNPs/GCE (**curve f**). The catalytic effect of combining PPyox with Ag-Au NPs as evidenced by the remarkable enhancement in the peak height for anthracene oxidation might be attributed to the adsorptive ability of PPyox film and its high nanoparticle-loading nano-porous structure allowing the deposition of the Ag-Au NPs which have high catalytic properties. A summary of the thermodynamic data obtained from Figure 34 is shown in table 6.

**Table 6. Anodic current response data for the development of the sensor (see Figure 34).**

Electrode	$E_{pa}$ (mV)	$I_{pa}$ (A)
Bare GCE	1148	$2.778 \times 10^{-5}$
AgNps/GCE	1150	$2.900 \times 10^{-5}$
AuNPs/GCE	1160	$3.193 \times 10^{-5}$
Ag-AuNPs/GCE	1162	$3.537 \times 10^{-5}$
PPyox/GCE	1162	$4.657 \times 10^{-5}$
PPyox/ Ag-AuNPs/GCE	1181	$5.225 \times 10^{-5}$

The effect of potential scan rate was investigated. Increasing the scan rates caused an increase in the peak current. Figure 35 shows the CV of PPyox/Ag-AuNPs/GCE upon addition of  $3.56 \times 10^{-4}$  M anthracene at different scan rates. The peak current for anthracene increased linearly with the square root of the sweep rate ( $v^{1/2}$ ) over the range 20-250  $\text{mV s}^{-1}$  with a linear regression of  $I_{pa}(\text{A}) = -4.911 \times 10^{-6} - 3.993 \times 10^{-6} v^{1/2}(\text{mV s}^{-1})^{1/2}$  ( $r^2 = 0.999$ ) (Figure.36) denoting that the electrochemical process was



limited by the rate of diffusion of anthracene from the solution to the electrode surface. Moreover, on increasing the scan rate, the magnitude of the peak current increased. However, the peak potentials shifted to more positive potentials. This also confirmed that the peak currents were diffusion-controlled [137]

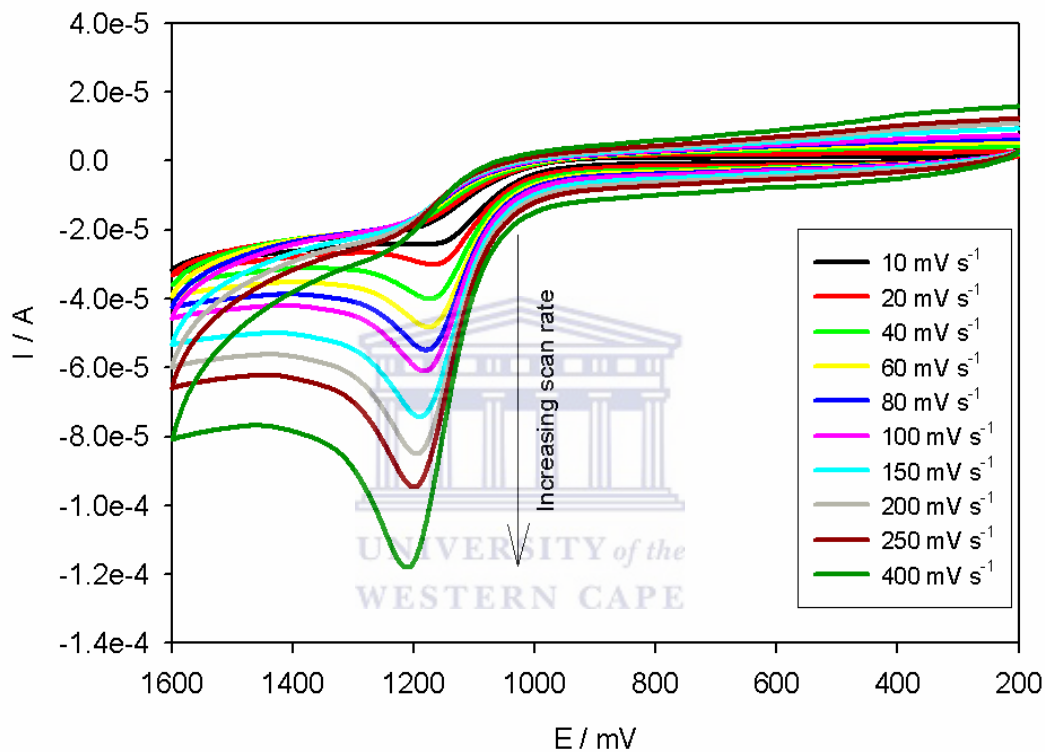


**Figure 35. CVs of PPyox/Ag-AuNPs/GCE upon addition of  $3.56 \times 10^{-4}$  M anthracene at different scan rates.**

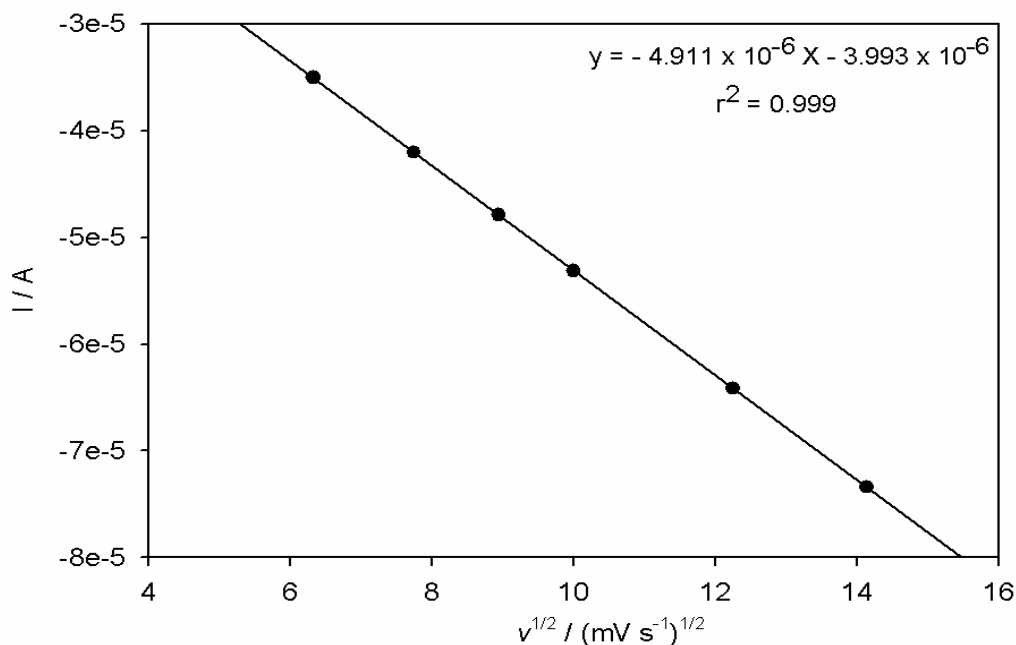


**Figure 36. A plot of root scan rate versus peak current.**

#### **5.1.1.1 Analytical application for anthracene detection.**

The cyclic voltammogram of PPyox/Ag-Au-modified electrode in acetonitrile and LiClO<sub>4</sub> (0.1 M) containing different concentrations of anthracene are shown in Figure 37. A calibration curve (Figure 38) based on the anodic peak heights from Figure 37, plotted against concentration, was found to be satisfactorily linear ( $r^2 = 0.995$ ) for analytical application of this sensor. The anodic peak potential of anthracene at the PPyox/Ag-Au film modified electrode was at about 1181 mV [72]. This was confirmed by the use of SWV in Figure 39 which showed similar results. Lower concentrations of anthracene were also determined using SWV (Figure 39 inset) and a calibration plot drawn as shown in Figure 40.

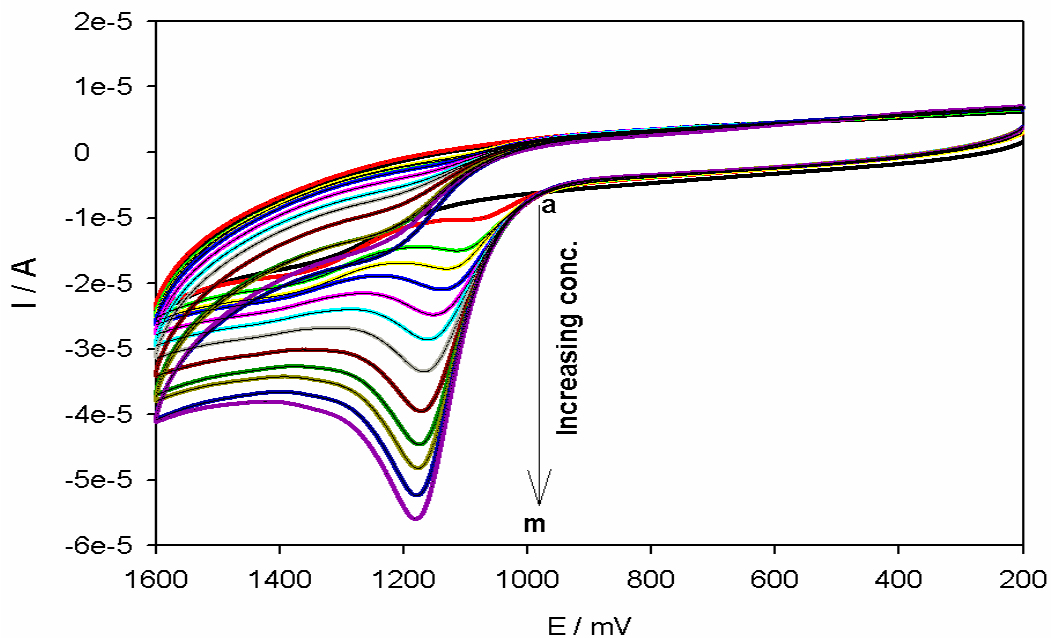


Figure 37. CV of PPyox/Ag-AuNPs/GCE in acetonitrile + 0.1 M LiClO<sub>4</sub> with different anthracene concentration: (a) 0, (b) 33, (c) 66 (d) 100 (e) 133 (f) 166 (g) 200 (h) 233 (i) 250 (j) 283 (k) 312 (l) 340 (m) 356  $\mu\text{M}$ ) at a scan rate of 100  $\text{mV s}^{-1}$ .

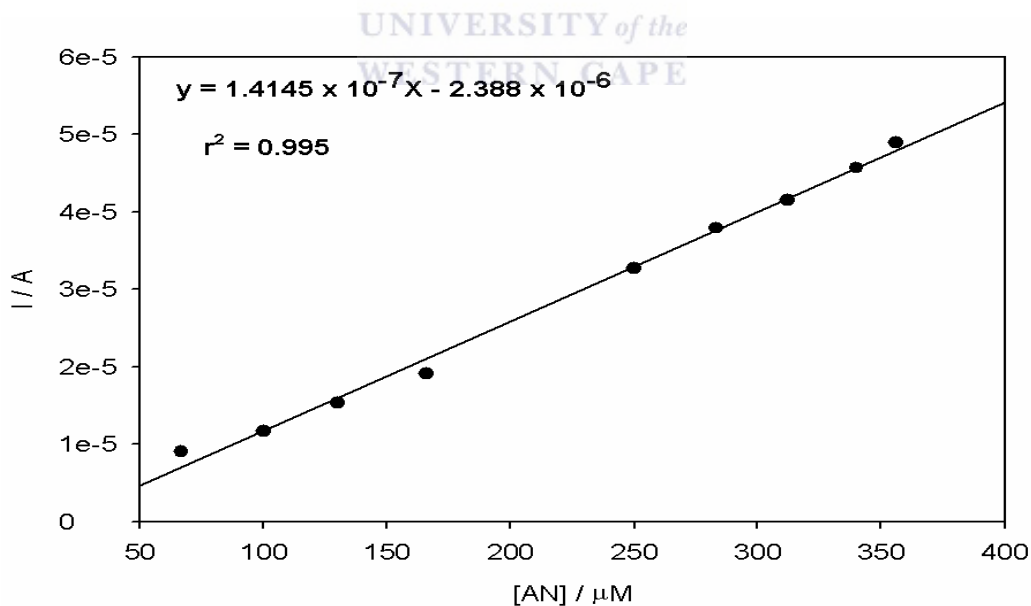


Figure 38. A calibration plot showing the relationship between oxidation current and concentration of anthracene.

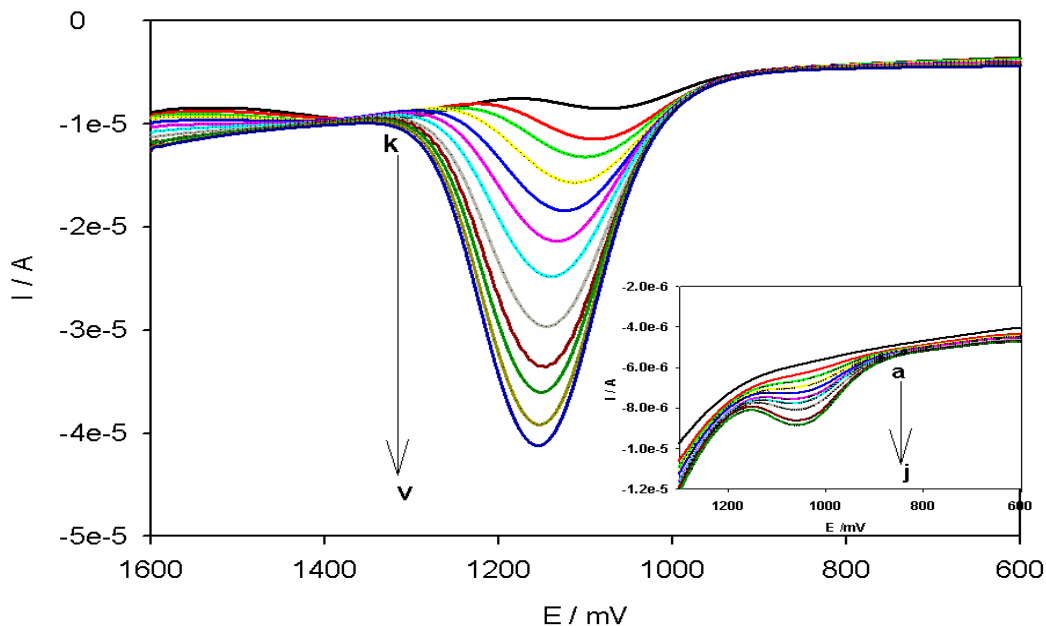


Figure 39. Anodic difference SWV of PPyox/Ag-AuNPs/GCE in acetonitrile + 0.1 M LiClO<sub>4</sub> with different anthracene concentration: (a) 0, (b) 3, (c) 6, (d) 10, (e) 13, (f) 16, (g) 20, (h) 23, (i) 26, (j) 28, (k) 33, (l) 66, (m) 100, (n) 133, (o) 166, (p) 200, (q) 233, (r) 250, (s) 283, (t) 312, (u) 340, (v) 356  $\mu$ M. Inset shows the curves at low concentrations.

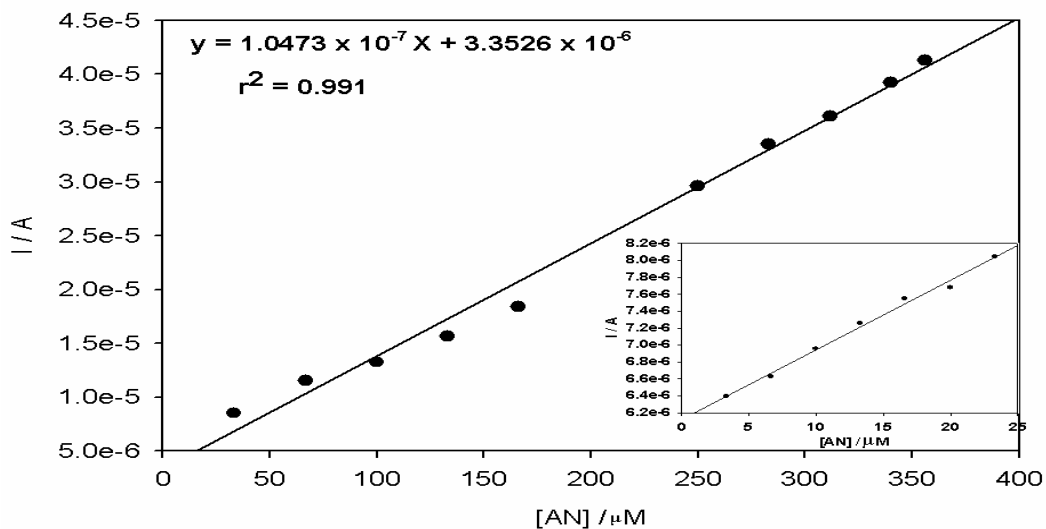
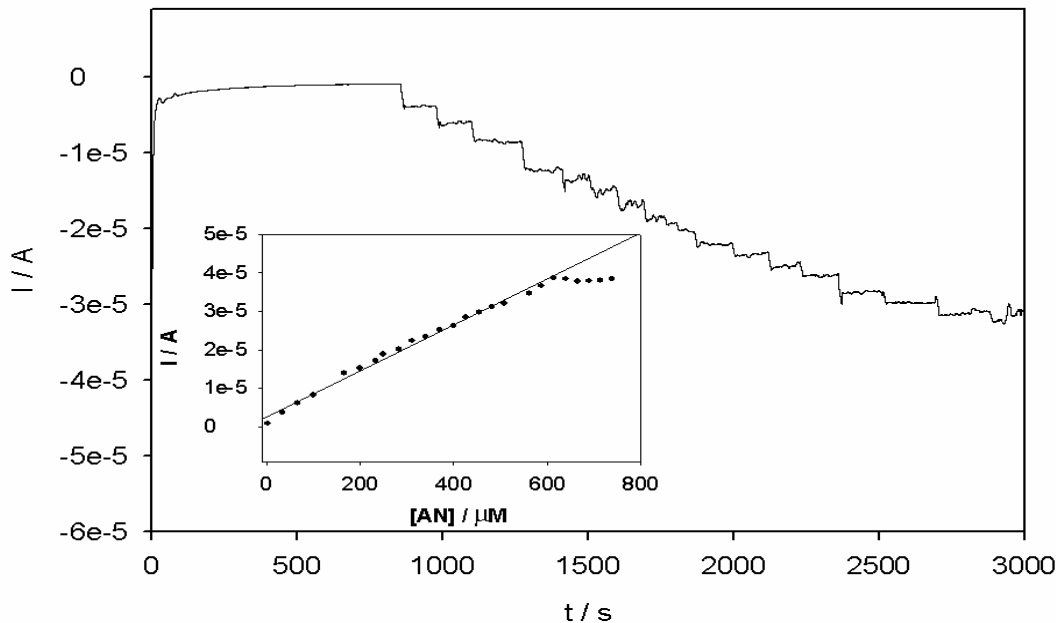


Figure 40. A calibration plot showing the relationship between current and concentration of anthracene. Inset shows a calibration plot at low concentration.

Based on the SWV measurements, a linear relationship between the anodic current and anthracene concentration was attained over the range of  $3.0 \times 10^{-6}$  to  $3.56 \times 10^{-4}$  with a correlation coefficient of 0.991. The limit of detection for anthracene from standard solutions, calculated as the concentration corresponding to the signal three times the standard deviation of blank measurements was  $1.69 \times 10^{-7}$  M.

While the above calibration was based on kinetic principle, it was also interesting to see how the electrode would perform under steady state condition. Figure 41 shows the steady state amperometry response of the sensor for successive additions of anthracene ( $3.0 \mu\text{M}$  each time) into the acetonitrile and  $0.1 \text{ M LiClO}_4$  solution sequentially. From the steady state amperogram (Figure 41), successive additions of AN resulted in favorable responses on the PPyox/Ag-AuNPs/GCE achieving steady state within 4 s. The linear dependence of current response on the AN concentration as shown in the calibration curve (Figure 41 inset) was linear in the range  $3.0 \times 10^{-6}$  to  $5.9 \times 10^{-4}$  M ( $r^2 = 0.992$ ).



**Figure 41.** Current-time plot for the electrochemical sensor response to successive addition of  $3.0 \mu\text{M}$  anthracene at a constant potential of  $1181 \text{ mV}$ . The measurements were carried out in a continuously stirred acetonitrile solution of  $\text{LiClO}_4$  ( $0.1 \text{ M}$ ). The inset shows a calibration plot of current against concentration.

#### 5.1.1.2. Interferences to AN detection.

During the over oxidation of pyrrole, higher density carbonyl groups such as  $>\text{C}=\text{O}$  and  $-\text{COO}^-$  can be generated on the backbone of the PPyox-film [11]. This is favorable for cation species (+) to be accumulated onto the film and then be catalytically oxidized at the electrode. Several metal cations are found in waste water thus the need to investigate how they affect the detection of the PAHs using the developed sensor. In the catalytic oxidation of anthracene, several interference substances have been reported. These substances include inorganic species such as  $\text{Na}^+$ ,  $\text{Cu}^{2+}$ ,  $\text{Fe}^{2+}$ ,  $\text{Mn}^{2+}$ ,  $\text{Cl}^-$ ,  $\text{SO}_4^{2-}$ , and  $\text{NO}_3^-$  [126]. Interference studies were therefore carried out with the above inorganic species. Figure 42 shows the SWV of the sensor in presence of anthracene and the interferences. The sensor in anthracene alone

generated a current of  $-2.706 \times 10^{-5}$  A while a mixture of anthracene and interferences showed a current of  $-2.627 \times 10^{-5}$  A upon addition of 1:1 quantity of the interferences and anthracene, with the anthracene concentration being  $3.12 \times 10^{-4}$  M. It was found that the addition of the interferences caused little decrease of the peak current and hence a negligible interference of 3.0% was observed. The inorganic species therefore were expected to cause no meaningful interference in the detection of anthracene.

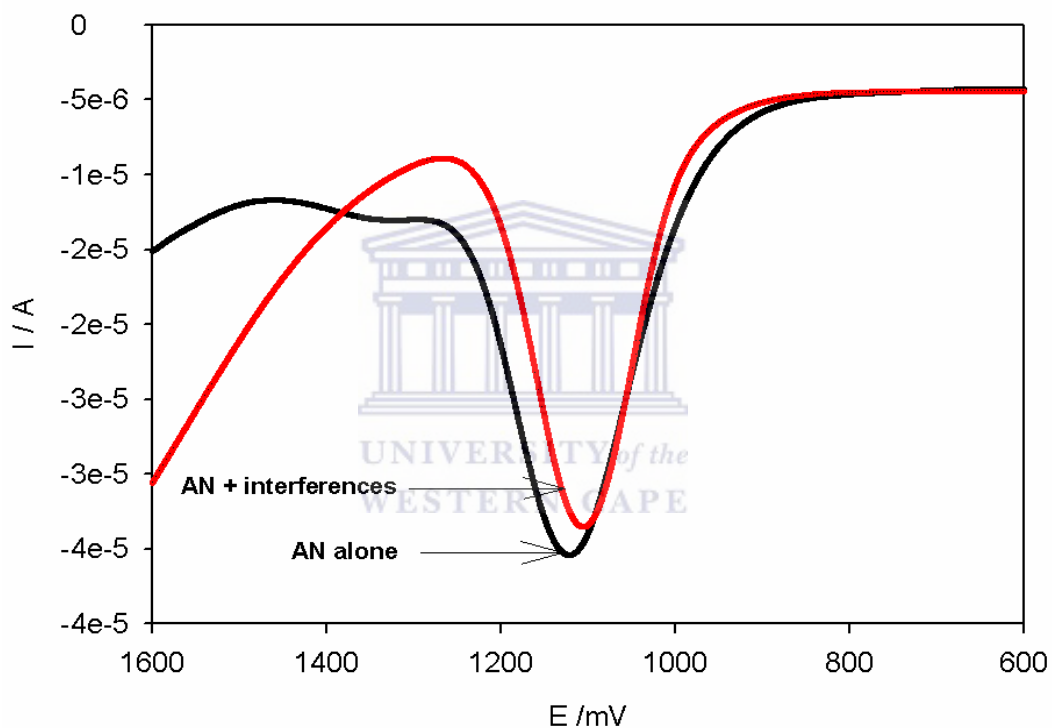


**Figure 42. SWV of PPyox/Ag-AuNPs/GCE in acetonitrile and 0.1 M LiClO<sub>4</sub> in presence of anthracene alone and a mixture of anthracene and interferences.**

### 5.1.1.3 Stability studies.

The stability of PPyox/Ag-AuNPs/GCE sensor was investigated by measuring the electrode response with  $3.56 \times 10^{-4}$  M anthracene every 4 days by SWV (Figure 43).

It was found that there was almost 19.26% decrease of the peak current response on

the modified electrode for  $3.56 \times 10^{-4}$  M after 2 weeks thus the modified electrode retained 80.74% of its initial response after it was kept in refrigerator at 4 °C for 12 days. This can be attributed to the excellent stability of the film.

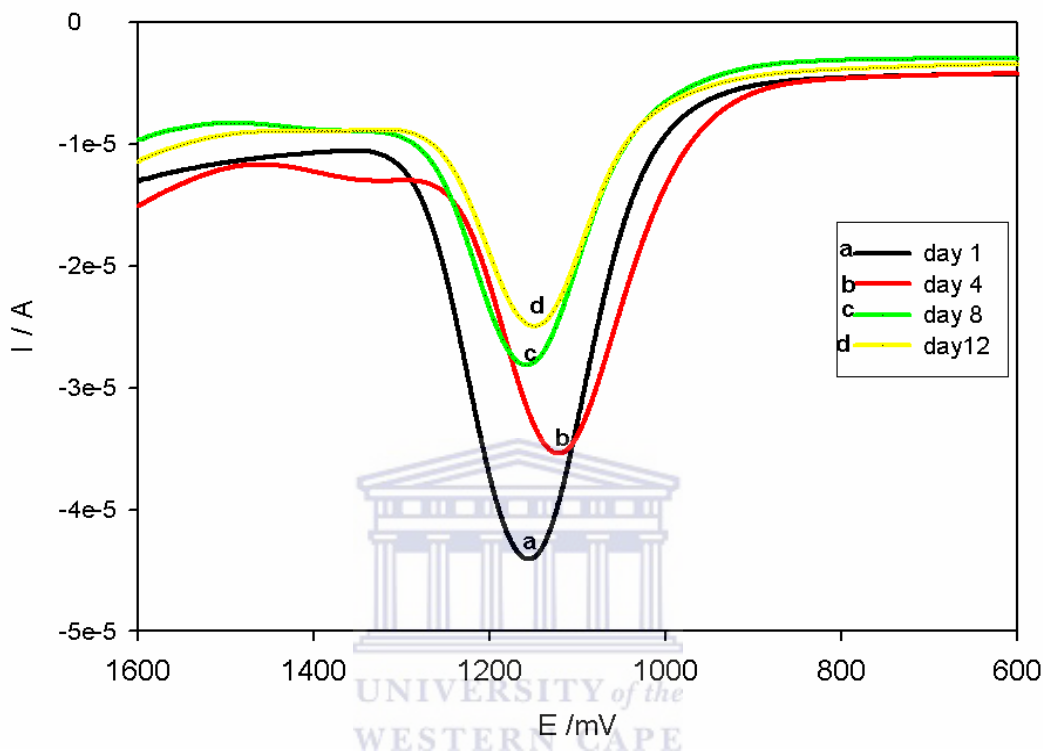


**Figure 43.** SWV of PPyox/Ag-AuNPs/GCE in acetonitrile and 0.1 M LiClO<sub>4</sub> in presence of anthracene ( $3.56 \times 10^{-4}$  M) at the 1<sup>st</sup> day, 4<sup>th</sup> day, 8<sup>th</sup> and 12<sup>th</sup> day.

#### 5.1.1.4. Reproducibility studies.

The stability and reproducibility are key elements of electrode performance. The reproducibility of the PPyox/Ag-Au nanoparticles modified electrode was investigated in the presence of  $3.56 \times 10^{-4}$  M anthracene in acetonitrile and 0.1 M LiClO<sub>4</sub>. Square wave voltammetric experiments were repeatedly performed 6 times with the same PPyox/Ag-Au nanoparticles modified electrode in the solution of  $3.56 \times 10^{-4}$  M anthracene. The relative standard deviation was 1.2% (n = 6) confirming that the results were reproducible.



### 5.1.2 Electrocatalytic oxidation of phenanthrene (PHE).

Comparative experiments on electrocatalytic oxidation of PHE were investigated using different electrodes. Compared with the response of PHE at bare GCE in acetonitrile containing  $2.5 \times 10^{-4}$  M PHE, PPyox/Ag-AuNPs/GCE exhibited much higher current response sensitivity towards the oxidation of phenanthrene. For control experiments, Ag-AuNPs/GCE and PPyox/GCE were used as working electrodes. The results indicated that the response sensitivity of PPyox/Ag-AuNPs/GCE towards phenanthrene electro oxidation was higher than those of bare GCE (Figure 44 **curve a**), Ag-AuNPs/GCE (Figure 44 **curve b**) and PPyox/GCE (Figure 44 **curve c**). It can be explained by the synergetic effect of Ag-Au alloy nanoparticles which were incorporated in the PPyox film and thus acted as nanoreactors facilitating electron transfer while the PPyox behaved like nanopores which enhanced adsorption of phenanthrene. Similar results were observed using SWV as shown in Figure 45.

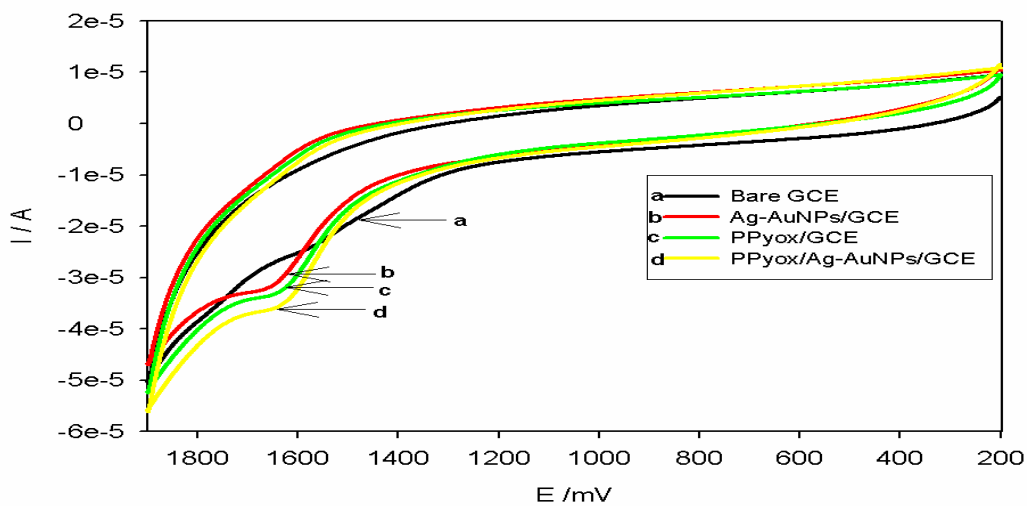


Figure 44. CV of  $2.5 \times 10^{-4}$  M PHE at bare GCE (curve a), Ag-AuNPs/GCE (curve b), PPyox/GCE (curve c) and PPyox/Ag-AuNPs/GCE (curve d) in acetonitrile and 0.1 M LiClO<sub>4</sub>.

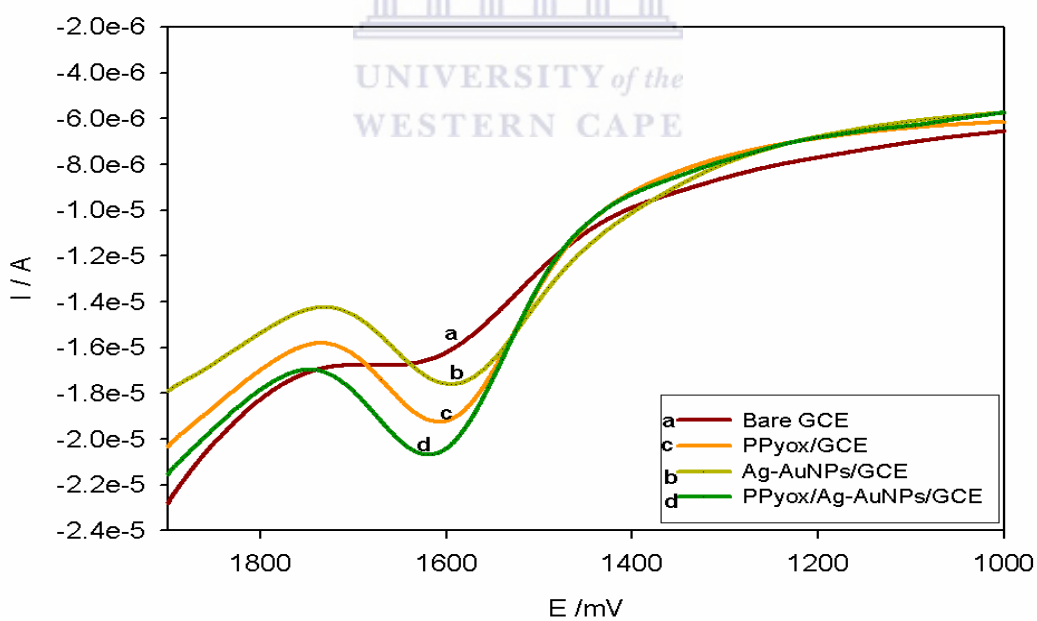
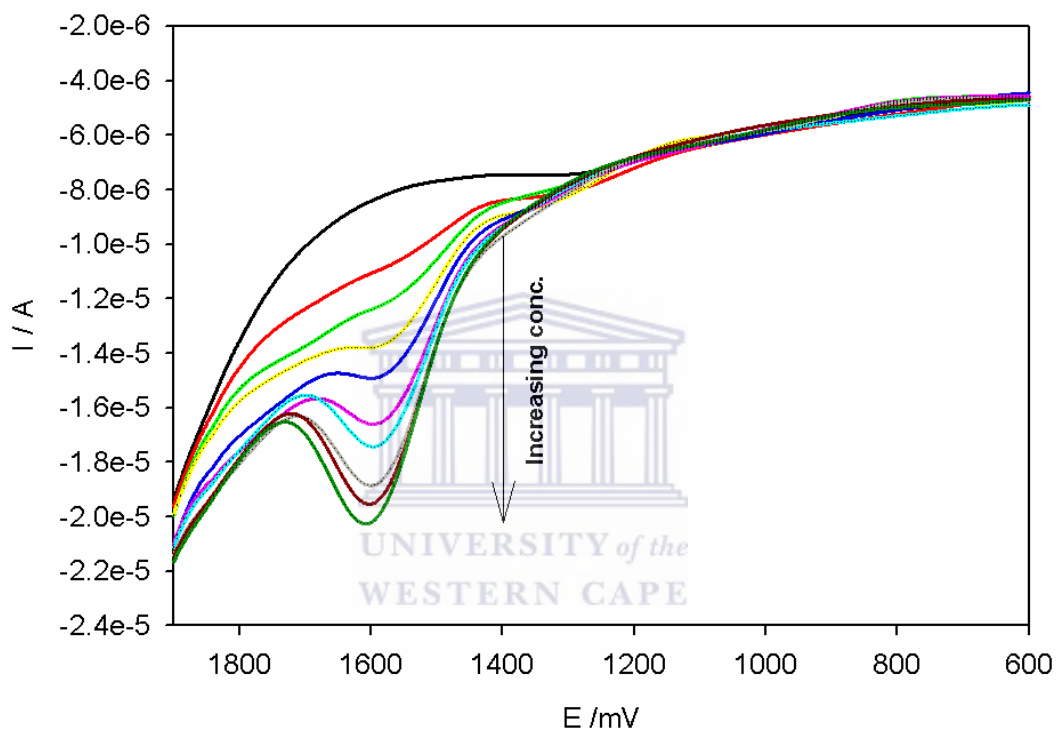
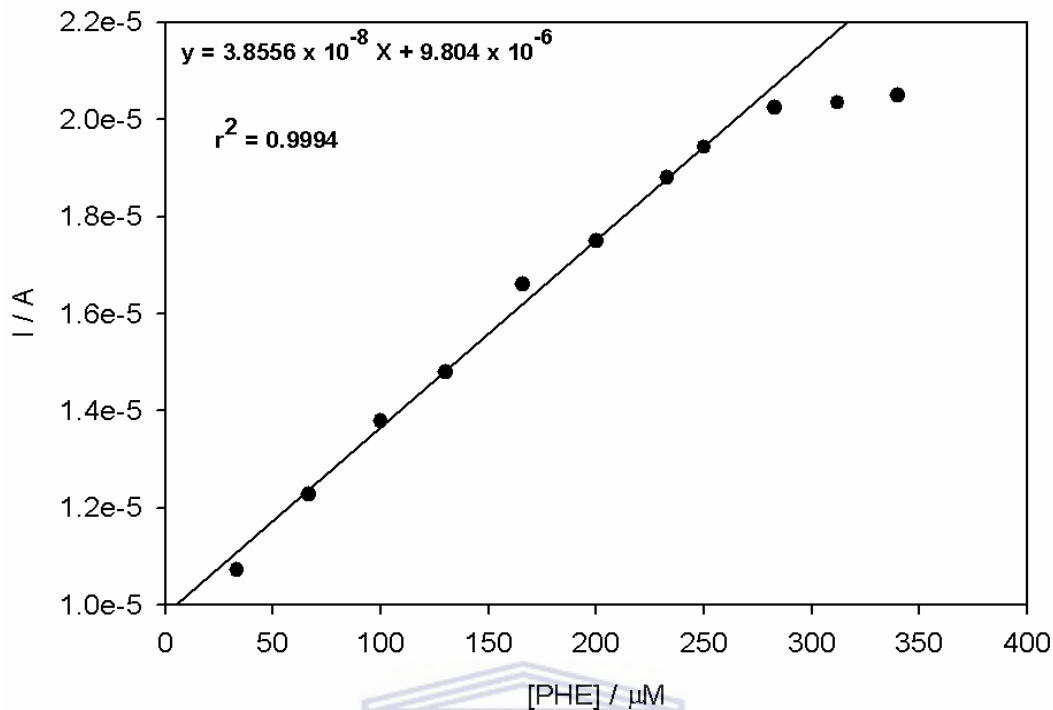


Figure 45. SWV of  $2.5 \times 10^{-4}$  M PHE at bare GCE (curve a), Ag-AuNPs/GCE (curve b), PPyox/GCE (curve c) and PPyox/Ag-AuNPs/GCE (curve d) in acetonitrile and 0.1 M LiClO<sub>4</sub>.

The SWV of the sensor at different concentrations of PHE is shown in Figures 46. The oxidation current displays a good linear response to the concentration of PHE ( $r^2 = 0.9994$ ) (Figure 47). A linear relationship between anodic current and PHE concentration was attained over the range of  $3.3 \times 10^{-5}$  to  $2.83 \times 10^{-4}$  M with detection limit of  $1.5983 \mu\text{M}$ ).



**Figure 46. Anodic difference SWV of PPyox/Ag-Au NPs/GCE in acetonitrile + 0.1 M LiClO<sub>4</sub> with different PHE concentrations: 0, 33, 66, 100, 133, 166, 200, 233, 250, 283  $\mu\text{M}$ ).**



**Figure 47. A calibration plot showing the relationship between oxidation current and concentration of PHE.**

The effect of potential scan rate was investigated as shown in Figure 48. The oxidation peak current increased with the increase in scan rate and exhibited a linear relation to the square root of the scan rate,  $v^{1/2}$ , (Figure 49) in the range from 20-80  $\text{mV s}^{-1}$ , with linear regression equation  $I_{pa}/A = -1.5735 \times 10^{-5} - 4.675 \times 10^{-6} v^{1/2}/(\text{mV s}^{-1})^{1/2}$  (correlation coefficient,  $r^2 = 0.996$ ), suggesting that the oxidation of PHE at the PPyox/Ag-AuNPs modified electrode was a diffusion controlled process.

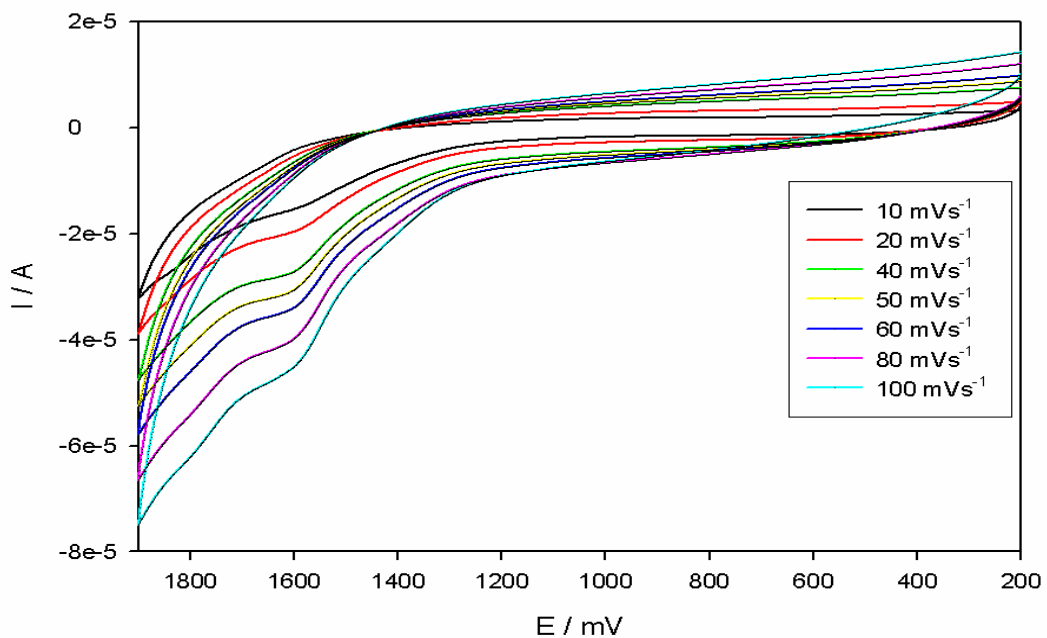


Figure 48. CV of PPyox/Ag-AuNPs/GCE in acetonitrile and 0.1 M LiClO<sub>4</sub> at different scan rates upon addition of  $2.33 \times 10^{-4}$  M PHE.

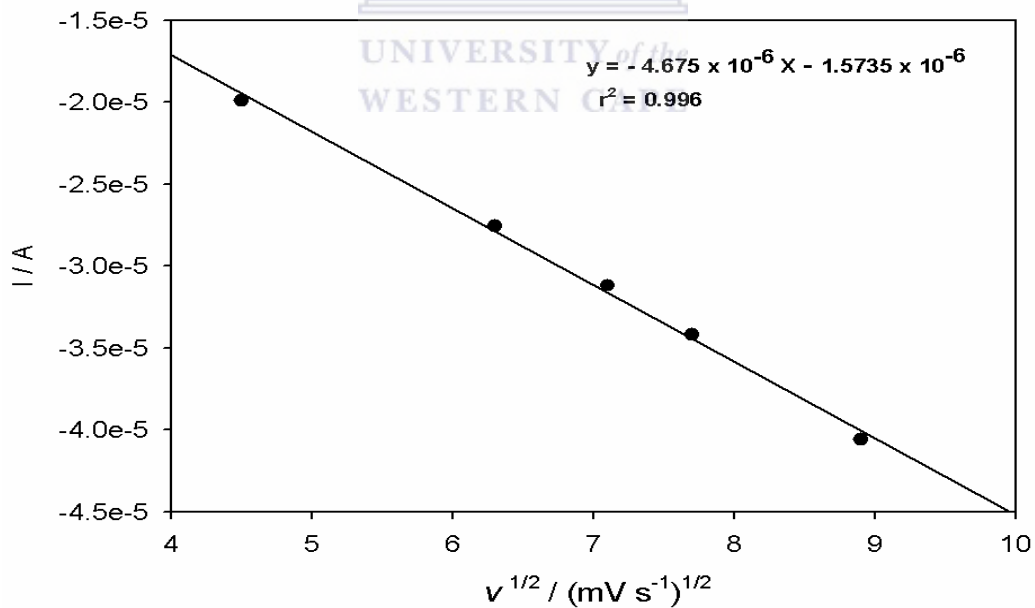


Figure 49. A plot of root scan rate versus peak current of PHE.

### ***5.1.2.1 Reproducibility studies.***

The reproducibility of the PPyox/Ag-Au nanoparticles modified electrode was investigated in the presence of  $2.5 \times 10^{-4}$  M PHE in acetonitrile and 0.1 M LiClO<sub>4</sub>. SWV experiments were performed 6 times with the same PPyox/Ag-Au nanoparticles modified electrode in a solution of  $2.5 \times 10^{-4}$  M PHE. The sensitivity remained almost the same with a relative standard deviation of 5.06% at all the six times confirming that the results were reproducible.

### ***5.1.2.2 Interference studies.***

In the catalytic oxidation of phenanthrene, several interference substances have been reported. These substances include inorganic species such as Na<sup>+</sup>, Cu<sup>2+</sup>, Fe<sup>3+</sup>, Mn<sup>2+</sup>, Cl<sup>-</sup>, SO<sub>4</sub><sup>2-</sup>, and NO<sub>3</sub><sup>-</sup> [126]. Interference studies were carried out with the above inorganic species. Using SWV measurements, PHE alone generated a current of  $-4.824 \times 10^{-6}$  A while a mixture of PHE and interferences generated  $-4.723 \times 10^{-6}$  A upon addition of 1:1 of the interferences when the PHE concentration was  $2.5 \times 10^{-4}$  M. It was found that the addition of the interferences caused little decrease of the anodic peak current and hence a negligible interference of 2.1% was observed as shown in Figure 50.

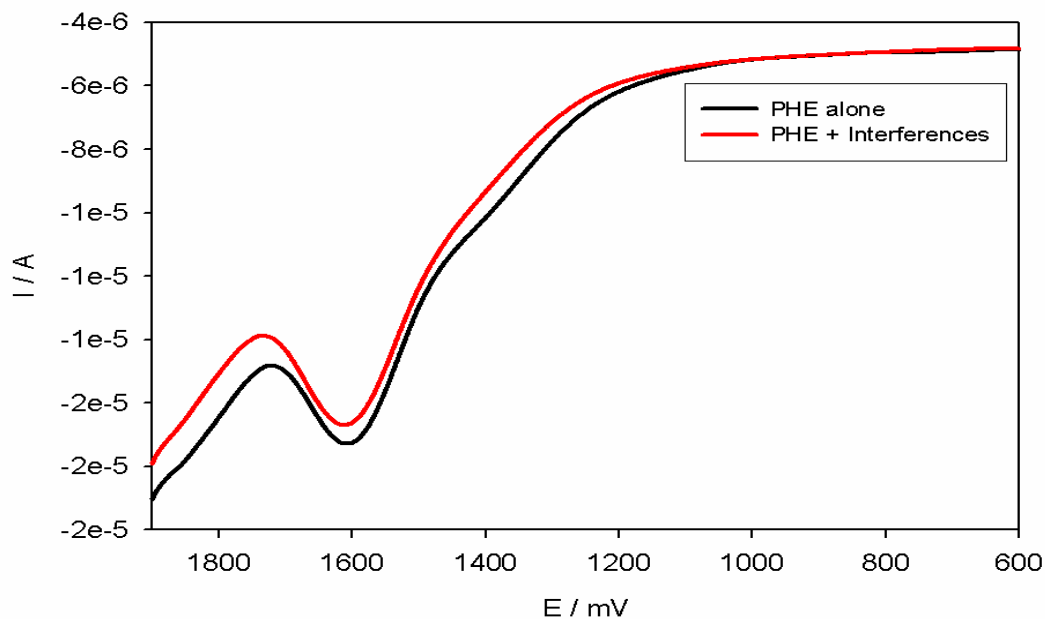


**Figure 50. SWV of PPyox/Ag-AuNPs/GCE in acetonitrile and 0.1 M LiClO<sub>4</sub> in presence of PHE alone and a mixture of PHE and interferences.**

### 5.1.3. Electrocatalytic oxidation of AN and PHE.

PHE and AN have similar structures and properties. Their simultaneous determination was done using the developed sensor (PPyox/Ag-AuNPs/GCE). Figure 51 shows cyclic voltammograms of AN (**curve a**), PHE (**curve b**) and blank (acetonitrile and 0.1M LiClO<sub>4</sub>) (**curve c**) at a scan rate of 50 mV s<sup>-1</sup> in acetonitrile and 0.1 M LiClO<sub>4</sub>. From Figure 51, one oxidation peak was observed for AN (**curve a**) and PHE (**curve b**), respectively. The modified electrode showed no response when no addition of AN and PHE was done (**curve c**). It is noteworthy that the oxidation peaks for the PHE and AN were at distinct potentials.

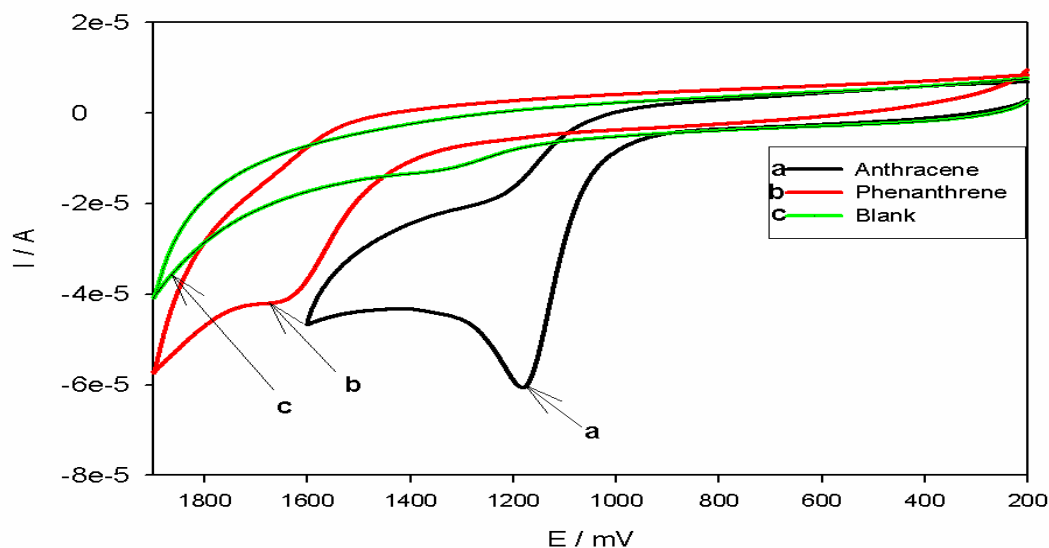


**Figure 51.** Voltammetric curves of  $3.56 \times 10^{-4}$  M solution of AN (curve a),  $2.30 \times 10^{-4}$  M solution of PHE (curve b) and 0.1 M LiClO<sub>4</sub> in acetonitrile (curve c) using PPyox/Ag-AuNPs/GCE.

For simultaneous oxidation of AN and PHE, a mixture of PHE and AN ( $2.30 \times 10^{-4}$  M each) were spiked into the electrolyte and acetonitrile and mixed thoroughly by the use of a magnetic stirrer. Two peaks were obtained corresponding to the oxidation of AN and PHE respectively as shown in Figure 52 (peaks a and b). Similar results were obtained using SWV as shown in Figure 53. It was evident that the voltammogram peaks i.e. both CV and SWV of the mixture solution of AN and PHE correlated well with that of their individual solutions (Figure 51). It is noteworthy that, elimination of the fouling of the electrode surface by the oxidation products could be achieved and the precise oxidation of AN in the presence of PHE is possible at the PPyox/Ag-AuNPs/GCE. The voltammetric signals of AN and PHE remained unchanged in the subsequent sweeps, indicating that the PPyox/Ag-AuNPs modified electrode does not undergo surface fouling.



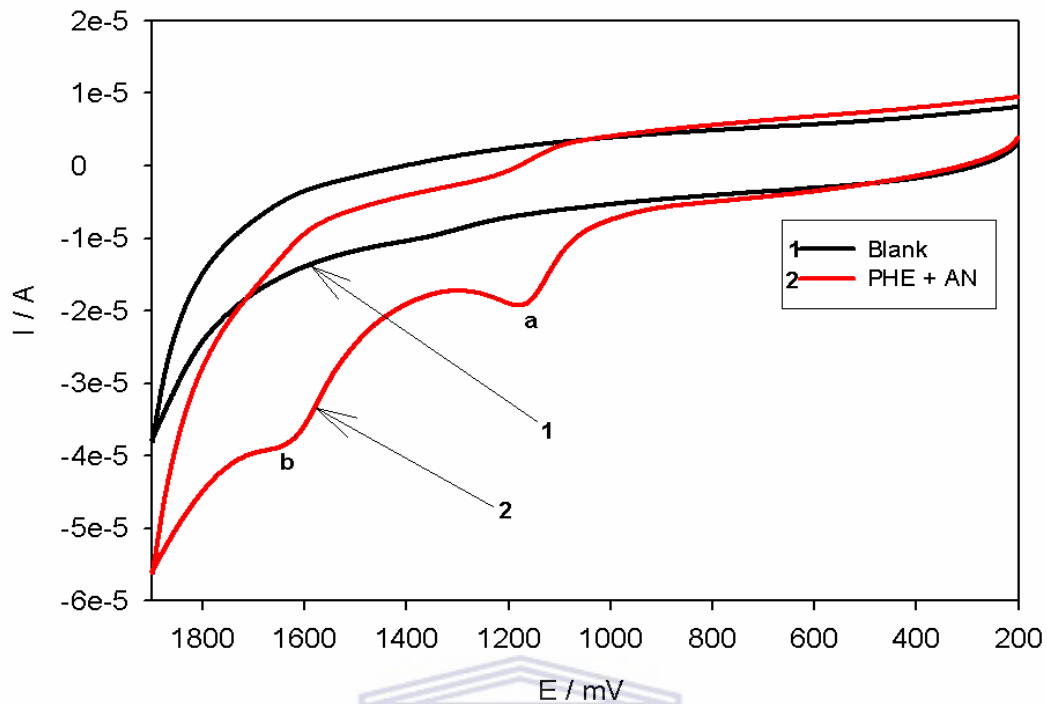


Figure 52. CVs of PPyox/Ag-AuNPs/GCE in acetonitrile and 0.1 M LiClO<sub>4</sub> (blank) (1) and a mixture of AN and PHE (2) at a scan rate of 50 mV s<sup>-1</sup>.

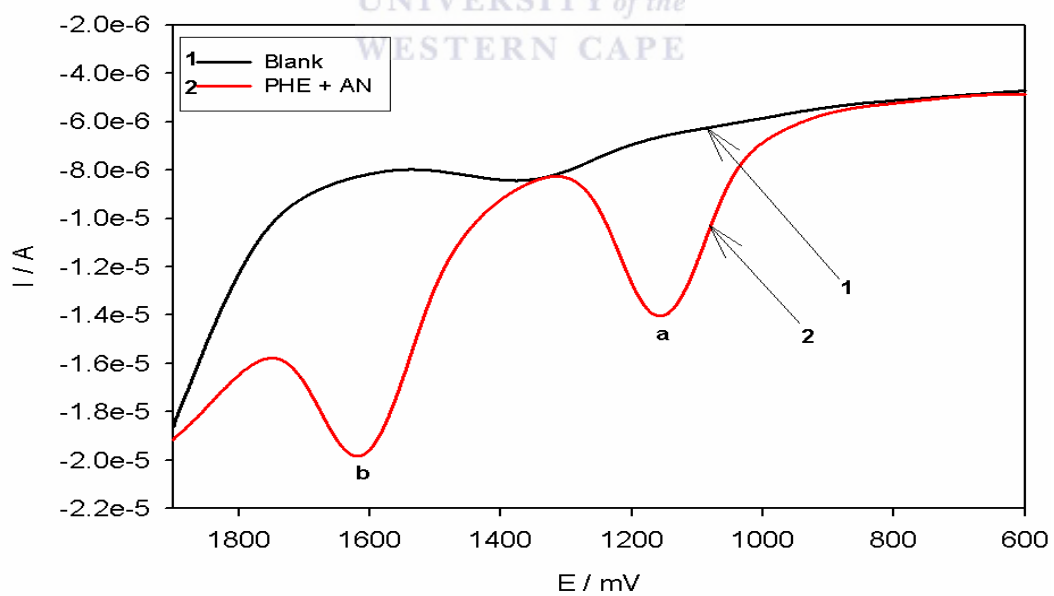


Figure 53. SWVs of PPyox/Ag-AuNPs/GCE in acetonitrile and 0.1 M LiClO<sub>4</sub> (blank) (1) and a mixture of AN and PHE (2).

### 5.1.3.1 Effect of scan rate on the peak current in the binary mixture of AN and PHE.

Figure 54 shows the cyclic voltammograms for the binary mixtures of  $2.30 \times 10^{-4}$  M AN and  $2.30 \times 10^{-4}$  M PHE in 0.1 M LiClO<sub>4</sub> and acetonitrile at the PPyox/Ag-AuNPs modified electrode at different scan rates. The oxidation peak potentials of the two compounds were observed to shift positively with the increase in scan rate. In addition, the oxidation peak current for the oxidation of AN exhibited a linear relation to the square root of the scan rate,  $v^{1/2}$ , in the range from 20 to 450 mV s<sup>-1</sup>, with the linear regression equation  $I_{pa}/A = -1.446 \times 10^{-6} - 8.604 \times 10^{-7} v^{1/2}$  (mV s<sup>-1</sup>)<sup>1/2</sup> (correlation coefficient,  $r^2 = 0.9981$ ), suggesting that the oxidation of AN at the modified electrode was diffusion-controlled process (Figure 55). Simultaneously, the oxidation peak current for the oxidation of PHE also exhibited a linear relation to the square root of the scan rate,  $v^{1/2}$ , in the range from 20 to 450 mV s<sup>-1</sup>, with the linear regression equation  $I_{pa}/A = -4.115 \times 10^{-6} - 2.826 \times 10^{-6} v^{1/2}$  (mV s<sup>-1</sup>)<sup>1/2</sup> (correlation coefficient,  $r^2 = 0.9995$ ), suggesting that the oxidation of PHE at the modified electrode was also a diffusion-controlled process (Figure 56).

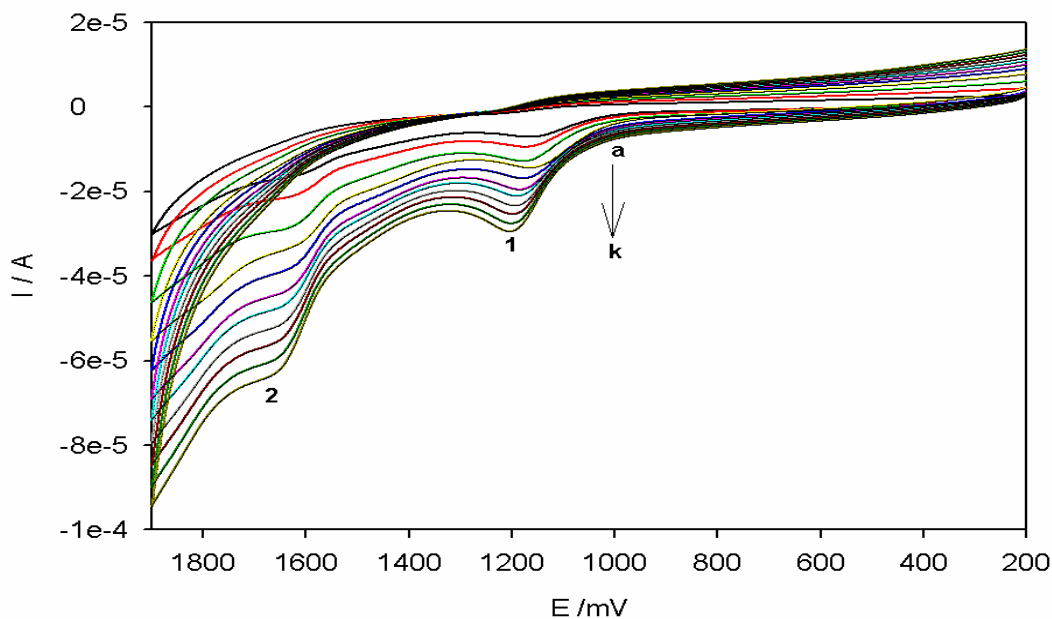


Figure 54. CVs for the binary mixtures of  $2.30 \times 10^{-4}$  M AN and  $2.30 \times 10^{-4}$  M PHE in 0.1 M LiClO<sub>4</sub> and acetonitrile at the PPyox/Ag-AuNPs/GCE at different scan rates: (a)  $20 \text{ mV s}^{-1}$  (b)  $40 \text{ mV s}^{-1}$  (c)  $80 \text{ mV s}^{-1}$  (d)  $100 \text{ mV s}^{-1}$  (e)  $150 \text{ mV s}^{-1}$  (f)  $200 \text{ mV s}^{-1}$  (g)  $250 \text{ mV s}^{-1}$  (h)  $300 \text{ mV s}^{-1}$  (i)  $350 \text{ mV s}^{-1}$  (j)  $400 \text{ mV s}^{-1}$  (k)  $450 \text{ mV s}^{-1}$ .

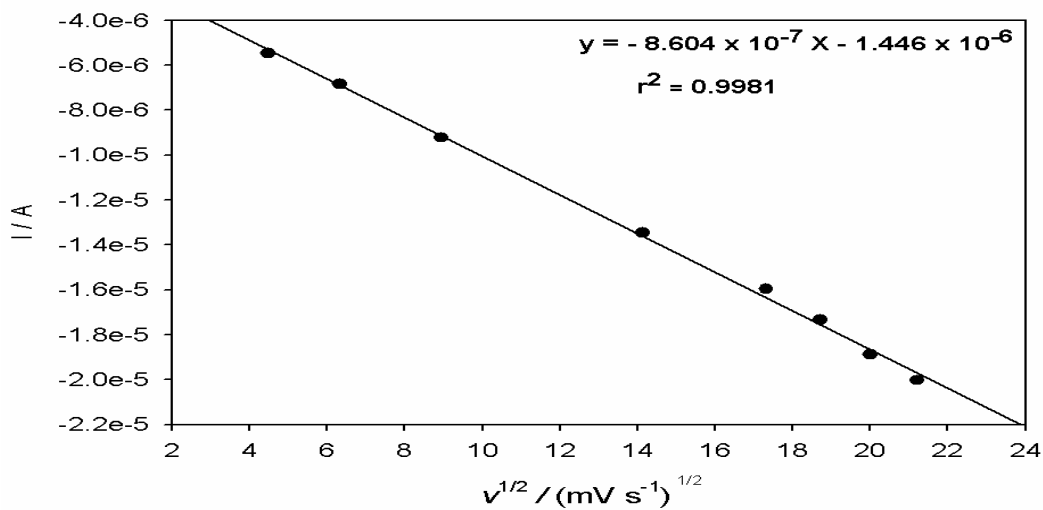
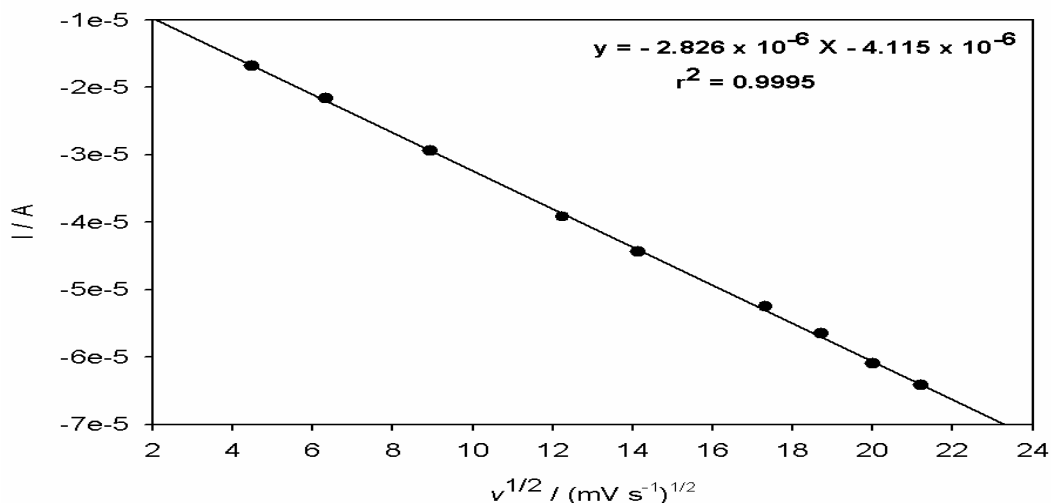


Figure 55. A plot of root scan rate versus peak current of AN.



**Figure 56. A plot of root scan rate versus peak current of PHE.**

### 5.1.3.2. Simultaneous determination of AN and PHE.

A series of mixture standard solutions of PHE and AN, in which the concentration of one component was varied and the other was fixed were prepared and determined. Figure 57 shows the SWV obtained when the concentration of PHE was kept constant and the concentration of AN was increased successively. The oxidative peak current for AN increased linearly with the increase in AN concentration in the range of  $3.0 \times 10^{-5}$  M to  $3.12 \times 10^{-4}$  M. The linear regression equation was  $I_{pa}/A = -9.268 \times 10^{-7} + 2.736 \times 10^{-8} C / \mu M$  (correlation coefficient,  $r^2 = 0.9987$ ) (see Figure 58) and the detection limit was  $23.0 \mu M$  in the presence of  $2.30 \times 10^{-4}$  M PHE. It can be observed that, with increasing concentration of AN, the amperometric current increased (Figure 57, peak 1) while that of PHE (peak 2) kept almost constant. Thus it can be confirmed that the responses of AN and PHE at the modified electrode are independent.

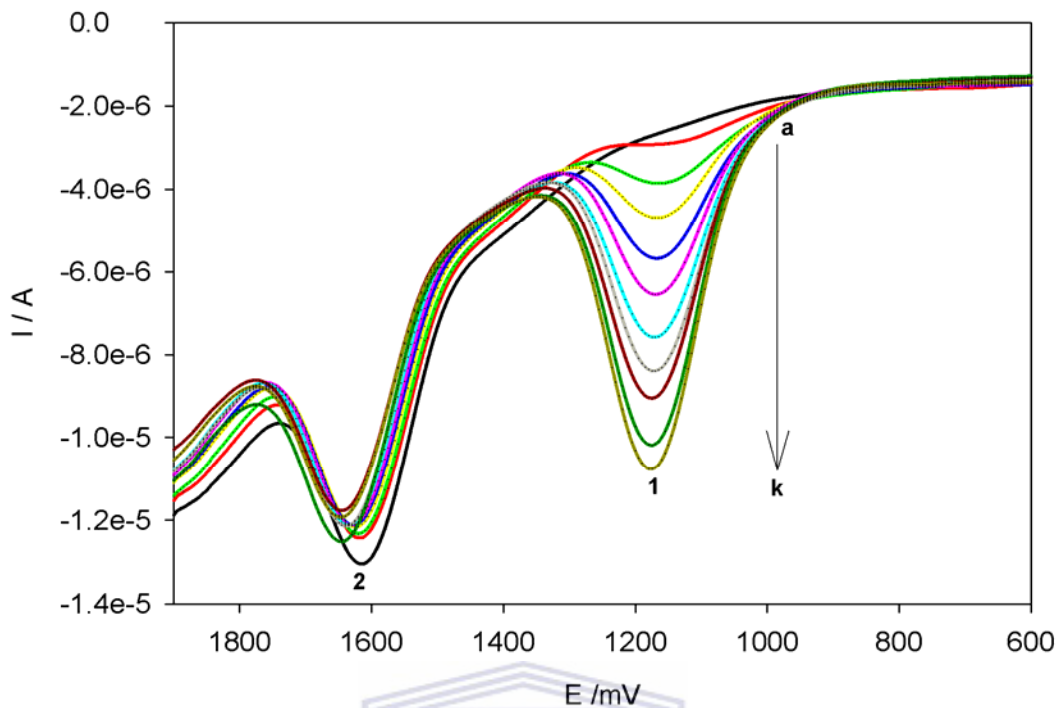


Figure 57. SWV for the binary mixtures of AN and PHE at PPyox/Ag-Au NPs/GCE in 0.1 M LiClO<sub>4</sub> and acetonitrile, [PHE] was kept constant and [AN] was changed (i.e. [AN]: (a) 0 (b) 30 (c) 60 (d) 100 (e) 130 (f) 166 (g) 200 (h) 230 (i) 250 (j) 280 (k) 312 μM).

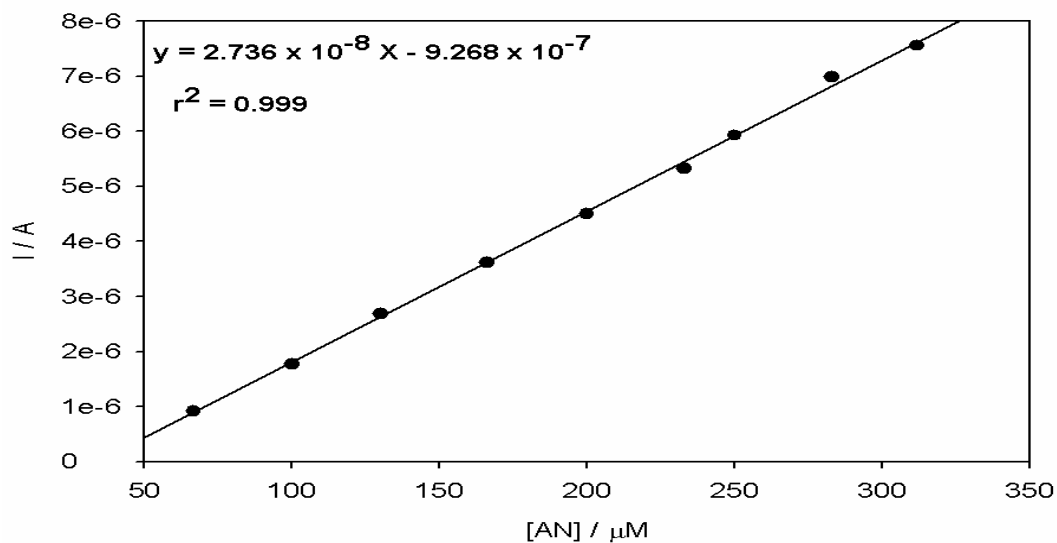
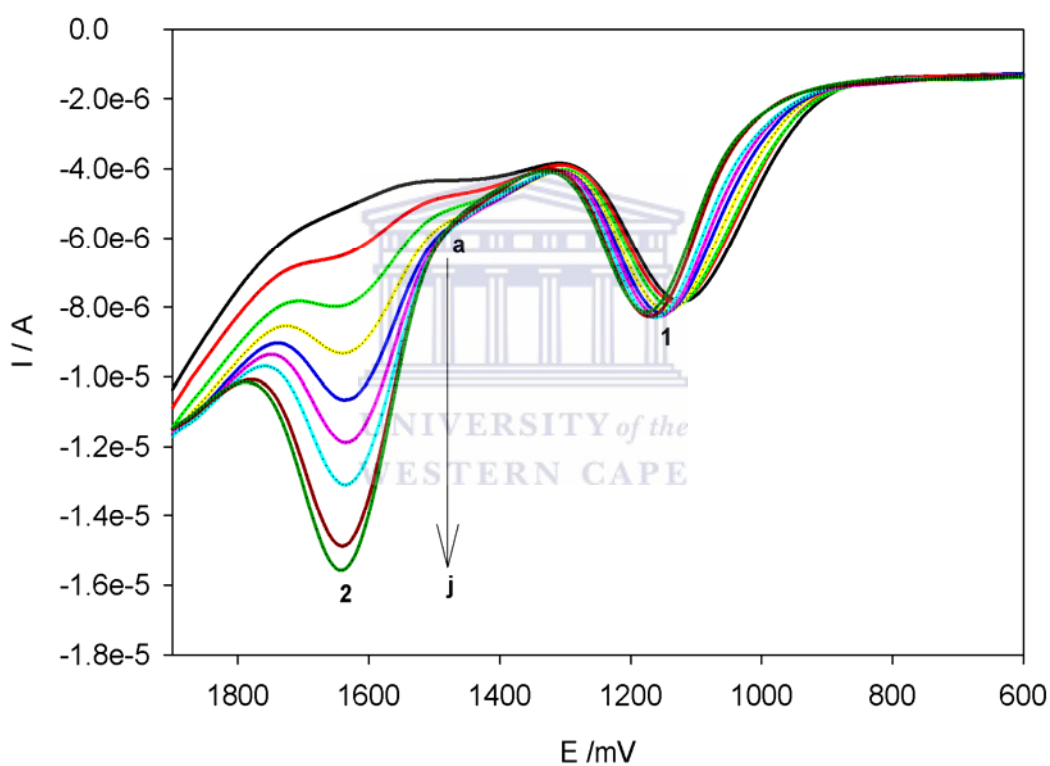
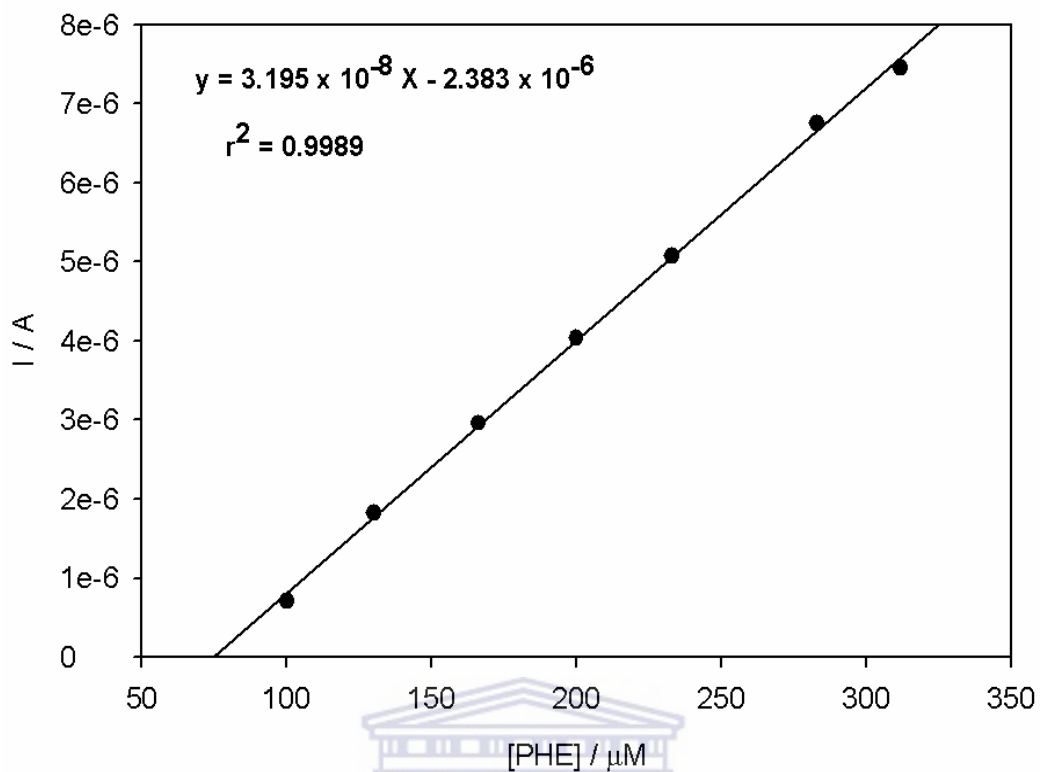


Figure 58. A calibration plot of concentration versus peak current of AN.

When the concentration of AN was kept constant and PHE concentration increased, there was a peak current increase with increase in concentration of PHE (Figure 59 peak 2) while that of AN kept almost constant (Figure 59 peak 1). The oxidative peak current increased linearly in the range of  $3.0 \times 10^{-5}$  M to  $2.80 \times 10^{-4}$  M. The linear regression equation was  $I_{pa}/A = -2.383 \times 10^{-6} + 3.195 \times 10^{-8} C / \mu\text{M}$  (correlation coefficient,  $r^2 = 0.9989$ ) (Figure 60) and the detection limit was  $24.0 \mu\text{M}$  in the presence of  $2.30 \times 10^{-4}$  M AN.



**Figure 59.** SWV for the binary mixtures of AN and PHE at PPyox/Ag-Au NPs/GCE in 0.1 M LiClO<sub>4</sub> and acetonitrile, [AN] was kept constant and [PHE] was changed (i.e. [PHE]: (a) 0 (b) 30 (c) 60 (d) 100 (e) 130 (f) 166 (g) 200 (h) 230 (i) 250 (j) 280  $\mu\text{M}$ ).



**Figure 60. A calibration plot of concentration versus peak current of PHE.**

Figure 61 represents the SWV measurements at increasing concentrations of AN and PHE. As can be seen, there was peak enhancement upon addition of both AN (Figure 61 peak 1) and PHE solutions (Figure 61 peak 2).

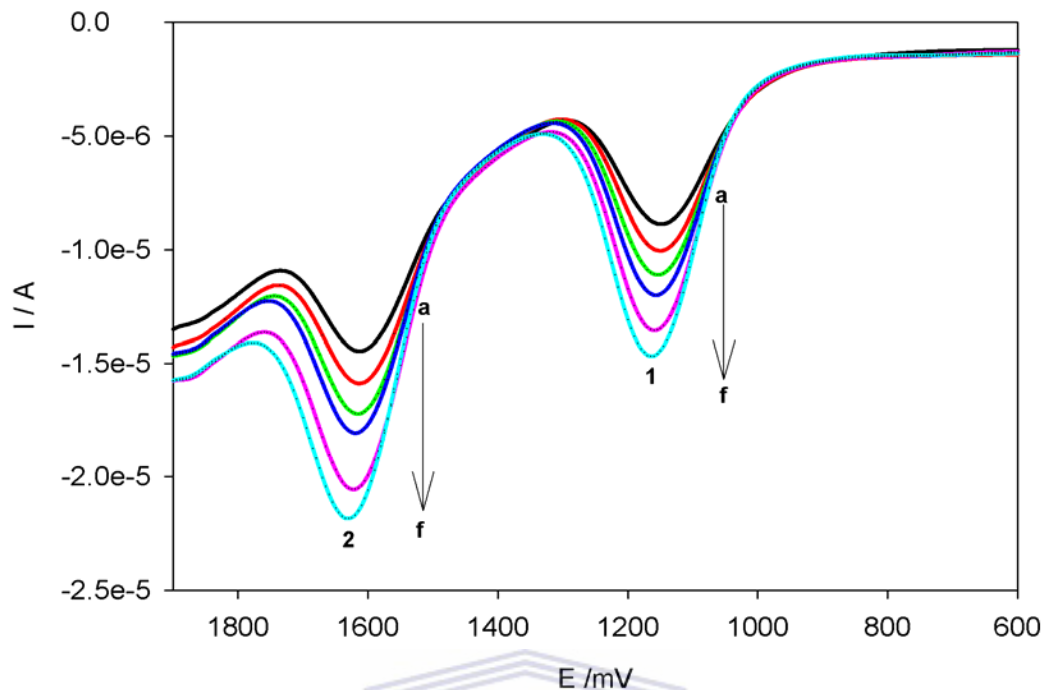


**Figure 61.** SWV for the binary mixtures of AN and PHE at PPyox/Ag-Au NPs/GCE in 0.1 M LiClO<sub>4</sub> and acetonitrile, at increasing [AN] and [PHE] (i.e. (a) 250 (b) 280 (c) 312 (d) 340 (e) 356 (f) 380  $\mu$ M).

It can be observed that the sensor was able to simultaneously detect AN and PHE in a mixture and that increasing the concentration of one does not affect the detection of the other. Thus, the responses of AN and PHE at the developed sensor are independent and that it showed excellent sensitivity, selectivity and antifouling properties.

#### 5.1.4 Determination of pyrene (Py).

The PPyox/Ag-AuNPs/GCE sensor was used to detect pyrene which is one of the known teratogenic, carcinogenic and mutagenic polyaromatic hydrocarbons. Figure 62 shows the bare and the modified electrodes in the presence of  $2.80 \times 10^{-4}$  M pyrene. A remarkable increase in oxidation current can be seen at the PPyox/Ag-



AuNPs/GCE (**curve d**) compared to the other modified electrodes. This demonstrated the cooperative effect of PPyox and Ag-Au nanoparticles in the electrocatalytic oxidation of pyrene.

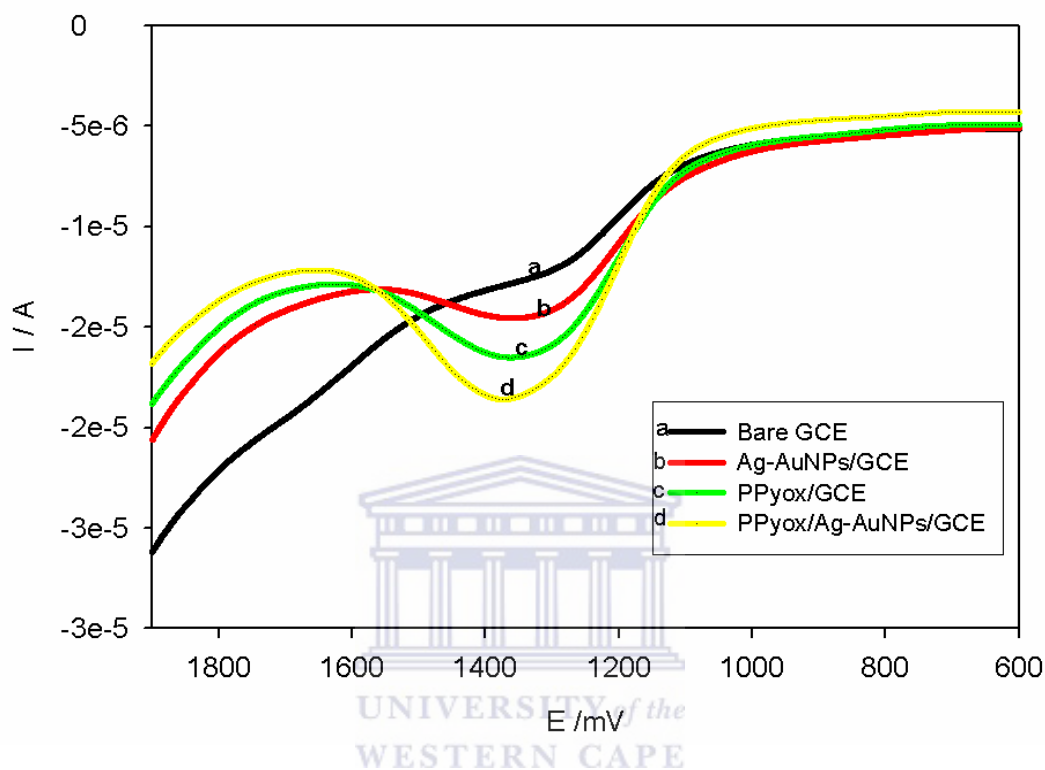


**Figure 62.** SWV of  $2.80 \times 10^{-4}$  M pyrene at bare/GCE (curve a), Ag-AuNPs/GCE (curve b), PPyox/GCE (curve c) and PPyox/Ag-AuNPs/GCE (curve d) in acetonitrile and 0.1 M LiClO<sub>4</sub>.

SWV measurements at increasing concentration of pyrene are shown in Figure 63. After pyrene was added in the acetonitrile and 0.1 M LiClO<sub>4</sub>, the peak current increased obviously. A calibration curve of oxidation peak current and concentration of pyrene was plotted (Figure 64) with a linear regression equation of  $I_{pa}/A = 9.8834 \times 10^{-6} + 5.302 \times 10^{-8} C / \mu\text{M}$  (correlation coefficient,  $r^2 = 0.997$ ). A linear relationship between anodic current and pyrene concentration was attained over the range of  $3.3 \times 10^{-5}$  to  $1.66 \times 10^{-4}$  M with a detection limit of 2.7  $\mu\text{M}$ .

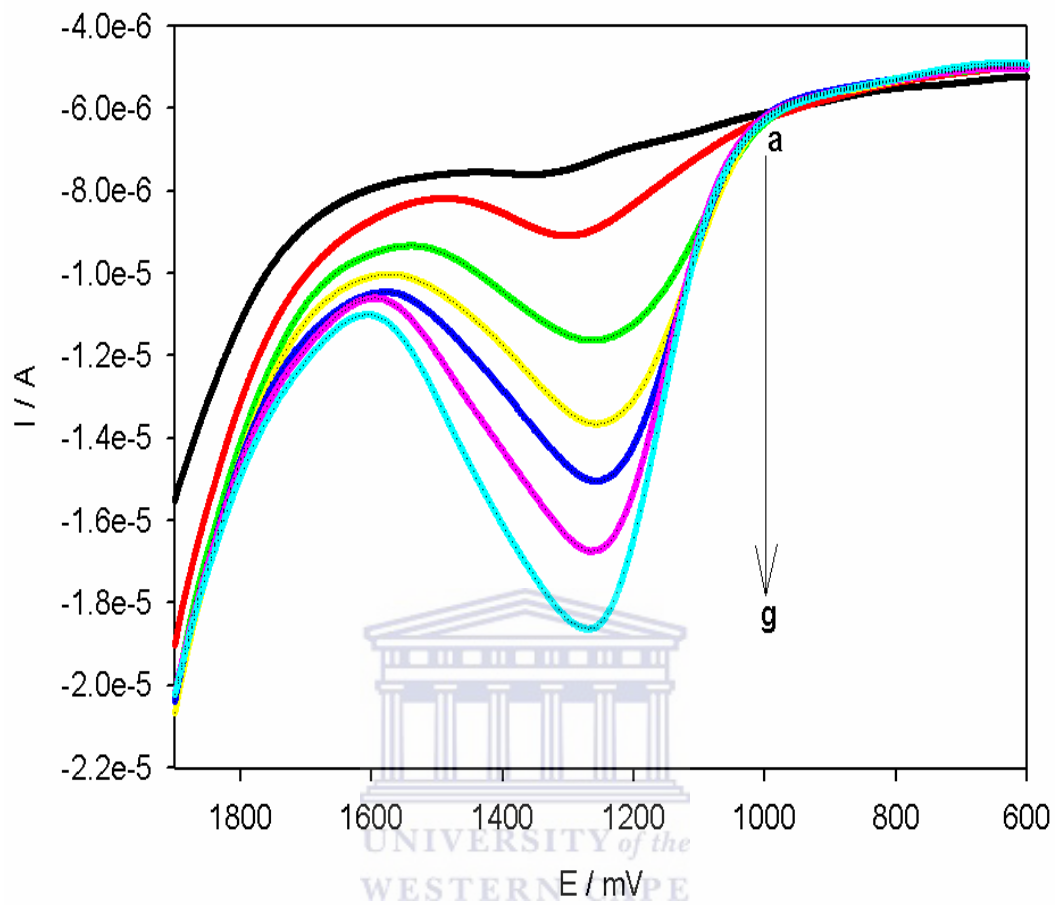


**Figure 63. SWV of PPyox/Ag-AuNPs/GCE at increasing concentration of pyrene (a) 0 (b) 10 (c) 33 (d) 66 (e) 100 (f) 130 (g) 166  $\mu M$ ).**

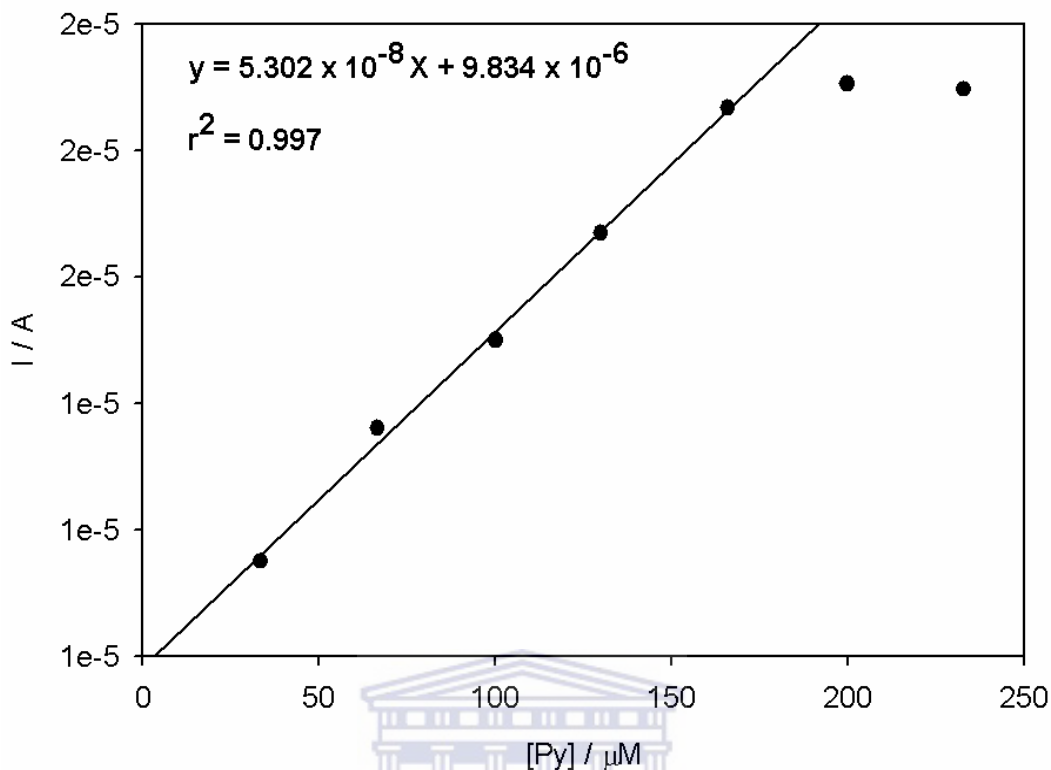


**Figure 64. A calibration plot of current verses concentration of pyrene**

UNIVERSITY of the  
WESTERN CAPE

#### **5.1.4.1 Reproducibility.**

The reproducibility of the PPyox/Ag-Au nanoparticles modified electrode was investigated in the presence of  $2.80 \times 10^{-4}$  M pyrene in acetonitrile and 0.1 M LiClO<sub>4</sub>. SWV experiments were performed for 6 times with the same PPyox/Ag-Au nanoparticles modified electrode. The sensitivity remained almost the same with a relative standard deviation (R.S.D) of 8.16% at all the six times confirming that the results were reproducible. The results demonstrated that the PPyox/Ag-AuNPs/GCE would improve both the sensitivity and reproducibility for the determination of pyrene using SWV.

## CHAPTER 6.

### 6.0 CONCLUSION AND RECOMMENDATIONS

#### 6.1 Conclusion

Highly catalytic, stable and well dispersed Ag-Au alloy nanoparticles were successfully prepared by the reduction of  $\text{HAuCl}_4$  and  $\text{AgNO}_3$  with sodium citrate. The alloy formation was confirmed by optical absorption spectroscopy and TEM. Consequently, overoxidized-polypyrrole was electrochemically synthesized and characterized by electrochemical methods. A novel electrochemical sensor was successfully fabricated based on the construction of nano-porous overoxidized-polypyrrole (PPyox) template- deposited Ag-Au alloy nanoparticles which formed a composite nano-electrode sensor, PPyox/Ag-AuNPs/GCE. The sensor exhibited a strong electrocatalytic activity towards the oxidation of anthracene, phenanthrene and pyrene. Moreover, the modified electrode with antifouling properties was able to simultaneously detect anthracene and phenanthrene. This makes the method better compared to the immunoassay techniques reported in literature.

In SWV determination, lower detection limits of anthracene, phenanthrene and pyrene were estimated to be about  $1.69 \times 10^{-7}$  M,  $1.59 \times 10^{-6}$  M and  $2.70 \times 10^{-6}$  M, respectively. Although these detection limits are slightly higher than those obtained using High performance Liquid Chromatography (HPLC) and Gas Chromatography (GC) techniques, they are within the concentration range of polyaromatic hydrocarbons (PAHs) in contaminated waste water [13]. The work presented opens an entirely new approach in the detection of PAHs by the use of polymers coupled with

alloy nanoparticles leading to the development of a simple, cheap, less time consuming and environmentally friendly electrochemical method with antifouling properties and lower detection limits.

## **6.2 Future work and Recommendation:**

- My thesis opens up an entirely new approach in the application of electroanalytical techniques for the detection of PAHs by the use of polymers coupled with alloy nanoparticles. Though, I used Ag-Au alloy nanoparticles for my work, future work to further establish how other alloy nanoparticles would behave is worthwhile.
- Further optimization of this method and its application in the detection of anthracene, phenanthrene and pyrene in waste water.
- Chemical methods were used in the synthesis of the alloy nanoparticles. Further investigation of the use of electrochemical method of synthesis is worthwhile.
- Further investigation on the use of the developed sensor in the detection of more than two PAHs in waste water.

## References.

1. West, L., *World Water Day: A Billion People Worldwide Lack Safe Drinking Water*. 2006 [cited 17 April, 2010]; Available from: <http://environment.about.com/od/environmentalevents/a/waterdayqa.htm>.
2. Carson, R., *From silent spring to silent night : endocrine disruption , amphibian declines, and environmental justice*. memorial lecture, pesticides news; 70, December, 2005.
3. Jose Luis V., Lilia, A., and Alberto N., *Application of Isotope Dilution to the determination of anthracene in environmental samples by headspace solid-phase microextraction and Gas Chromatography-Mass spectroscopy*. *Microchimica Acta*, 2006. **155**: p. 435-439.
4. Fetzer, J.C., *The chemistry and Analysis of the large polyaromatic hydrocarbons*. *polyaromatic hydrocarbons*, 2007. **27**(2).
5. Blumer, M., *Polycyclic aromatic compounds in nature*. *Scientific American Journal*, 2003. **234**: p. 34-35.
6. Laura, C., Liliana, A., Marina, B., Licia, S., Omar, L., Carla V., Piero, E.C., Irene, M., Vito, F.C, Fustinoni, *Biological monitoring of exposure to polycyclic aromatic hydrocarbons by the determination of unmetabolized compounds in urine*. *Toxicol, Lett.*, 2006. **162**: p. 132-138.
7. Saravanabhavan, G., Helferty, A., Hodson, P.V., Brown, R.S., *A multi-dimensional high performance liquid chromatographic method for figure printing polycyclic hydrocarbons and their alkyl-homologs in the heavy gas oil fraction of Alaskan North Slope crude*. *J. Chromatogr. A*, 2007. **1156**: p. 124-133.

8. Sram, R.j., Beskid, O., Rossnerova, A, Rossner, P., Lnenickova, Z., Milkova, A., Solansky, I., Binkova, B., *Environmental exposure to carcinogenic polyaromatic hydrocarbons-the interpretation of cytogenetic analysis by fish.* Toxicol. Lett., 2007. **172**: p. 12-20.
9. Mielke, H.W., Wang, G.D., Gonzales, C.R., Powell, E.T., Le, B., Quach, V.N., *PAHs and metals in the soils of inner –city and suburban New Orleans , Louisiana, USA.* Environ. Toxicol. Pharmacol, 2004. **18**: p. 243-247.
10. Fährnich, K.A., Pravda M., and Guilbault G.G., *Disposable amperometric immunosensor for the detection of polycyclic aromatic hydrocarbons (PAHs) using screen-printed electrodes.* Biosensors and Bioelectronics, 2003. **18** (1): p. 73-82.
11. Li, J., and X.-Q. Lin, *Electrodeposition of gold nanoclusters on overoxidized polypyrrole film modified glassy carbon electrode and its application for the simultaneous determination of epinephrine and uric acid under coexistence of ascorbic acid.* Analytica Chimica Acta, 2007. **596**(2): p. 222-230.
12. WHO, *Guidelines of drinking-water Quality* Geneva, 1998. **vol. 1**(2<sup>nd</sup> edition).
13. Kabzinski, A.K.M., J.C., Juszczak, R., *Determination of polycyclic aromatic hydrocarbons in water (including drinking water) of Lodz.* Journal of environmental studies, 2002. **11**(6): p. 695-706.
14. Sun, F., Littlejohn, D., and David Gibson M., *Ultrasonication extraction and solid phase extraction clean-up for determination of US EPA 16 priority pollutant polycyclic aromatic hydrocarbons in soils by reversed-phase liquid chromatography with ultraviolet absorption detection.* Analytica Chimica Acta, 1998. **364**(1-3): p. 1-11.

15. Woodward K.L.A., G.M., *Determination of polyaromatic hydrocarbon using immunoassays*. Science Total Environment, 1984. **32**: p. 103.
16. Colmsjo A., A.H.N., *The handbook of environmental chemistry part 1, PAHs and related compounds*. springer-verlag, 1998. **3**: p. 55.
17. Ferrer, R., Guiteras J., and Beltrán J.L., *Development of fast-scanning fluorescence spectra as a detection system for high-performance liquid chromatography Determination of polycyclic aromatic hydrocarbons in water samples*. Journal of Chromatography A, 1997. **779** (1-2): p. 123-130.
18. Andrade Eiroa, A., E.V.B., López Mahía, P., Muniategui Lorenzo, S., Prada Rodríguez, D. and Fernández Fernández. E., *Determination of polycyclic aromatic hydrocarbons (PAHs) in a complex mixture by second-derivative constant-energy synchronous spectrofluorimetry*. Talanta, 2000. **51**: p. 677-684.
19. Szolar, O.H.J., *Separation of PAHs by capillary electrophoresis (CE) equipped with laser-induced fluorescence* journal of molecular Rec., 1996. **9**: p. 515.
20. Geffard, O., Geffard, A., His, E., Budzinski, H., *Assessment of the bioavailability and toxicity of sediment-associated polycyclic aromatic hydrocarbons and heavy metals applied to Crassostrea gigas embryos and larvae*. Marine Pollution Bulletin, 2003. **46**(4): p. 481-490.
21. Cai, Z.-Q., Zhu Y.-X., and Zhang Y., *Simultaneous determination of dissolved anthracene and pyrene in aqueous solution by synchronous fluorimetry*. Spectrochimica Acta Part A: Molecular and Biomolecular Spectroscopy, 2008. **69**(1): p. 130-133.



22. Roman Edmund Sioda, B.F., *Voltammetric oxidation of naphthalene derivatives*. Journal of Electroanalytical chemistry, 2008. **612** p. 147-150.
23. Zhou, M., Shiyo, Z., Houyi Ma, O., *One-step synthesis of Au-Ag alloy nanoparticles by a convenient electrochemical method*. Physica E: Low-dimensional Systems and Nanostructures, 2006. **33** (1): p. 28-34.
24. Grova, N.E.A., *Detection of polycyclic aromatic hydrocarbon level in milk collected near potential contamination sources*. Journal of Agricultural and Food chemistry, 2002. **50**: p. 4640.
25. Lundstedt, S., Haglud, P., and Orberg, L., *Degradation and formation of polycyclic aromatic compounds during bioslurry treatment of an aged gasworks soil*. Journal of Environmental Toxicological Chemistry, 2003. **22**: p. 1413. .
26. De Voogt, P., V.H.P., Leonards, P., Klamer, J.C., Govers, H., *Bioconcentration of polycyclic aromatic hydrocarbons in the guppy ( poecilia reticulata)*. A quat Toxicol, 1991. **20**: p. 169-194
27. Djomo, J.E., Ferrier, V., Narbonne, J.F., Monkiedje, A., Njine, T., Garrigues, P., *Toxic effects of some major polyaromatic hydrocarbons found in crude oil and aquatic sediments on Scenedesmus subspicatus*. Water Research, 2004 **38** p. 1817–1821.
28. Wilson, S.C & Jones, K.C., *Bioremediation of soil contaminated with polynuclear aromatic hydrocarbons (PAHs); a review*. . Environ. Pollut., 1993. **81**: p. 229-249.
29. Kielhorn, J.B., *Guidelines for drinking water quality, Health criteria and other supporting information, world health organisation, Geneva*. 1998. **2**: p. 123-152.

30. Potin, O., E. & Rafin, C., *Biodegradation of polycyclic aromatic hydrocarbons (PAHs) by *Clasporium sphaerospermum* isolated from an aged PAH contaminated soil*. FEMS Microbiology Ecology 2004. **51**: p. 71-78.
31. Quantin, C., Joner, E.J., and Portal, J.M, *PAH dissipation in contaminated river sediment under oxic and anoxic conditions*. Journal of Environmental pollution, 2005. **134 (2)**: p. 315-322.
32. Associates, R.T.A., *Persistent, bioaccumulative and toxic chemicals in central and eastern European countries –state of the art report*. Brno. 2004. **17.08**, .
33. Ghosh U., S.G., Luthy R.G., Zare R.N., *Microscale location, characterization and association of polycyclic aromatic hydrocarbons on harbor sediment particles*. Environ. sci. Techno., 2000. **34**: p. 1729-1736.
34. Doong, R.A, C.K.P., Sun Y.C, Liao P.L., *Composition and distribution of organochlorine pesticide residues in surface sediments from Wu-shi river estuary, Taiwan*. mar. pollut. Bull., 2002. **45**: p. 246-253.
35. Mackay, A.A., P.M.G., *Enhanced concentrations of PAHs in groundwater at a coal tar site*. Environ. sci. Technol., 2001. **35**: p. 1320-1328.
36. (ATSDR)., A.D.R., *Public Health Statement, Polycyclic Aromatic Hydrocarbons*. Atlanta, GA: U.S. Department of Health and Human Services, 1990.
37. Faust, R.A., *Oak Ridge National Laboratory, Chemical Hazard Evaluation Group. Toxicity summary for Phenanthrene*. Oak Ridge, 1993.
38. White, K.L., *An overview of immunotoxicology and carcinogenic polycyclic aromatic hydrocarbons*. Environ. Carnog.Rev.C4 1986: p. 163-202.
39. Sims, R.C., M.R.O., *Fate of polynuclear aromatic compounds (PNAs) in soil-plant systems*. Residue Rev., 1983. **88**: p. 1-68.

40. Cerniglia, C.E., *Microbial metabolism of polycyclic aromatic hydrocarbons*. *Adva. Appl. Microbiol.*, 1984. **30**: p. 31-71.
41. Lim, L.H., R.M.H., Harrad, S., *The contribution of traffic to atmospheric concentrations of polycyclic aromatic hydrocarbons*. *Environ. Sci. Technol.*, 1999. **33**: p. 3538-3542.
42. Cai, Q.Y., C.H.M., Wu, Q.T., Zeng Q.Y., Katsoyiannis A., Ferard J.F., *Bioremediation of polycyclic aromatic hydrocarbons (PAHs)-contaminated sewage sludge by different composting process*. *J. Hazard . Mater.*, 2007. **142** p. 535-542.
43. ATSDR., *Public Health Statement, Polycyclic Aromatic Hydrocarbons*. Atlanta, GA: U.S. Department of Health and Human Services, 1990.
44. De Jong, W.H.E.A., *Detection of immunotoxicity of benzo(a)pyrene in a subacute toxicity study after oral exposure in rats*, . *Toxicological Sciences*, 1999. **50**: p. 214.
45. Mueller, J.G., Chapman, P. & Pritchard, P., *Creosote-contaminated Sites*. *Journal of environmental science and technology*. , 1997. **23**: p. 1197-1201.
46. Pickering, R.W., *A toxicological review of polycyclic aromatic hydrocarbons*. *Journal of Toxicology*, 1999. **18**: p. 101-135.
47. EUHCP, *Polycyclic aromatic hydrocarbons-occurrence in food dietary exposures and health effects, European Union Health and consumer products Directorate General*, 2002.
48. Nieva –Cano, M.J.R.-B., and Santos –Delgado, M.J, *Determination of PAH in food samples by HPLC with fluoremetric detection following sonication extraction without clean-up*. *Analyst*, 2001. **126**: p. 1326.

49. Charis, P., Marston, C.P., Jennifer, F., Kay F., Olaf, H., Wan-Mohaiza, D., William, M.B., *Effects of complex environmental mixture from coal tar containing polycyclic aromatic hydrocarbons (PAHs) on tumor initiation , PAH-DNA binding and metabolic activation of carcinogenic PAH in mouse epidermis*, carcinogenesis, 2001. **22**: p. 1077.
50. Melikkian, M., *Identification of benzo(a)pyrene metabolites in cervical mucus and DNA adducts in cervical tissues in humans by gas chromatography –mass spectrometry*. cancer letter, 1999. **146**: p. 127.
51. Simko, P., *Determination of polycyclic aromatic hydrocarbons in smoked meat product and smoke flavoring food additives*. Journal of chromatography B, 2002. **770**: p. 3.
52. Agency for Toxic Substances and Disease Registry (ATSDR), *Toxicological profile for polycyclic aromatic hydrocarbons*,. Atlanta, GA: U.S. Department of Health and Human Services, Public Health Service, 1995.
53. Ferrer, R., Guiteras, J., and Beltrán, J. L., *Development of fast-scanning fluorescence spectra as a detection system for high-performance liquid chromatography determination of polycyclic aromatic hydrocarbons in water samples*. Journal of Chromatography A, 1997. **779**: p. 123-130.
54. Andrade Eiroa, A., E.V.B., López Mahía, P., Muniategui Lorenzo, S., Prada Rodríguez, D., and Fernández Fernández, E., *Determination of polycyclic aromatic hydrocarbons (PAHs) in a complex mixture by second-derivative constant-energy synchronous spectrofluorimetry*. Talanta, 2000. **51**: p. 677-684.
55. Cai, Z.-Q., Zhu, Y.X., and Zhang, Y., *Simultaneous determination of dissolved anthracene and pyrene in aqueous solution by synchronous fluorimetry*.

- Spectrochimica Acta Part A: Molecular and Biomolecular Spectroscopy, 2008.  
**69**: p. 130-133.
56. Szekacs, A., L.H.M., Knopp D., Niessner R., *A modified enzyme-linked immunosorbent assay (ELISA) for polyaromatic hydrocarbons*. Analytica chimica acta, 1999. **399**: p. 127-134.
57. Li, K., Chen, R., Zhao B., Liu, M., Karu A.E, Roberts V.A., Li, q., *Monoclonal Antibody-Based ELISAs for Part-per-Billion Determination of Polycyclic Aromatic Hydrocarbons: Effects of Haptens and Formats on Sensitivity and Specificity*. Analytical Chemistry, 1998. **71**(2): p. 302-309.
58. Meisenecker, K., Knopp, D., Niessner, R., *Development of an enzyme-linked immunosorbent assay (ELISA) for pyrene*. analytical methods instru., 1993. **2**(1): p. 114-118.
59. Herikstad B. V., S.Ø., Haugen A. and Hagen, *Determination of polycyclic aromatic hydrocarbons in urine from coke-oven workers with a radioimmunoassay*. carcinogenesis, 1993. **14**(2): p. 307-309.
60. Kado, N.Y., Wei, E.T., *Radioimmunoassay for benzo (a) pyrene*. J Natl Cancer Inst., 1978. **61**(1): p. 221-225.
61. Liu, M., Li; Q.X, Rechnitz, G.A., *Flow injection immunosensing of polycyclic aromatic hydrocarbons; effect of haptens and formats on sensitivity and specificity*. Anal. chem., 1999. **71**: p. 302-309.
62. Liu, M., Rechnitz, G.A., Li, K., *Capacitive immunosensing of polycyclic aromatic hydrocarbons and protein conjuctes*. Anal. lett., 1998. **31**(12): p. 2025-2038.

63. Vo-Dinh, T., B.J.T., Griffin G. D., Ambrose K. R., Sepaniak M. J., and Gardenhire E. M., *Antibody-Based Fiberoptics Biosensor for the Carcinogen Benzo(a)pyrene*. Appl. Spectrosc., 1987. **41**: p. 735-738.
64. Lee, H.J., J.V., Cullen, D.C., Kim, B.C., Gu, M.B, *Monitoring and classification of PAH toxicity using an immobilized bioluminescent bacteria*. biosens. bioelectron., 2003. **18**: p. 571-577.
65. Chang, S.T., *Enhancement in the sensitivity of an immobilized cell-based soil biosensor for monitoring PAH toxicity*. sensors and actuators B, 2004. **97**: p. 272-276.
66. Pandey, P.C., Weetall, H.H., *Detection of aromatic compounds based on DNA intercalation using an evanescent wave biosensor*. Anal. chem., 1995. **67**: p. 787-792.
67. Gu, M.B., S.T.C., *Soil biosensor for the detection of PAH toxicity using an immobilized recombinant bacterium and a biosurfactant*. biosensens. bioelectron., 2001. **16**: p. 667-674.
68. Ruey-an Doong, H.-M., Shih-hui Lee, *Sol-gel-derived array DNA biosensor for detection of polycyclic aromatic hydrocarbons in water and biological samples*. sensora and actuators B, 2005: p. 323-330.
69. Vazquez-Duhalt, R., Fedorak P.M., *Lignin peroxidase oxidation of aromatic coumpounds in systems containing organic solvents*. Appl. Environ. Microbio., 1994. **60**: p. 459.
70. Rajeshwar, K., *Environmental Electrochemistry Fundamentals and Applications in Pollution Abatement*. Academic Press, New York, 1997.

71. Doong, R.-A., Shih H.-M., and Lee S., *Sol-gel-derived array DNA biosensor for the detection of polycyclic aromatic hydrocarbons in water and biological samples*. Sensors and Actuators B: Chemical, 2005. **111-112**: p. 323-330.
72. Bouvrette, P., Hrapovic, S., Male, K.B., Luong, J.T., *Analysis of the 16 Environmental Protection Agency priority polycyclic aromatic hydrocarbons by high performance liquid chromatography-oxidized diamond film electrodes*. Journal of Chromatography A, 2006. **1103**(2): p. 248-256.
73. Ahuja, T., M.I.A., Kumar, D., *Bimolecular immobilization on conducting polymers for biosensing application*. Biomaterials, 2007. **28**: p. 791-794
74. Malhotra, B.D, C.A., *Prospects of conducting polymers in biosensors*. Analytical Chimica Acta, 2006. **578**: p. 60-61.
75. Kuang-Hsuan Yang, Y.-C.L., Chung-Chin Yu., *Temperature effect of electrochemically roughened gold substrates on polymerization electrocatalysts of polypyrrole*. Analytica Chimica Acta. 2009. **631**: p. 40-46.
76. Ngece, R.F., *Electrochemical dynamics of cytochrome P450 (2D6) biosensors for selective serotonin re-uptake inhibitors (SSRIs)*. unpublished MSc. Thesis in chemistry, 2007. University of the Western Cape, South Africa.
77. Said Sadki, P.S., Nancy Brodie and Guillaume Sabouraud, *The mechanism of pyrrole polymerization*. Royal society of Chemistry, 2000. **29**: p. 283-293.
78. Dodlhofer, K., and Rajeshwar K., *Handbook of conducting polymers, 2nd ed*, New York ,USA, 1998. **531**.
79. Lyons, M.E.G., *Advances in Chemical Physics, Polymeric systems, 2<sup>nd</sup> ed*. John Wiley Sons, New York, USA, 1997: p. 297.

80. Vernitskaya, T.V.E., *Polypyrrole: a conducting polymer; its synthesis, properties and applications*. Russian Chemical Reviews, 1997. **66**(5): p. 443-457.
81. Kaplin, D.A., and Qutubuddin, S., *Electrochemically synthesized polypyrrole films: effects of polymerization potential and electrolyte type*. Polymer, 1995. **36**(6): p. 1275-1286.
82. Gao, Z., Minxian Z., and Beshen C., *The influence of overoxidation treatment on the permeability of polypyrrole films*. Journal of Electroanalytical Chemistry, 1994. **373**(1-2): p. 141-148.
83. Beck F., P.B., Oberst, M., Bunsenges Ber., *Organic electrochemistry in the solid state-overoxidation of polypyrrole*. journal of physical chemistry, 1987. **91**(9): p. 967-974.
84. Benzhi, Liu, L.L., Min Wang and Yanqin, Z., *A study of nanostructured gold modified glassy carbon electrode for the determination of trace Cr(VI)*. J. chem. Sci., 2008. **5**: p. 493-498.
85. Xiliang Luo, A.M., Anthony J. Killard, Malcolm R. Smyth, *Application of Nanoparticles in Electrochemical Sensors and Biosensors*. electroanalysis, 2005. **18**(4): p. 319 - 326.
86. Liu, T., Kang, T., Lu, L., Zhang, Y., Cheng, S., *Au-Fe(III) nanoparticle modified glassy carbon electrode for electrochemical nitrite sensor*. Journal of Electroanalytical Chemistry, 2009. **632**(1-2): p. 197-200.
87. Masato Tominaga, T.S., Makoto N., Isao T., *Composition-activity relationships of carbon electrodes-supported bimetallic gold-silver nanoparticles in electrocatalytic oxidation of glucose*. journal of electroana. Chem., 2008. **615** p. 51-61.



88. Liping Wang, W.M., Dandan Ni, Junwei Di, Ying Wu, Yifeng Tu, *Direct electrodeposition of gold nanoparticles of to indium/ tin oxide glass.* *electrochemistry comm.*, 2008. **10**: p. 673-676.
89. Xiahuang Kang, Z.M., Xiaoyong Zou, Peiang cia, Jinyuan Mo, *A novel glucose biosensor based on immobilization of glucose oxidase in Chitosan on a glassy carbon electrode modified with gold-platinum alloy nanoparticles / multiwall carbon nanotubes.* *Analytical Biochemistry*, 2007. **369** p. 71-79.
90. Gole, A., C.D., Ramakrishnan, V., Sainkar, S.R., Mandale, A.B., Rao, M., Sastry, M., *Pepsin-gold colloid conjugates: Preparation, characterization, and enzymatic activity.* *Langmuir*, 2001. **17**(5): p. 1674-1679.
91. Gole, A., Vyas, S., Phadtare, S., Lachke, A., Sastry, M., *Studies on the formation of bioconjugates of Endoglucanase with colloidal gold.* *Colloids and Surfaces B: Biointerfaces*, 2002. **25**(2): p. 129-138.
92. Zhuo, Y., Yuan, R., Chai, Y., Tang, D., Zhang, Y., Wang, N., Li, X., Zhu, Q., *A reagentless amperometric immunosensor based on gold nanoparticles/thionine/Nafion-membrane-modified gold electrode for determination of [alpha]-1-fetoprotein.* *Electrochemistry Communications*, 2005. **7**(4): p. 355-360.
93. Retna, Raj, C., Takeo Ohsaka T.O., *Gold nanoparticle arrays for the voltammetric sensing of dopamine.* *Journal of Electroanalytical Chemistry*, 2003. **543** p. 127-133.
94. Tianyan You, O.N., Masato T., and Shigeru H., *Characterization of Platinum Nanoparticle-Embedded Carbon Film Electrode and Its Detection of Hydrogen Peroxide.* *Anal. Chem.*, 2003. **75**(9 ): p. 2080–2085.

95. Liu, T., Gan X., Fan C., Li G., and Matsuda N., *Wiring electrons of cytochrome c with silver nanoparticles in layered films*. ChemPhysChem, 2003. **4**: p. 1364-1366.
96. Murielle Dequaire, C.D., and Benoît L., *An Electrochemical Metalloimmunoassay Based on a Colloidal Gold Label*. Anal. Chem., 2000. **72** (22): p. 5521–5528.
97. Jing-Juan Xu, W.Z., Xi-Liang Luo and Hong-Yuan Chen, *A sensitive biosensor for lactate based on layer-by-layer assembling MnO<sub>2</sub> nanoparticles and lactate oxidase on ion-sensitive field-effect transistors*. The Royal Society of Chemistry, 2005: p. 792–794.
98. Min Zhou, S.C., Shiyonb Z., Houyi M., *One-step synthesis of Ag-Au alloy nanoparticles by convenient electrochemical method* physica E, 2006. **33**: p. 28-34.
99. Supriya Devarajan, B.V., Sampath S., *Phase transfer of Au–Ag alloy nanoparticles from aqueous medium to an organic solvent: effect of aging of surfactant on the formation of Ag-rich alloy compositions*. Journal of Colloid and Interface Science, 2004. **278**: p. 126–132.
100. Okomoto H., T.B.M., in, *Phase diagrams of binary Gold alloys*. international, metals park, 1987.
101. Link, S., "Alloy formation of gold-silver nanoparticles and the dependence of the plasmon absorption on their composition". Journal of physical chemistry B., 1999. **103**:p. 3529-3533.
102. Pal, A., Shah, S., Kulkarni, V., Murthy, R.S., Devi, S., *Template free synthesis of silver-gold alloy nanoparticles and cellular uptake of gold nanoparticles in*

- Chinese Hamster Ovary cell*. Materials Chemistry and Physics, 2009. **113**(1): p. 276-282.
103. Devarajan, S., Vimalan B., and Sampath S., *Phase transfer of Au-Ag alloy nanoparticles from aqueous medium to an organic solvent: effect of aging of surfactant on the formation of Ag-rich alloy compositions*. Journal of Colloid and Interface Science, 2004. **278**(1): p. 126-132.
104. Ai Qin Wang, Y.-P.H., Yong-Fan Chen, Chung-Yuan Mou, *Au-Ag alloy nanoparticles as catalyst for CO oxidation : effect of Si/Al ratio of mesoporous support*. Journal of catalysts, 2006. **237** p. 197-206.
105. Xiangling Ren, X.M., Fangqiong Tang, *Preparation of Ag-Au nanoparticles and its application to glucose biosensor*. sensors and actuators, B 2005. **110** p. 358-363.
106. Stetter, J.N., Sheng Y., *Sensors chemical sensors, electrochemical sensors and ECS*. J. Electrochem Soc., 2003. **150**: p. S11-16.
107. Nelson, R., Stradiotto, H.Y., *Electrochemical sensors: A powerful tool in analytical chemistry*. J. Braz. Chem. soc., 2003. **14**(2): p. 159-173.
108. You Wang, Hui Xu, J.Z., *Electrochemical sensors for clinic analysis sensors*, 2008. **8**: p. 2043-2081.
109. Bard, A.J., and Faulkner, L.R., *Electrochemical Methods : Fundamentals and applications (2nd edition)*. Newyork, USA: John Willey & Sons, 2000.
110. Monk, P.M.S, *Fundamentals of electroanalytical chemistry*. Newyork, USA: John Willey & Sons, 2001: p. 158-159.
111. David, K., Gosser, J., *Cyclic voltammetry, simulation and Analysis of Reaction Mechanisms*. VCH publishers, 1994: p. 42-43.

112. Haines, F.W., *Environmental analytical chemistry*. blackie academic and professional, an imprint of chapman & hall, 2nd edition, 1995: p. 197-223.
113. Williams-Dottin, A.R., *Monosubstituted Squarate Ligands and their transition metal and Lanthanide Complexes: Structural and Electrochemical Studies, PhD Thesis in Chemistry*,. University of the West Indies, St. Augustine, 2001.
114. Kounaves, S.P., *Voltammetric Techniques: Handbook of Instrumental Techniques for Analytical Chemistry*. 2007, **Chapter 37**: p. 709-725.
115. Akinyenye, R.O., *Nanostructured polypyrrole impedimetric sensors for anthropogenic organic pollutants*, unpublished PhD Thesis in Chemistry, University of the Western Cape, South Africa, 2008.
116. Brett, C.M.A.B., A.M.O., *Electrochemistry Principles, Methods and Applications*. Oxford University Press, United States, New York, 2005.
117. Kang, X.M., Zhibin Zou, Xiaoyong Cai, Peixiang Mo, Jinyuan, *A novel glucose biosensor based on immobilization of glucose oxidase in chitosan on a glassy carbon electrode modified with gold-platinum alloy nanoparticles/multiwall carbon nanotubes*. Analytical Biochemistry, 2007. **369**(1): p. 71-79.
118. Fernández-Sánchez, C., McNeil, C.J. & Rawson, K., *Electrochemical impedance spectroscopy studies of polymer degradation: application to biosensor development*. Trends in Analytical Chemistry 2005. **24** (1): p. 37-48.
119. Skoog, E.A., *Principles of Instrumental analysis. 6th ed.* Thomson Brooks/Cole, 2007: p. 169-173.
120. Jihad Rene Albani, *Principles and application of fluorescence spectroscopy*. Wiley-Blackwell, 2007. **978-1-4051-3891-8**.

121. Fang, J., Zhong C., and Mu R., *The study of deposited silver particulate films by simple method for efficient SERS*. Chemical Physics Letters, 2005. **401**(1-3): p. 271-275.
122. Asta Sileikaite, I.P., Judita Puiso, Algimantas Juraitis, Asta Guobiene, *Analysis of Silver nanoparticles produced by chemical reduction of Silver salt solution*. Material science, 2006. **12**: p. 4.
123. McFarland, A.D., Mirkin, C.A , Van Duyne, R.P. and Godwin, H.A, *Synthesis of gold nanoparticles*. Journal of chemical education, 2004. **81**: p. 544A.
124. Yongsoon shin, I.-T.B., Bruce Arey, W., and Gregory Exarhos, J., *Facile stabilization of Gold-Silver alloy nanoparticles on cellulose nanocrystal*. Journal of physical chem. C, 2008. **112**: p. 4844-4848.
125. Fry, A., Britton, W.E, , *Laboratory Techniques in electroanalytical Chemistry, 1st edition*, New York, USA, 1984. **chapter 3**.
126. Matschulat Diana, A.D., Niessner Reinhard, Knopp Dietmar, *Development of a highly sensitive monoclonal antibody based ELISA*. Royal society of Chemistry, cambridge, 1877, 2005. **130**: p. 1078-1086.
127. Zhu, J., *Theoretical study of the optical absorption properties of Au-Ag bimetallic nanospheres*. Physica E: Low-dimensional Systems and Nanostructures, 2005. **27**(1-2): p. 296-301.
128. Angshuman Pal, A., Sunil Shah, A., Surekha, D., *Preparation of Silver–Gold Alloy Nanoparticles at Higher Concentration Using Sodium Dodecyl Sulfate*. Journal of Chemistry, 2008. **61**: p. 66.
129. Link S., L.W., El-Sayed M.A., *Alloy Formation of Gold–Silver Nanoparticles and the Dependence of the Plasmon Absorption on Their Composition*. Journal of physical chemistry B, 1999. **103** (18): p. 3529–3533.

130. Poovathinthodiyil Raveendran, J.F., *A simple and green method for the synthesis of Au, Ag, and Au–Ag alloy nanoparticles*. The Royal Society of Chemistry, 2006. **8**: p. 34-38.
131. Alqudami, S.A., Shivaprasad G.S.M., *Ag–Au alloy nanoparticles prepared by electro-exploding wire technique*. Journal of Nanoparticle Research, 2007. **10**: p. 1027-1036
132. Ehret, R., Baumann, W., Brischwein, M., Schwinde, A., Stegbauer, K., Wolf, B., *Monitoring of cellular behaviour by impedance measurements on interdigitated electrode structures*. Biosensors and Bioelectronics, 1997. **12**(1): p. 29-41.
133. Kang, X., Mai, Z., Zou, X., Cai, P., Mo, J., *A novel glucose biosensor based on immobilization of glucose oxidase in chitosan on a glassy carbon electrode modified with gold-platinum alloy nanoparticles/multiwall carbon nanotubes*. Analytical Biochemistry, 2007. **369**(1): p. 71-79.
134. Speiser, B., Stratman, M., unwin P.R. (Eds.), *Encyclopedia of Electrochemistry*. WILEY-VCH Verlag GmgH and CO. kGaA, Weinheim, 2003. **(chapter 2)**.
135. Monk, P.M.S., *Fundamentals of Electroanalytical Chemistry*. Newyork, USA: John Wiley & Sons., 2001: p. 264-266.
136. Arotiba, O.A., Owino, J.H., Baker, P.G., Iwuoha, E.I., *Electrochemical impedimetry of electrodeposited poly(propylene imine) dendrimer monolayer*. Journal of Electroanalytical Chemistry, 2010. **638**(2): p. 287-292.
137. Mathebe, N.G.R., Morrin A., and Iwuoha E.I., *Electrochemistry and scanning electron microscopy of polyaniline/peroxidase-based biosensor*. Talanta, 2004. **64**(1): p. 115-120.

138. Christensen, P.A., and Hamnett A., *In situ spectroscopic investigations of the growth, electrochemical cycling and overoxidation of polypyrrole in aqueous solution*. *Electrochimica Acta*, 1991. **36**(8): p. 1263-1286.
139. Martin, C.R., Van Dyke L.S., and Cai Z., *Template-synthesis--a method for enhancing the ionic and electronic conductivity in electronically conductive polymers*. *Electrochimica Acta*, 1992. **37**(9): p. 1611-1613.
140. Van Dyke, L.S. and Martin C.R., *Fibrillar electronically conductive polymers show enhanced rates of charge transport*. *Synthetic Metals*, 1990. **36**(2): p. 275-281.
141. Paddon, C.A., Banks, C.E.D., Compton, I.G., Richard, G., *Oxidation of anthracene on platinum macro- and micro-electrodes: Sonoelectrochemical, cryoelectrochemical and sonocryoelectrochemical studies*. *Ultrasonics Sonochemistry*, 2006. **13**(2): p. 126-132.
142. Tominaga, M., Shimazoe, T., Nagashima, M., Taniguchi, I., *Composition-activity relationships of carbon electrode-supported bimetallic gold-silver nanoparticles in electrocatalytic oxidation of glucose*. *Journal of Electroanalytical Chemistry*, 2008. **615**(1): p. 51-61.